CHALMERS

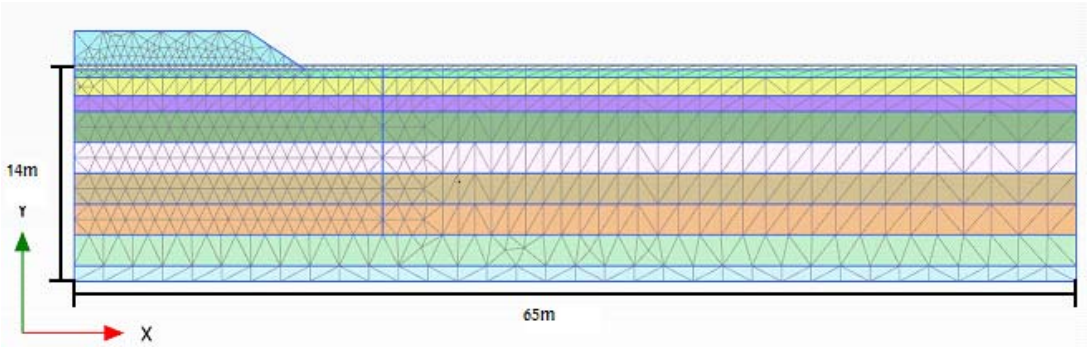

Numerical study of different creep models used for soft soils

Master of Science Thesis in the Master's Programme Geo and Water Engineering

PÄR GUSTAFSSON
TANG TIAN

Department of Civil and Environmental Engineering
Division of GeoEngineering

Geotechnical Engineering Research Group

CHALMERS UNIVERSITY OF TECHNOLOGY
Gothenburg, Sweden 2011
Master's Thesis 2011:41

MASTER'S THESIS 2011:41

Numerical study of different creep models used for soft soils

Master of Science Thesis in the Master's Programme Geo and Water Engineering

PÄR GUSTAFSSON

TANG TIAN

Department of Civil and Environmental Engineering
Division of GeoEngineering
Geotechnical Engineering Research Group
CHALMERS UNIVERSITY OF TECHNOLOGY
Gothenburg, Sweden 2011

Numerical study of different creep models used for soft soils

Master of Science Thesis in the Master's Programme Geo and Water Engineering

PÄR GUSTAFSSON
TANG TIAN

Examensarbete / Institutionen för bygg- och miljöteknik,
Chalmers tekniska högskola 2011:41

Department of Civil and Environmental Engineering
Division of GeoEngineering
Geotechnical Engineering Research Group
Chalmers University of Technology
SE-412 96 Gothenburg
Sweden
Telephone: + 46 (0)31-772 1000

Cover:
The finite element model of the test fill at Lilla Mellösa drawn in PLAXIS.

Chalmers Reproservice
Gothenburg, Sweden 2011

Numerical study of different creep models used for soft soils

Master of Science Thesis in the Master's Programme Geo and Water Engineering

PÄR GUSTAFSSON
TANG TIAN
Department of Civil and Environmental Engineering
Division of GeoEngineering
Geotechnical Engineering Research Group
Chalmers University of Technology

ABSTRACT

Nowadays, more and more construction activities are carried out on highly compressible layers of soft soil. The engineering challenges for this kind of soil material lie in that it commonly exhibits large amount of creep strains in time, it experiences anisotropy in the fabric as well as some inter-particle bonding within the soil structures. This finally makes an accurate prediction of soft soil behaviour quite problematic.

In this master's thesis, three different material models concerning settlements in soft soils, including creep deformations, have been studied and evaluated. The material models are the Soft Soil Creep model (SSC), the Anisotropic Creep Model (ACM) and the non-associated creep model for Structured Anisotropic Clay (n-SAC). These models have been implemented into the finite element software PLAXIS which can perform the large amount of calculations that is needed.

Standard laboratory tests for determining the soil parameters required by the models are described in this thesis, including the oedometer tests (mainly the Constant Rate of Strain test) and the undrained triaxial test. The method of how to evaluate those important soil parameters from test data is also discussed.

The practical work for this thesis is simulations of several laboratory tests and a field case. The modelling of laboratory tests is carried out on materials taken from the building of the new E45 highway between Trollhättan and Gothenburg on the Swedish west coast. Data for the real case scenario modelling has been received from the test fill located at Lilla Mellösa outside Stockholm, Sweden.

The overall aim of this master's thesis was to evaluate the performances of three different material models. The results demonstrate that all three models are capable to simulate the small-scale laboratory tests and describe the creep effect. However, regarding to the full-scale field test, the ACM model showed a deficiency to achieve the long-term settlement calculations, while the SSC and the n-SAC model captured the soil deformations well. Given that the ACM and the n-SAC models are recently developed, more future researches are of necessity. In general, all the three models are attractive when dealing with soft soil behaviour, however if considering numerical analysis, more testing works are suggested to be done so as to achieve full and stable applications of these models in geotechnical engineering practices.

Key words: soft soil, creep, long term settlement, soil anisotropy, destructuration, SSC, ACM, n-SAC

Numerisk studie av olika krypningsmodeller för användning i lösa jordarter
Examensarbete inom Geo and Water Engineering

PÄR GUSTAFSSON
TANG TIAN
Institutionen för bygg- och miljöteknik
Avdelningen för geologi och geoteknik
Forskargrupp geoteknik
Chalmers tekniska högskola

SAMMANFATTNING

Fler och fler konstruktioner byggs idag på högkompressibla lösa jordarter. Den ingenjörsmässiga utmaningen med att uppföra konstruktioner på dessa material är att de ofta uppvisar stora krypningseffekter som utvecklas med tiden, anisotropi samt bindningseffekter mellan partiklarna i jordstrukturen. Detta medför att möjligheten att förutse beteendet hos lösa jordarter försvåras.

I detta examensarbete studeras och utvärderas tre olika materialmodeller som avser sättningar i lösa jordarter. Dessa modeller inkluderar krypningseffekter. Modellerna är *Soft Soil Creep model* (SSC), *Anisotropic Creep Model* (ACM) och *non-associated creep model for Structured Anisotropic Clay* (n-SAC). Dessa modeller har implementerats i det finita elementmetodprogrammet PLAXIS, vilket används för att utföra de stora mängder ekvationer som krävs.

Vidare kommer standardlaboratorietester att beskrivas, vilka används för att bestämma de jordparametrar som behövs i modellerna. Testerna inkluderar ödometerförsök (huvudsakligen CRS-försök) och det odränerade triaxialförsöket. Den metod som används för att utvärdera parametrarna från försöken kommer också att beskrivas.

Arbetet med detta examensarbete genomförs genom simuleringar av flera laboratorietester samt ett fältfall. Data till laboratorietesterna erhålls från byggandet av den nya motorvägen E45 som sträcker sig mellan Göteborg och Trollhättan på västkusten. Data till fältfallet erhålls från ett geotekniskt testområde som är lokaliserat i Lilla Mellösa utanför Stockholm.

Målet med detta examensarbete är att utvärdera de tre materialmodellernas kapacitet ur geoteknisk synvinkel. Resultatet från simuleringarna visar att alla tre modellerna är kapabla att simulera de småskaliga laboratorietesterna och att beskriva krypningseffekterna. Dock så visar utvärderingen också att ACM-modellen är bristfällig att utvärdera sättningar över lång tid medan SSC- och n-SAC-modellerna lyckas med detta på ett bra sätt. Det ska även nämnas att ACM- och n-SAC-modellerna är nyutvecklade och att mer forskning och utveckling krävs för att bli mer precisa. Överlag så är samtliga tre modeller bra att använda när lösa jordarter utvärderas. Dock rekommenderas att fler tester utförs på modellerna för att de ska bli fullt stabila och kapabla för att användas inom det geotekniska området.

Nyckelord: lösa jordarter, krypning, sättningar över lång tid, anisotropi, SSC, ACM, n-SAC

Contents

Preface

The work with this thesis was performed during January to June 2011 at the Division of GeoEngineering, Department of Civil and Environmental Engineering at Chalmers University of Technology, Gothenburg, Sweden. The examiner was Professor Claes Alén and supervisors were Mats Olsson and Anders Kullingsjö.

First, we would like to thank our supervisors Mats Olsson and Anders Kullingsjö for taking their time to answer numerous questions and helping us with various problems that have arisen during our work. We are grateful to the division's research engineer Peter Hedborg for guiding us through the study of the laboratory tests.

We would also like to thank the staff and the other master's thesis students at the division for creating a positive atmosphere during this demanding but instructive time.

Finally, we want to express our appreciations to our parents for their endless support and love. It is because of their love that we are brave to go further and enjoy the exploration.

Gothenburg, June 2011

Pär Gustafsson Tang Tian

Notations

Below follows a summary of the parameters used in this master's thesis.

Roman upper case letters

C_c	Compression index
C_p	Preconsolidation index
C_s	Swelling index
C_α	Secondary compression index
E_{ref}	Young's modulus reference
E_{oed}^{ref}	Oedometer Young's modulus reference
F	Force
K_0	Lateral earth pressure ratio
K_0^{NC}	Lateral earth pressure ratio in the NC-region
M	Compression modulus
M	Slope of the critical state line
M_c	Slope of the critical state line in compression
M_e	Slope of the critical state line in extension
M_f	Load angle dependent critical state line in p'-q space
M_{fC}	Critical state line in compression loading
M_L	Compression modulus for the normal consolidated range
M_0	Compression modulus for the over consolidated range
Q	Potential surface
R	Time resistance

Roman lower case letters

c	Cohesion
c_k	Coefficient of permeability
c_v	Coefficient of consolidation
c'	Cohesion
d	Depth
e	Void ratio
e_{init}	Initial void ratio
e_0	Initial void ratio
k	Permeability
m'	Modulus number
n	Over consolidation ratio
p_c	Preconsolidation pressure
p_{ref}	Reference stress
p_p^{eq}	Equivalent preconsolidation pressure
p^{eq}	Equivalent effective stress
p'	Mean effective stress
p'_{eq}	Equivalent mean effective stress
p'_m	Reference stress
p'_{mi}	Intrinsic reference stress
p'_p	Preconsolidation pressure

q	Deviatoric stress
r_s	Time resistance number
r_{si}	Intrinsic time resistance number
$r_{s,min}$	Minimum measured time resistance number
r_1	Minimum time resistance number
t	Time
t_c	Consolidation time
t_r	Reference time
t_0	Reference time
t'	Effective creep time
u	Pore water pressure
w_n	Natural water content
x	Number of instable structures
z	Depth

Greek upper case letters

β_d	Deviatoric rotational vector
$\beta_{K_0^{NC}}$	Internal model parameter

Greek lower case letters

α	Scalar quantity
$\dot{\alpha}$	Rotation hardening parameter
α_d	Deviatoric rotational vector
$\alpha_{K_0^{NC}}$	Rotation of the potential surface in K_0^{NC}-loading
α_s	Coefficient of secondary compression
α_0	Initial inclination
γ	Unit weight
γ_w	Weight of water
γ'	Weight of soil grains
$\dot{\gamma}^c$	Deviatoric creep strain rate
δl	Change in length
δv	Change in volume
ε	Strain
ε_v	Vertical strain
$\dot{\varepsilon}_v$	Volumetric strain rate
ε_c	Creep strain
ε_{creep}	Creep strain
ε_v^c	Volumetric creep strain
ε_v^p	Plastic volumetric creep strain
ε^c	Creep strain
$\dot{\varepsilon}^c$	Creep strain rate
ε^e	Elastic strain
$\dot{\varepsilon}^e$	Elastic strain rate
ζ_i	Intrinsic viscoplastic compressibility coefficient
$\eta_{K_0^{NC}}$	Mobilization in K_0^{NC}-loading
κ^*	Modified swelling index

λ_i^*	Normal compression line for a reconstituted soil sample
λ^*	Modified compression index
μ^*	Modified creep index
ν	Poisson's ratio
ν_{ur}	Poisson's ratio for unloading-reloading
σ	Total stress
σ_a	Axial stress
σ_d	Deviatoric stress vector
σ_p	Preconsolidation pressure
σ_r	Radial stress
σ'	Effective stress
σ_p'	Preconsolidation pressure
σ_v'	Vertical effective stress
σ_0'	In-situ effective stress
σ_c'	Preconsolidation pressure
τ	Reference time
τ_c	Time parameter
φ	Friction angle
φ'	Friction angle
φ_{cv}'	Critical state friction angle
φ_{cs}	Critical state friction angle
ψ	Dilatancy angle
ω	Rate of rotation parameter
ω	Deviatoric destructuration parameter
ω_d	Rate of shear rotation parameter

Abbreviations

ACM	Anisotropic Creep Model
CRS	Constant Rate of Strain
CSL	Critical State Line
IL	Incremental Loading
LIR	Load Increment Ratio
MCC	Modified Cam Clay model
NCL	Normal Consolidated Line
n-SAC	non-associated creep model for Structured Anisotropic Clay
OCR	Over Consolidation Ratio
POP	Pre-Overburden Pressure
SSC	Soft Soil Creep model

1 Introduction

The introduction chapter of this master's thesis aims to provide the background to the subject studied, define the main objectives and scope and as well the method and limitations.

1.1 Background

There are increasing conflicts between the limited land resources and the ascending modern construction activities worldwide. Soft soils that were previously considered as inappropriate for constructions because of high compressibility are more and more adopted as the subsoil in infrastructural engineering nowadays.

Accurate predictions of the amount of and the rate of settlement of the ground under an applied load are of great importance as geotechnical designs are largely driven by serviceability limit state conditions. Conventional calculation methods that did not consider the time-dependent strains of the soft soil however can't achieve the demanded accuracy and consequently needs to be modified.

Several advanced material models have recently been developed which incorporate creep effects in soft soil. Besides the characteristics of time-dependency, these models are also trying to consider the influence of anisotropy and the structures of the mechanical behaviour of natural clay. While the more factors are being included, the more complexity these models turn out to have. Understanding of the required input parameters and validations of these models' performances are therefore necessary so as to promote their applicability in geotechnical practices.

1.2 Aim

The major aim of this master's thesis is to study the three different material models within the finite element software PLAXIS, including the Soft Soil Creep model (SSC), Anisotropic Creep Model (ACM), and the non-associated creep model for Structured Anisotropic Clay (n-SAC). Although the first model, SSC, has obtained a relatively wide application in PLAXIS so far, the other two models are newly developed and needs further improvements. The objectives of this thesis work include the verifications of simulation results from those material models against laboratory tests as well as a real field case scenario. The laboratory test data originates from the modernization of highway E45 between the cities of Trollhättan and Gothenburg, Sweden. The real field case is a test fill constructed in the mid 1940's at Lilla Mellösa, Sweden, from which unique data has been extracted since its construction. Moreover, discussions within the different models in terms of input parameters evaluation from lab tests, and the inter-relationship between various model parameters will be done.

1.3 Scope of work

The work in this thesis is carried out in stages as follows so as to achieve the objectives:

- Literature studies about the time-dependent strains in soft soil incorporating the influences of fabric anisotropy and destructuration;
- Understanding the fundamental theories of three advanced soil models – SSC, ACM and n-SAC;
- Discussions of the evaluation method for the required input soil parameters from laboratory tests;
- Investigating the model performances by simulating the CRS tests and undrained triaxial tests in the finite element software PLAXIS;
- Further investigations of the models' capability to predict the soft soil behaviour by simulating a field case – the Lilla Mellösa test fill;
- Discussions with the advantages and drawbacks regarding to apply these soil models in practice.

1.4 Method

The work with this master's thesis started with a literature survey of creep theories and the soil models that will be used. Since none of the writers of this thesis has worked with PLAXIS before, several tutorial exercises in PLAXIS have been done firstly in order to learn the basics of the software. Moreover, in order to understand the determinations of soil parameters, several soil tests such as the incremental loading (IL) tests, constant rate of strain (CRS) tests and the triaxial tests were studied and practiced in the geo-engineering laboratory at Chalmers. The laboratory test data for the highway E45 were provided by the supervisor and the field measurement data for the test fill in Lilla Mellösa were digitalized from the SGI report 29 (Larsson, 1986) and SGI report 70 (Larsson, 2007).

1.5 Limitations

Due to the complexity within the applications of numerical tools, a couple of limitations have been set in this thesis and therefore not been taken into account including:

- The mesh dependency in finite element software;
- Programs for dealing with three-dimensional conditions.

2 Fundamental studies of soft soil behaviour

When using the term soft soil, it is usually included near-normally consolidated clays, clayey silts and peat while in this report, studies will be focusing on soft clay; i.e. normally consolidated clays and slightly over consolidated clays. Clay is primarily composed of irregular arranged particles which have typical dimension of less than 2 μm. The particles are gathered in aggregates which are connected by bondings/links. These links are usually the smallest particles (Hansbo, 1975).

In a view of engineering practice, what distinguishes soft clay from other soil types is that they have a high grade of compressibility. If performing for instance an oedometer test it can be shown that normally consolidated clays behave ten times softer than normally consolidated sands (Vermeer & Neher, 1999).

The high compressibility of soft clay, their fabric anisotropy (particle arrangement) and their structures (inter-particle bondings) will be studied in this chapter.

2.1 Compressibility

In this section, basic soil mechanics regarding to the stress-strain relationship as well as the time-dependent strain behaviour is described.

2.1.1 Stress-strain behaviour

To describe the stress-strain behaviour, a typical stress-strain curve for soft clay with one-dimensional first loading and an unloading-reloading sequence is illustrated in Figure 2.1.

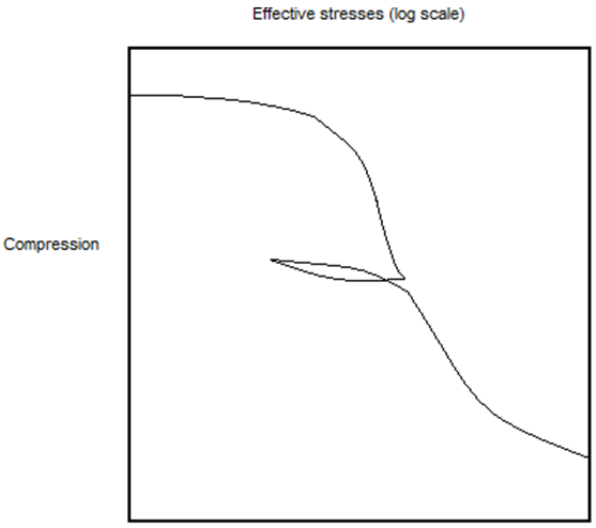

Figure 2.1. A stress-compression curve with a first loading and unloading-reloading sequence (Wood, 1990).

Initially, within a certain range of overburden pressure, the soil behaves stiff and only a small amount of compression has been reached. When stress increases, there is a transition from stiff to less stiff response, which usually is defined as yielding of soil.

When the soil is unloaded to a less pressure state, only a small part of the compression is recovered, i.e. the elastic strain and the plastic strain are left in the soil as permanent deformations. If the soil is loaded again, it behaves stiffer in the beginning until the stress exceeds the previous reached loading pressure. The compression line would then follow the same trend as in the first loading. The yield point of irrecoverable plastic strains is associated to the maximum pressure that the soil has been experienced in the past, which is also the definition of the preconsolidation pressure. This is because unlike metals, soil has a stress memory which would affect the current stress-strain relations significantly.

The preconsolidation pressure is usually evaluated from an oedometer test and the evaluation method will be described in details later in the laboratory tests chapter, see Chapter 4.1. Sample disturbance, temperature and strain rate are commonly considered as factors influencing the evaluation of preconsolidation pressure in laboratory tests.

Natural clays usually show an over consolidation effect, i.e. a higher preconsolidation pressure than in-situ effective stress. This could be explained by different reasons. The upper layer of the ground usually has a complex stress history due to the groundwater fluctuation. Its preconsolidation pressure is corresponding to the lowest groundwater level. If a soil layer has a current groundwater level in the ground surface and the lowest groundwater down to a depth of d in history, then the over consolidation ratio along the depth z is shown in Figure 2.2 and equation (2.1).

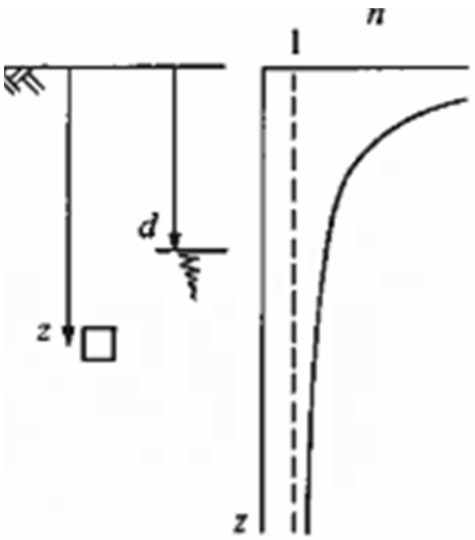

Figure 2.2. A profile of the over consolidation ratio with depth (Wood, 1990).

$$n = OCR = 1 + \frac{\gamma_w d}{\gamma' z} \tag{2.1}$$

where γ_w = weight of water

γ' = weight of soil grains

When without the presence of groundwater level changes, soft soil also presents an over consolidation effect which is more related to the aging effect. As shown in Figure 2.3, a 3000-year old clay sample when loaded in the laboratory test would show a preconsolidation pressure determined by the combination of its current void ratio and the duration of sustained loading.

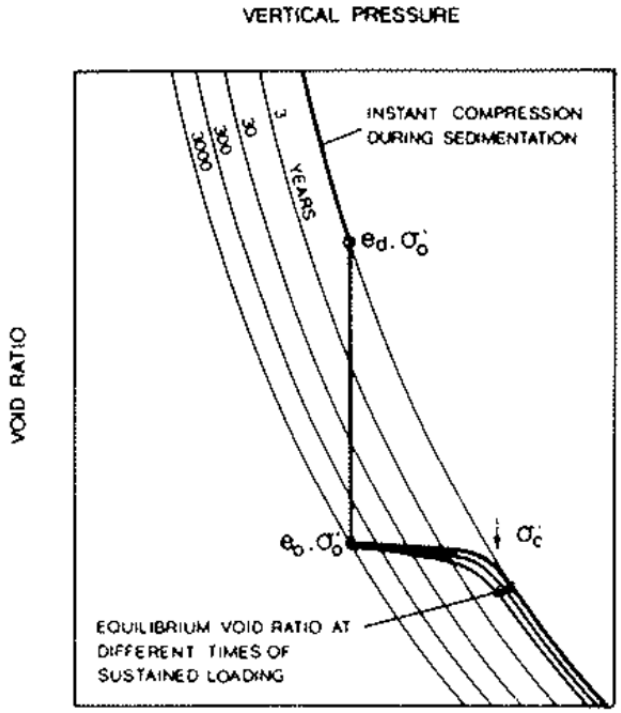

Figure 2.3. Aging effect of clay (Bjerrum, 1967).

2.1.2 Time-dependent strain behaviour

Several researchers have reported that the time plays an important role in soft soil behaviour. Buisman (1936) firstly proposed a creep law based on empirical data, which expresses that under constant effective stresses, the strain increases linearly with the logarithm of time. Later on, several researchers attempted to investigate this time-dependent behaviour elaborately through different approaches.

2.1.2.1 Delayed compression

Bjerrum (1967) put forward with the term of "instant" and "delayed" compression. The former is to describe the strains occurring simultaneously with the increase of effective stresses and the latter represents strains under unchanged effective stresses. See Figure 2.4 for an illustration of this approach.

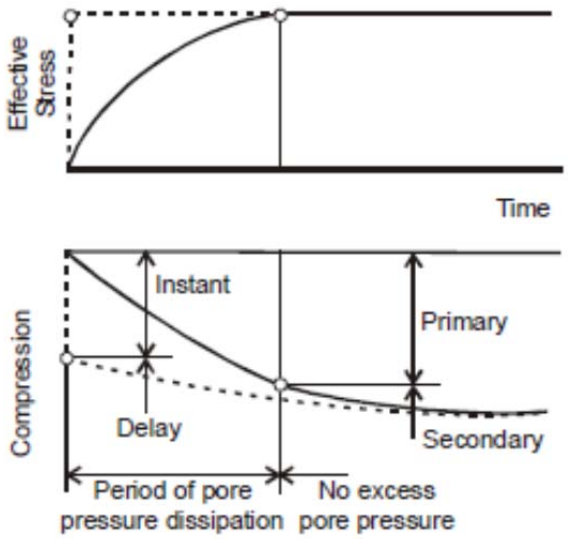

Figure 2.4. Definition of "instant" and "delayed" compression compared with "primary" and "secondary" compression illustrated by the broken and solid line respectively (Bjerrum, 1967).

The solid line is presenting the time-delayed effective increase due to excess pore pressure dissipation. In the figure, Bjerrum (1967) also applied different "time lines" to simulate the delayed compression. The decreased distance between time lines is describing the reduced creep strain rate.

2.1.2.2 Strain-rate effect

A common observation in laboratory tests is that the preconsolidation pressure is dependent on the strain rate; the higher the strain rate, the higher the apparent preconsolidation pressure. This is shown by conducting CRS tests with different strain rates as in Figure 2.5a. Based on large amount of CRS tests data, it is also found that there is a linear variation of preconsolidation pressure versus the strain rate when plotted in a log-log scale as in Figure 2.5b (Adachi & Oka, 1982; Vermeer & Neher, 1999; Kim & Leroueil, 2001).

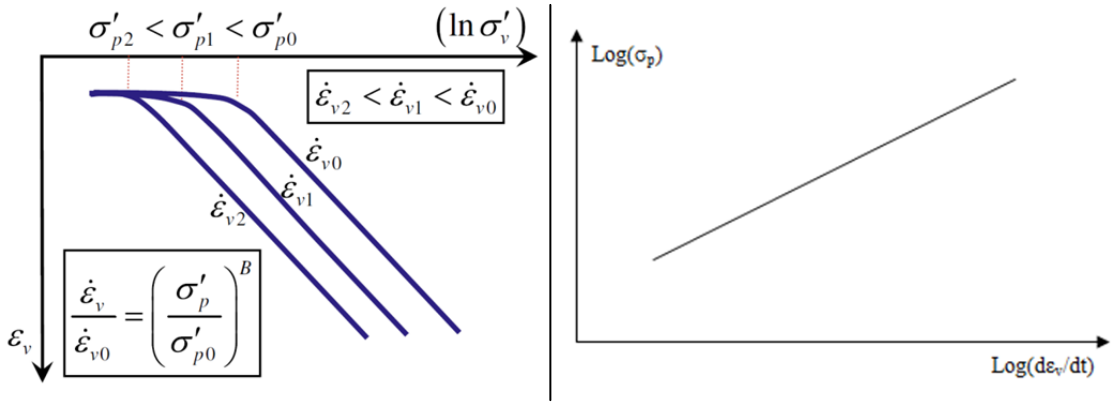

Figure 2.5. *a) A comparison of stress-strain curves under different strain rates (Yin et al., 2010).*

b) Schematic plot of the relationship between the strain rate and the apparent preconsolidation pressure (after Claesson, 2003).

Šuklje, in 1957, systematically described this rate effect by using an isotache model as shown in Figure 2.6 below, where the unique relationship between effective stresses, void ratio and strain rate are illustrated. Šuklje (1957) also suggested the soil layer thickness, permeability and drainage condition are influencing the rate-dependent strains.

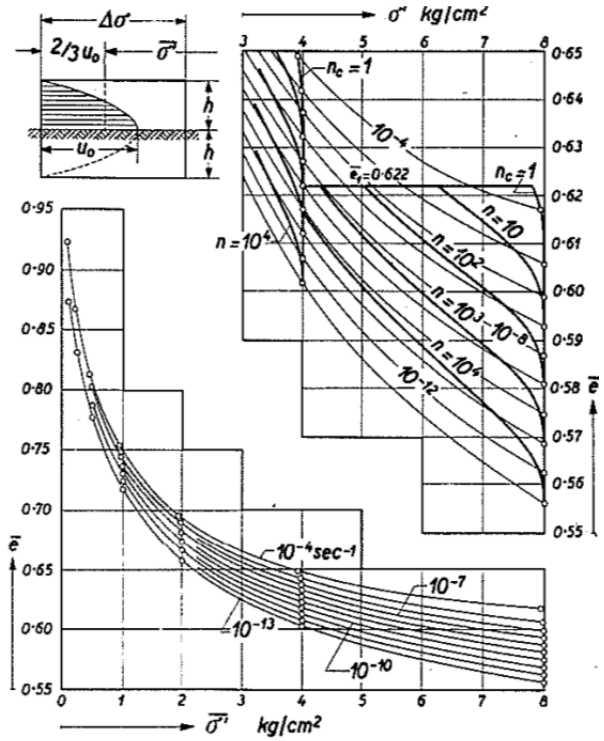

Figure 2.6. Šuklje's isotache model (Šuklje, 1957).

2.1.2.3 Time-resistance concept

The resistance concept is commonly applied in physics such as thermal resistance and electrical resistance which both show a general relation as equation (2.2).

$$R_x = \frac{incremental-action:dx}{incremental-response:dy} \tag{2.2}$$

Janbu (1969) creatively applied the resistance concept into soil behaviour by defining the time as an action and the strain as a response, described by equation (2.3).

$$R_t = \frac{dt}{d\varepsilon} \tag{2.3}$$

When plotting the time resistance against the time, it is found that there eventually is a linear relationship between the time resistance and the time, which defines the time resistance number r_s. Figure 2.7 illustrates the time resistance R and resistance number r_s in incremental loading oedometer test (Janbu, 1998).

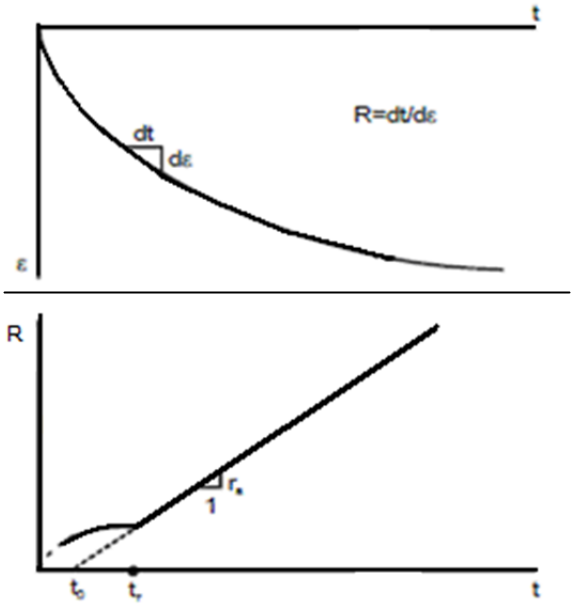

Figure 2.7. Definition of time resistance R and resistance number r_s in incremental loading oedometer test (Janbu, 1998).

Equation (2.4) describes the calculation of the time resistance R.

$$R = r_s(t - t_r) \tag{2.4}$$

where t = time

t_r = reference time

The derivation of the relationship between creep strain and time based on the time resistance number is expressed in equation (2.5) as follows.

$$\dot{\varepsilon}_{creep} = \frac{\partial \varepsilon_{creep}}{\partial t} = \frac{1}{R} = \frac{1}{r_s(t-t_r)} \tag{2.5}$$

By integration of equation (2.5) from t_0 to t, creep strain during this time period can be estimated, as equation (2.6).

$$\Delta\varepsilon_{creep} = \frac{1}{r_s}\int_{t_0}^{t} \frac{1}{(t-t_r)} = \frac{1}{r_s}\ln\frac{t-t_r}{t_0-t_r} \tag{2.6}$$

Meanwhile, time resistance number, r_s, can be calculated as equation (2.7).

$$r_s = \frac{\partial \ln t}{\partial \varepsilon_{creep}} \tag{2.7}$$

Typical values of the resistance number for the normally consolidated, saturated clays are estimated as in the range of 100-500 for natural water content within 30-60% (Havel, 2004).

2.2 Consolidation

The consolidation sequence can be divided into two sub-categories; primary consolidation and secondary consolidation. Primary consolidation is defined as the deformation that occurs during the pore water pressure dissipation and secondary consolidation when the load is exposed to the structure of the clay and thereby deforming it. Both consolidations will be explained further in this section.

2.2.1 Primary consolidation

Consolidation is the process of volume decrease of a soil due to a hydrodynamic delayed dewatering from the pores of the soil (Hansbo, 1975). A soil with a high permeability has an instantaneous deformation and a soil with a low permeability has a delayed deformation due to that it takes some time for the water to leave the pores of the soil. Soils with low permeability, such as clay and silt, are therefore characterized of time-dependency (Sällfors, 2001). If clay with a low permeability is exposed to a load, the increased stress will create an excess pore water pressure in the clay. Figure 2.8 illustrates a simple model of consolidation. The model consists of a container filled with water (which can be regarded as a saturated clay), springs (the structure of the clay), standpipes and a lid with holes in it (where the holes represent the pores in

the clay). The water level in the standpipes represents the pore water pressure at each level.

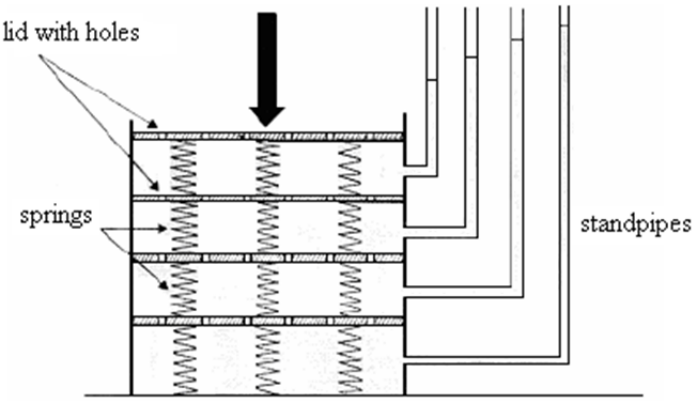

Figure 2.8. Rheological model of consolidation theory (Hansbo, 1975).

Initially, the entire load is held up by the pore water, but as the water is leaving the system, the load is transferred to the structure of the clay which will then be compressed and creates settlements in the clay. At the same time, the excessive pore water pressure is decreasing and the effective stress is increasing as illustrated in Figure 2.9. The total stress is constant during the process which is illustrated by the figure and shown with equation (2.8).

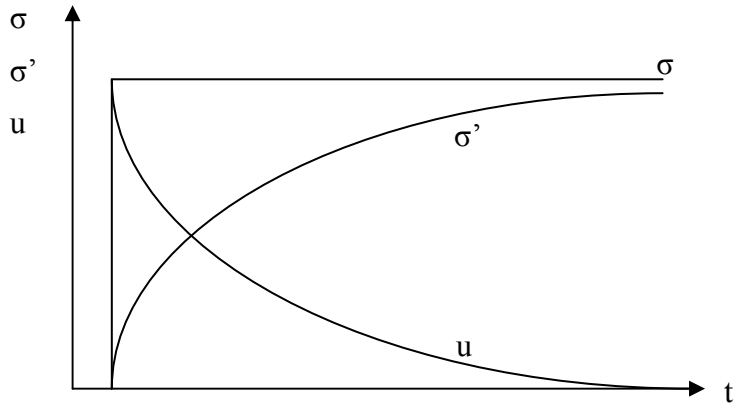

Figure 2.9. Change of load from excessive pore water pressure to effective stress (modified after Sällfors, 2001).

$$\sigma = \sigma' + u \tag{2.8}$$

where σ = total stress

σ' = effective stress

u = pore water pressure

2.2.2 Secondary consolidation

The phenomenon of creep settlements continuing after complete pore water equalization at a constant effective stress is called secondary consolidation, and is the time-dependency of the effective stress-strain relation. It is also known under the names secondary compression, plastic resistance to compression, time resistance and strain rate effects. But the common name is creep deformations (Larsson, 1986).

Creep deformations occur when all the excess pore water pressure is zero and the load put on the clay is exposed to the structure of the clay. Creep is a slow process and does not create any hydraulic gradient (Hansbo, 1975). Secondary consolidation in clay is the result of viscous deformations in the micro structural fracture zones which are created during the primary consolidation. It is also the result of a time dependent re-orientation of the particles in the aggregates due to a re-storage and increase of stress that occurs (Hansbo, 1975). The strength in the aggregates that are created increases the resistance of deformations which means that the speed of creep is reduced with time and will eventually reach zero.

There have been many attempts to incorporate the time effects into settlement calculation models. It has been assumed that Terzaghi's (1923) consolidation theory has been valid during the primary consolidation and that the secondary consolidation started after the excess pore water pressure had been equalized. It was assumed that it commenced at a continuously decreasing speed since it was regarded to be a linear function of the logarithm of time (Larsson, 1986). However, it has been shown that this assumption is inadequate. Šuklje (1957) has presented a model where there is made no difference between when the primary and secondary consolidations started. In the model, the void ratio and the effective stress relation continuously changes with the rate of deformation (Larsson, 1986). This would mean that creep deformation is not a process that starts immediately after the pore water pressure equalization but rather that the two compression sequences occur at the same time, apart from the hydrodynamic delay during the primary consolidation.

2.2.3 Terzaghi's classical consolidation theory

Terzaghi's model for consolidation in one dimension was introduced in 1923. There are several prerequisites for the model to be valid (Hansbo, 1975):

- The soil is saturated and homogenous;
- Pore water flow and soil deformation only occur in one dimension; vertically;
- Darcy's law is valid when deciding pore water flow;
- The total stress is always constant, changes in pore water pressure results in equal change in effective stress;
- The pore water and the soil particles are incompressible;
- The compression of the soil is only dependent of the effective pressure.

The model can be described with equation (2.9) (Hansbo, 1975).

$$\frac{\partial u}{\partial t} = M \frac{\partial}{\partial z}\left(\frac{k}{\gamma_w}\frac{\partial u}{\partial z}\right) \quad (2.9)$$

where u = pore water pressure

t = time

z = depth coordinate

M = compression modulus

k = permeability

γ_w = unit weight of water

If the permeability k is independent from the depth z, i.e. k is constant with the depth as well as the compression modulus M, the consolidation coefficient can be used to simplify the model. The consolidation coefficient is a parameter that provides information about which speed the settlement is developing. The coefficient can be expressed as equation (2.10) (Hansbo, 1975).

$$c_v = \frac{kM}{\gamma_w} \quad (2.10)$$

Equation (2.10) can then be rewritten as equation (2.11).

$$\frac{\partial u}{\partial t} = c_v \frac{\partial^2 u}{\partial z^2} \quad (2.11)$$

2.2.4 Corrections of the consolidation theory

However, Terzaghi's consolidation theory loses its validation when time-dependent strain is considered. In reality, the consolidation phase is prolonged since the creep strains induce more pore pressure and therefore act as a hydro break, preventing the excess pore pressure to dissipate. Figure 2.10 illustrates the excess pore pressure development with and without creep.

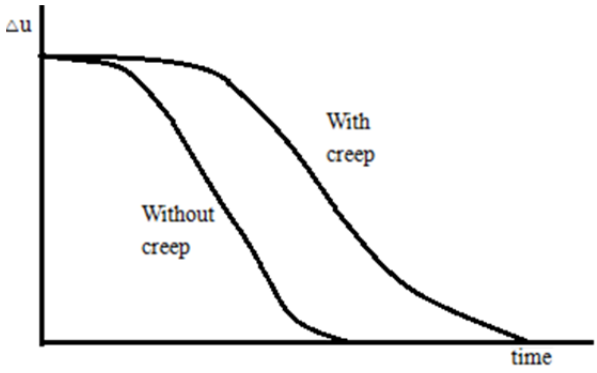

Figure 2.10. A schematic diagram of the excess pore pressure development with and without creep.

The new models investigated in this thesis would therefore correct the estimation of excess pore pressure and the deformation by combining the creep effect.

2.3 Anisotropy

Natural soft clay tends to have a considerable degree of anisotropic fabric, which is developed during the deposition, sedimentation and consolidation sequences. Anisotropy can also be induced in soil when experiencing subsequent strains, re-orientation of particles and changes in particle contacts (Wheeler et al., 2003b).

Anisotropy affects the stress-strain behaviour of soil regarding of both elastic and plastic strains. When talking about normally consolidated or slightly over consolidated soft clay which shows predominant plastic deformation compared with relatively small elastic strains, the plastic anisotropy therefore is of more importance in engineering practice than elastic anisotropy.

Both empirical and numerical investigations show that plastic anisotropy has a great influence on the soil stiffness and strength (Tavenas & Leroueil, 1977; Burland, 1990; Wheeler et al., 2003b). To illustrate this, Figure 2.11 shows the stress-strain curve of Gloucester clay, where different samples at various angles i relative to the vertical direction are tested in undrained triaxial compression condition. The different undrained shear strength can therefore be well explained to be corresponding to the anisotropy of soil.

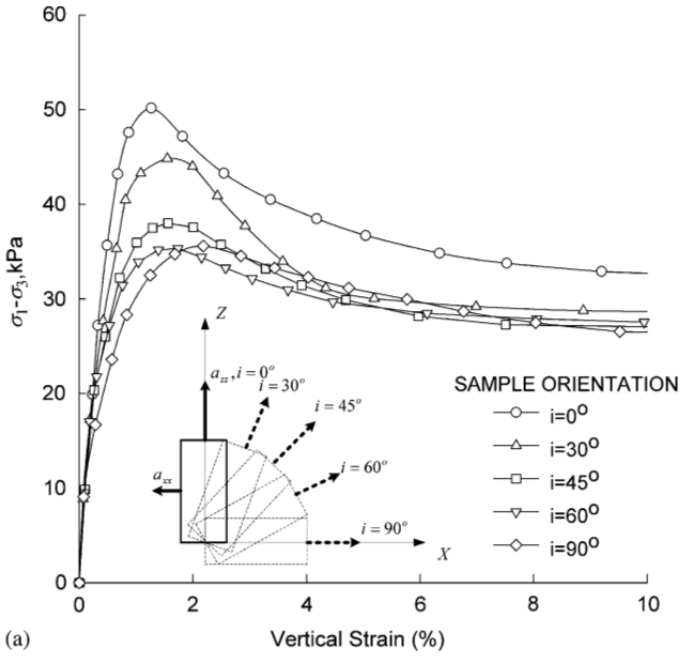

Figure 2.11. The influence of sample orientation on the response of Gloucester clay in undrained triaxial compression tests (Hinchberger, Qu & Lo, 2010).

2.4 Structures and destructuration

Burland (1990) described the "structure" of a natural soil as two components:

- The fabric, which is referred to the spatial arrangement of soil particles and inter-particle contacts.
- The "bonding" between soil particles, which can be progressively destroyed during loading.

The term of "destructuration" was first presented by Leroueil et al. in 1979 to define the post-yield disruption of the structure of clay. In this thesis, the destructuration is solely meant to be the progressive elimination of inter-particle bondings under plastic strains for more clear comparison since the fabric would be considered into anisotropy.

So far, there are firm provenances for the influence of structure on the strength of soft clay by conducting laboratory tests both on natural (undisturbed) sample and reconstituted material under loading and finally compare the different responses. In Figure 2.12, the behaviour of natural and remoulded Rosemere clay under isotropic consolidated drained (CID), triaxial compression tests are compared. Undisturbed clay gained additional strength from the presence of structure which is shown by the hatched area. Moreover, in Figure 2.13, oedometer tests on natural clay show an initial compression curve above that of the remoulded sample. As stresses increased the compression curve of natural clay it is gradually approaching the compression line of the remoulded clay, which is describing the destruction of bonding during plastic strains.

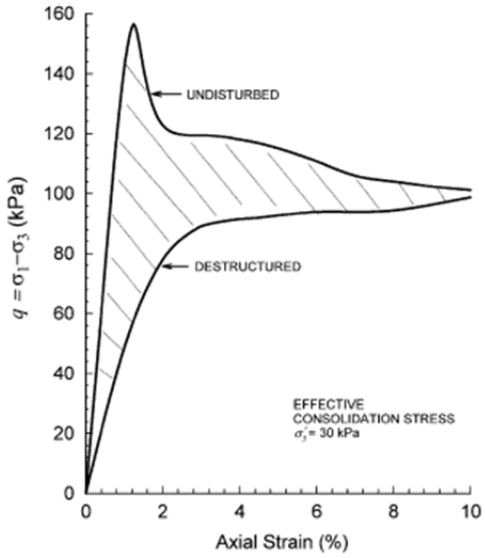

Figure 2.12. Structured and destructured stress-strain response of Rosemere clay during CID triaxial compression test (Lefebvre, 1981).

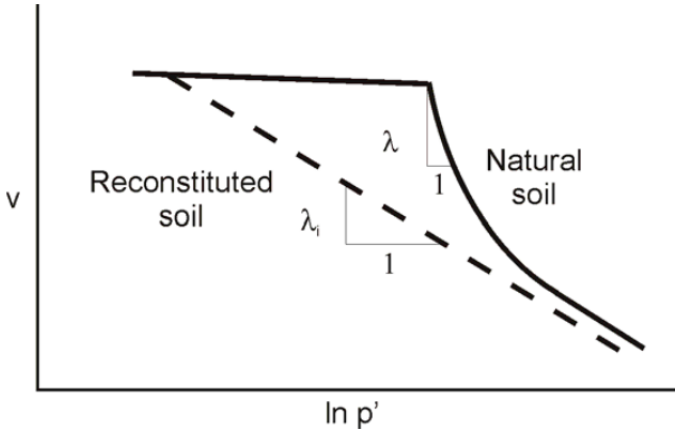

Figure 2.13. The influence of destructuration during oedometer loading (Wheeler et al., 2003a).

3 Different models for simulating soft soil behaviour

To be able to perform more realistic simulations of soft soil behaviour, three different soil models that all incorporate creep effects are studied in this chapter. These models are the Soft Soil Creep model (SSC), the Anisotropic Creep Model (ACM), and the non-associated creep model for Structured Anisotropic Clay (n-SAC), which have been implemented into the FE-code PLAXIS. The main objectives of investigating these three models are focusing on their capabilities to capture the time-dependent soil behaviour as well as the influence of anisotropy and structures of the creep effect.

3.1 Soft Soil Creep model

Described by Brinkgreve, Broere & Waterman (2006), the SSC model is an extension of the original Soft Soil model to take the time dependency of soft soil strains into account. Nowadays, it has become a widely used model in geotechnical engineering when the creep deformation is of great interest.

3.1.1 Basic characteristics of the SSC model

As an advanced soil model, the SSC possesses several characteristics that distinguish it from other models:

- Stress-dependent stiffness (logarithmic compression behaviour);
- Distinction between primary loading and unloading-reloading;
- Time-dependent compression;
- Memory of preconsolidation pressure;
- Soil strength following the Mohr-Coulomb failure criteria;
- Yield surface adapt from the Modified Cam Clay model;
- Associated flow rule for plastic strains.

3.1.2 Formulations of the SSC model

This section will explain the formulations of the SSC model.

3.1.2.1 The 1D creep model

The fundamental one dimensional creep model for the SSC model is constructed based on researches of Buisman (1936), Šuklje (1957), Bjerrum (1967) and Garlanger (1972). According to their ideas, the total strains are consisted of two parts; the elastic and the inelastic (visco-plastic or creep) strains, of which the inelastic part not only occur under constant effective stresses but also being incorporated into the consolidation phase. Moreover, the preconsolidation pressure is closely linked to the creep strain accumulated during the time (Bjerrum, 1967).

Consequently, an expression of total strains is formulated in equation (3.1) and illustrated in Figure 3.1.

$$\varepsilon = A \ln\left(\frac{\sigma'}{\sigma'_0}\right) + B \ln\left(\frac{\sigma'_c}{\sigma'_{c,0}}\right) + C \ln\left(\frac{\tau_c + t'}{\tau_c}\right) \qquad (3.1)$$

where the first part is the elastic strains due to an increase of effective stresses in the total given time period t. The second part considers the creep strains during the consolidation phase, described by the increase of preconsolidation pressure during t_c. The final part stands for a pure creep strain under constant effective stresses, started from the end of the consolidation, t'.

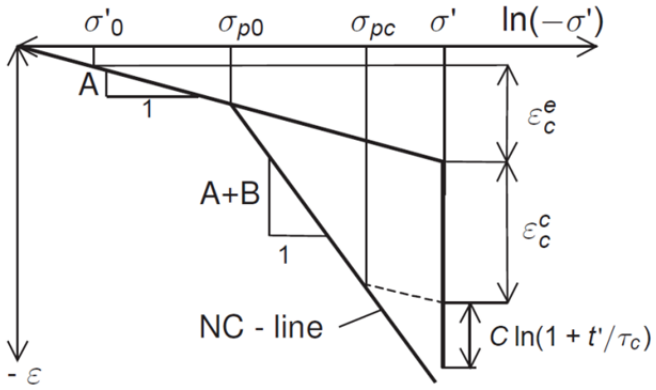

Figure 3.1. Idealized stress-strain curve with different strain increment (Vermeer & Neher, 1999).

The definition of different time parameters can be seen in Figure 3.2.

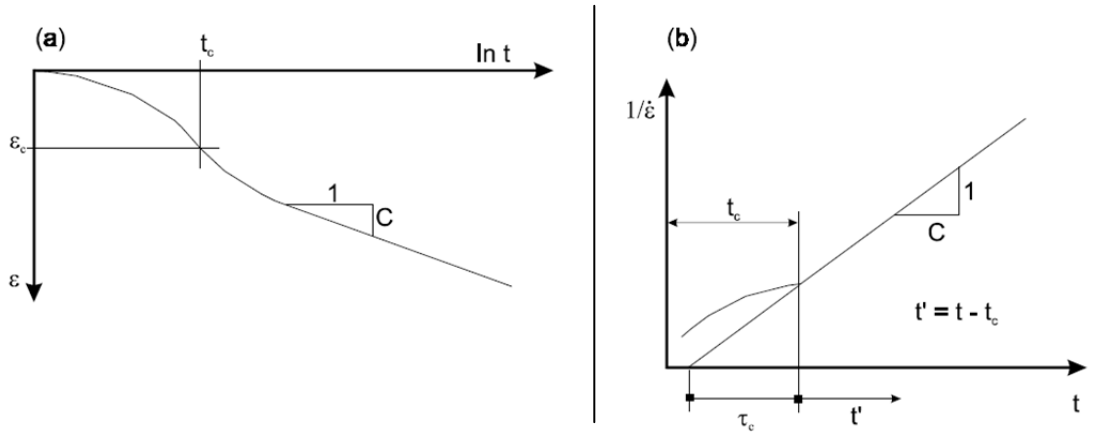

Figure 3.2. Illustration of the definition of C and different time parameters. t_c is the time at the end of consolidation (Vermeer & Neher, 1999).

An alternative expression of the total strain which dropped the time but only used the time-dependent preconsolidation pressure is formulated as equation (3.2).

$$\varepsilon = \varepsilon^e + \varepsilon^c = A \ln\left(\frac{\sigma'}{\sigma'_0}\right) + B \ln\left(\frac{\sigma'_c}{\sigma'_{c,0}}\right) \tag{3.2}$$

where $\sigma'_c = \sigma'_{c,0} \exp\left(\frac{\varepsilon_C}{B}\right)$ (3.3)

It is worth to mention that the SSC model imported the overstress theory which describes the possibility to reach states above the normal consolidation line. Particularly, in the SSC model, if a higher load is added on soil, the preconsolidation pressure would not increase immediately to that value, but will spend one day to reach to the new stress state. Therefore, if applying 1 day as a reference time when the compression curve precisely reached the NC-line, the following differential law, equation (3.4), can be deduced eventually (more details can be seen in Vermeer & Neher, 1999).

$$\dot{\varepsilon} = \dot{\varepsilon^e} + \dot{\varepsilon^c} = A\frac{\dot{\sigma'}}{\sigma'} + \frac{C}{\tau}\left(\frac{\sigma'}{\sigma'_c}\right)^{\frac{B}{C}} \tag{3.4}$$

3.1.2.2 The 3D creep model

The 3D creep model for the SSC model is an extension of the 1D version of it. While instead of using the principal stresses, the well-known stress invariants for isotropic stresses, *p'*, and deviatoric stresses, *q*, are adopted into the 3D model. Shown by Figure 3.3, ellipses from the Modified Cam Clay model in the p'-q plane are applied to represent different stress state, for instance, the current stress surface and the yield stress surface. Their sizes are decided by the equivalent stress p^{eq}, see equation (3.5), and the equivalent preconsolidation stress p_p^{eq}.

$$p^{eq} = p' + \frac{q^2}{M^2(p' - c'\cot(\varphi))} \tag{3.5}$$

where *M* is the slope of the critical state line (CSL).

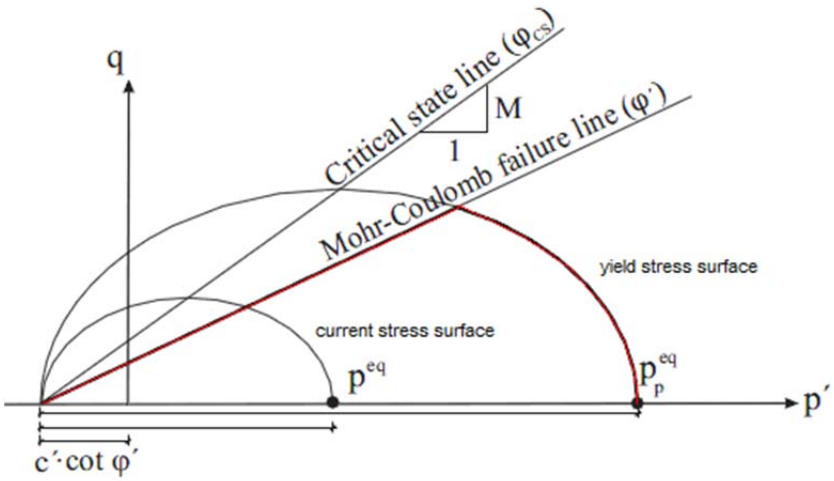

Figure 3.3. Ellipses of the Modified Cam Clay model (Neher, Wehnert & Bonnier, 2001).

The new stress-strain curve with different strain components in three-dimensional condition is shown in Figure 3.4.

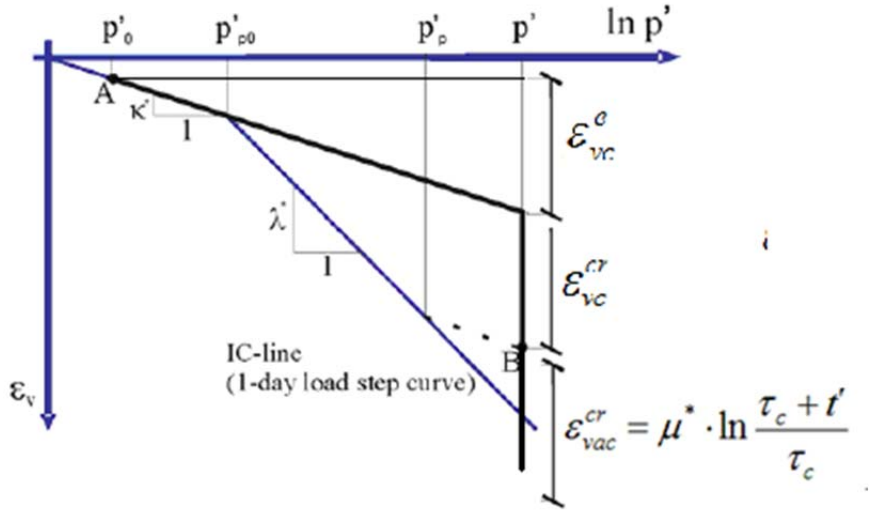

Figure 3.4. Idealized stress-strain curve for the 3D creep model (Wheeler et al., 2003a).

3.1.3 Soil parameters for the SSC model

Several soil parameters are required by the SSC model to fulfil the simulation. They are described in categories as following:

- Mohr-Coulomb failure parameters:
  - Friction angle, φ
  - Cohesion, c

    - Dilatancy angle, ψ
- Stiffness parameters:
    - Modified swelling index, κ^*
    - Modified compression index, λ^*
    - Modified creep index, μ^*
- Parameters defining the cap position and shape:
    - Initial over consolidation ratio, *OCR*
    - Slope of the critical state line, *M*

In order to properly capture the creep behaviour, the parameters have to be evaluated carefully. The *OCR*-value is defining at what creep rate the soil would deform when being exposed to loading, the creep index μ^* is specifying the creep rate after one day while the change of creep strain rate through the time is controlled by the combination of parameter κ^*, λ^*, and μ^*.

Even though the *OCR*-value has defined the location of cap, the slope of the critical state line is determining how steep the cap surface would be, which is in turn influencing the deviatoric plastic strains. In fact, *M* is a K_0^{NC}-related value which is calculated by equation (3.6) below.

$$M = 3\sqrt{\frac{\left(1-K_0^{NC}\right)^2}{\left(1+2K_0^{NC}\right)^2} + \frac{\left(1-K_0^{NC}\right)(1-2\nu_{ur})(\lambda^*/\kappa^*-1)}{\left(1+2K_0^{NC}\right)(1-2\nu_{ur})\lambda^*/\kappa^*-\left(1-K_0^{NC}\right)(1+\nu_{ur})}} \qquad (3.6)$$

In general, the parameters κ^* and λ^* are defined by the Modified Cam Clay model from the normal consolidation line (NCL) and the unloading-reloading line (URL) in a $\ln(p')$-v compression plane as shown in Figure 3.5. The creep parameter μ^* has the same definition as parameter *C* which was illustrated above in the 1D model, Figure 3.2. The evaluation methods for these parameters are to be discussed further in the next laboratory test chapter, see Chapter 4.1.

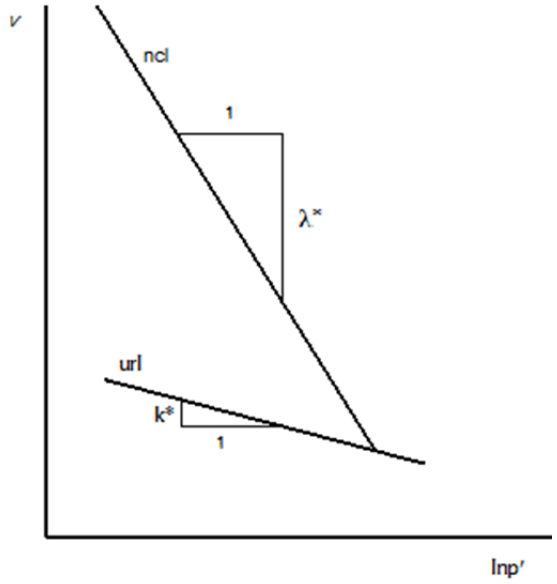

Figure 3.5. Diagram explaining the definition of κ and λ* (modified after Wood, 1990).*

3.2 Anisotropic Creep Model

As described in the fundamental studies of soft soil, Chapter 2, fabric anisotropy is commonly observed in natural clay. To incorporate the anisotropy into the time-dependent behaviour, a new anisotropic creep model was proposed by Leoni, Karstunen and Vermeer in 2008, to capture both the inherent and induced anisotropy in normally consolidated and lightly consolidated soft soils.

3.2.1 Basic characteristics of the ACM model

In a general view, besides from the capability of capturing the creep behaviour, the ACM model presents some more characteristics:

- For simplicity, it deals with the special case of cross-anisotropic soil samples that have been cut vertically from the ground;
- It focuses on plastic anisotropy (i.e. ignored elastic anisotropy);
- A rotated yield surface is adopted from the SCLAY-1 model;
- The application of extended overstress theory, assuming viscoplastic strains inside the yield surface;
- A rotational hardening law, capable to model induced anisotropy, is assumed;
- New soil parameters are introduced, which can be derived from conventional lab tests with no need for calibration.

3.2.2 Formulations of the ACM model

The new ACM model adopts the idea of the S-CLAY1 model and introduces a scalar quantity α to describe the orientation of yield surface based on the simple assumption of cross-anisotropy, see Figure 3.6 (Leoni, Karstunen & Vermeer, 2008). Also using the basic concept of the SSC model, there is an equivalent mean stress, p'_{eq}, determining the size of yield surface as shown in equation (3.7) below.

$$p'_{eq} = p' + \frac{(q-\alpha p')^2}{(M^2-\alpha^2)p'} \tag{3.7}$$

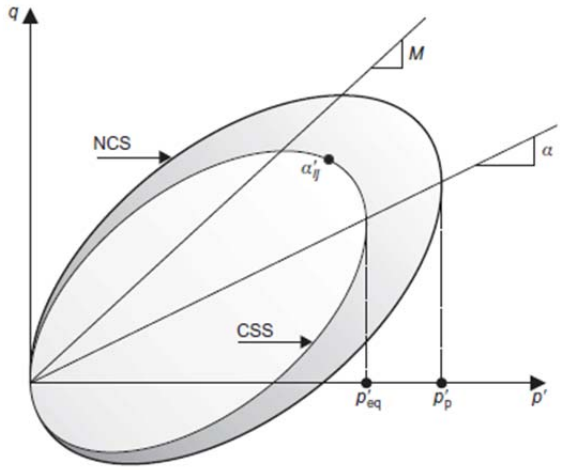

Figure 3.6. Anisotropic creep model: current state surface (CSS) and normal consolidation surface (NCC) in p'-q stress space (Leoni, Karstunen & Vermeer, 2008).

The scalar quantity α is a rotation hardening parameter and its evolution is determined by a combination of the volumetric creep strain and the deviatoric creep strain according to the rotational hardening law, see equation (3.8).

$$\dot{\alpha} = \omega \left[\left(\frac{3q}{4p'} - \alpha \right) \dot{\varepsilon}_v + \omega_d \left(\frac{q}{3p'} - \alpha \right) \dot{\gamma}^c \right] \tag{3.8}$$

where ω = rate of rotation parameter

ω_d = rate of shear rotation parameter

$\dot{\gamma}^c$ = deviatoric creep strain rate, defined according to equation (3.9) below:

$$\dot{\gamma}^c = \frac{2}{3} |\dot{\varepsilon}_1 - \dot{\varepsilon}_2| \tag{3.9}$$

Moreover, the size of yield surface, defined by the preconsolidation pressure, σ'_c, expands with the volumetric creep strains ε^c_v according to the hardening law, equation (3.10).

$$\sigma'_c = \sigma'_{c,0} \exp\left(-\frac{\varepsilon^c_v}{\lambda^* - \kappa^*}\right) \tag{3.10}$$

3.2.3 Soil parameters for the ACM model

Except from parameters like κ^*, λ^* and μ^* which have the same definition as in the SSC model, the ACM model requires another three parameters to describe the anisotropy and its evolution, including:

- Initial inclination of the ellipse, α_0
- The shear rotation parameter, ω_d
- The rate of rotation, ω

Although they are extra proposed parameters, there are evidences that they can be linked with other known soil parameters.

Based on a large amount of one-dimensional consolidation data, it is observed that there is a close correlation between the initial inclination α_0 and the K_0^{NC}. Their relation is expressed by equation (3.11) below.

$$\alpha_0 = \frac{\eta_0^2 + 3\eta_0 - M^2}{3} \tag{3.11}$$

where $\eta_0 = \frac{3(1-K_0^{NC})}{(1+2K_0^{NC})}$ (3.12)

$$M = \frac{6\sin\varphi'_{cv}}{3-\sin\varphi'_{cv}} = \frac{6(1-K_0^{NC})}{2+K_0^{NC}} \tag{3.13}$$

According to Jaky's formula, see equation (3.14), K_0^{NC} is defined as:

$$K_0^{NC} \approx 1 - \sin\varphi'_{cv} \tag{3.14}$$

Moreover, the shear rotation parameter ω_d is also found to correlate with the K_0^{NC}-value (Wheeler et al., 2003b), according to equation (3.15).

$$\omega_d = \frac{3}{8}\frac{4M^2 - 4\eta_0^2 - 3\eta_0}{\eta_0^2 - M^2 + 2\eta_0} \tag{3.15}$$

Another new material parameter, ω, is simply defined as a function of the compression index, λ^*. The reason behind this is derived from experimental evidence which shows that the initial anisotropy could be erased in isotropic stresses which are increasing to two or three times larger than the preconsolidation pressure (Anandarajah, Kuganenthira & Zhao, 1996). Consequently, it is obtained from laboratory testing that ω can be defined as equation (3.16).

$$\omega = \frac{1}{\lambda^*} \ln \frac{10M^2 - 2\alpha_0 \omega_d}{M^2 - 2\alpha_0 \omega_d} \tag{3.16}$$

Hence, all the new parameters can be obtained from available data and there would be no need for calibration.

Instead of using an increased *M*-value (compared with the Mohr-Coulomb failure slope) in the SSC model according to the Modified Cam Clay ellipse, the ACM model allows the *M*-value to correspond to the failure state, which ensures a realistic estimation of K_0^{NC} based on Jaky's formula. This improvement of the ACM model would show advantages to predict the horizontal displacements which are discussed in later chapters.

3.3 Non-associated creep model for Structured Anisotropic Clay (n-SAC)

Laboratory experiments performed on reconstituted clays found a base for different elasto-plastic models, for instance the Modified Cam Clay model. These models tend to adapt an associated flow rule which is then assumed to be true also for models that deal with natural clay. Laboratory experiments on natural soil however, show that this assumption is inadequate. In regard to this fact, a new model called non-associated creep model for structured anisotropic clay, abbreviated n-SAC, were proposed by Grimstad and Degago (2010).

3.3.1 Basic characteristics of the n-SAC model

In the beginning, it is necessary to describe the important features of the n-SAC model, differentiated from the previous SSC and ACM models.

- It applies the time-resistance concept to simulate the creep behaviour;
- Non-associated flow rule used, i.e. distinction between the yield surface and the plastic potential surface;
- Separate rotational hardening law for the two surfaces;
- A destructuration rule is adopted;
- Be able to model the "softening" response of soil in undrained shearing.

3.3.2 Formulations of the n-SAC model

Initially, rather than using the theory of volumetric viscoplastic strains, Grimstad et al. (2008) attempted to apply the time resistance to describe the rate of plastic multiplier, described in equation (3.17).

$$\frac{d\lambda}{dt} = \dot{\lambda} = \frac{1}{r_{si}\tau}\left(\frac{p^{eq}}{(1+x)p'_{mi}}\right)^{r_{si}\zeta_i} m_{K_0^{NC}} \tag{3.17}$$

where ζ_i = intrinsic viscoplastic compressibility coefficient

r_{si} = intrinsic time resistance number

p^{eq} = equivalent effective stress

$p_{mi}^{'}$ = intrinsic reference stress

τ = reference time

x = amount of instable structure, and

$$m_{K_0^{NC}} = \frac{M_{fC}^2 - \alpha_{K_0^{NC}}^2}{M_{fC}^2 - \eta_{K_0^{NC}}^2} \tag{3.18}$$

where α_{K0}^{NC} = rotation of the potential surface in K_0^{NC}-loading (virgin oedometer loading)

η_{K0}^{NC} = mobilization in K_0^{NC}-loading

M_{fC} = critical state line in compression loading

Moreover, the n-SAC model adopts the idea of an elasto-plastic model, the SCLAY1-S (Koskinen, Karstunen & Wheeler, 2002), to have two yield surfaces; the "intrinsic yield surface" and the real "natural yield surface" which are related by the expression equation (3.19). See Figure 3.7 for an illustration of the yield surfaces.

$$p'_m = (1 + x)p'_{mi} \tag{3.19}$$

where x stands for the amount of structure possessed by natural clay.

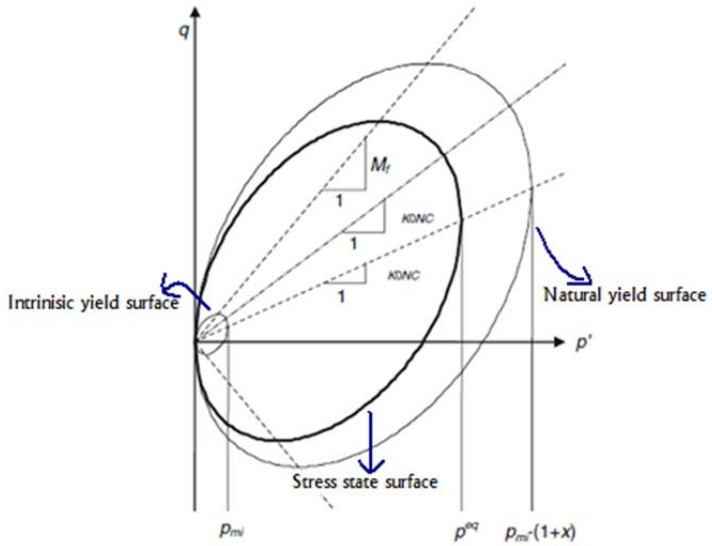

Figure 3.7. SCLAY1-S surfaces in triaxial stress space (Koskinen, Karstunen & Wheeler, 2002).

The "intrinsic yield surface" fulfils a hardening law which is solely dependent on the volumetric strain, see equation (3.20).

$$dp'_{mi} = \frac{p'_{mi}}{\zeta_i} d\varepsilon_v^p \tag{3.20}$$

where ζ_i = hardening parameter

The structure parameter x is following a destructuration law to be gradually decreased, which means that the natural yield surface would have the same size as the intrinsic yield surface when all the bondings are lost. The destructuration rate is controlled both by volumetric and deviatoric strains.

As non-associated flow is applied in this model, there are two different equations, equation (3.21) and (3.22), to define the reference surface (stress state surface) and the potential surface.

The reference surface is given by:

$$p^{eq} = p' + \frac{\frac{3}{2}\{\sigma_d - p'\beta_d\}^T\{\sigma_d - p'\beta_d\}}{\left(M^2 - \frac{3}{2}\beta_d^T\beta_d\right)p'} \tag{3.21}$$

where p' = mean effective stress

σ_d = deviatoric stress vector

β_d = deviatoric rotational vector

M = load angle dependent peak of the reference surface in p'-q space

The potential surface is expressed as:

$$Q = p' + \frac{\frac{3}{2}\{\sigma_d - p'\alpha_d\}^T\{\sigma_d - p'\alpha_d\}}{\left(M_f^2 - \frac{3}{2}\alpha_d^T\alpha_d\right)p'} - p_Q^{eq} = 0 \tag{3.22}$$

where M_f = load angle dependent critical state line in p'-q space

α_d = deviatoric rotational vector

Consequently, there are two rotational hardening laws for these two surfaces also, see equations (3.23) for the potential surface and (3.24) for the reference surface.

$$\frac{d\alpha_d}{d\lambda} = \frac{2}{\zeta_i(1+x)}\left(\frac{\alpha_{K_0^{nc}}}{\eta_{K_0^{nc}}}\frac{\sigma_d}{p'} - \alpha_d\right)\left\langle\frac{\partial Q}{\partial p'}\right\rangle \tag{3.23}$$

$$\frac{d\beta_d}{d\lambda} = \frac{2}{\zeta_i(1+x)}\left[\begin{array}{l}\left(\left(\frac{2}{9}M_C + \frac{1}{3}\right)\frac{\sigma_d}{p'} - \beta_d\right)\left\langle\frac{\partial p^{eq}}{\partial p'}\right\rangle + \\ \left(\frac{M_C}{3}\frac{\sigma_d}{p'} - \beta_d\right)\sqrt{\frac{2}{3}\left\{\frac{\partial p^{eq}}{\partial \sigma_d}\right\}^T\frac{\partial p^{eq}}{\partial \sigma_d}}\end{array}\right] \tag{3.24}$$

where ζ_i, M_C, α_{K0}^{NC} and β_{K0}^{NC} are internal model parameters (more details, see Grimstad & Degago, 2010).

3.3.3 Soil parameters for the n-SAC model

In general, there are some different soil parameters required by the n-SAC model.

- The creep parameters, r_{si} and $r_{s\,min}$, which are the intrinsic time resistance number and the minimum measured time resistance number respectively, see Figure 3.8.

In order to describe the influence of destructurations on the time-dependent strains, these two parameters are also in combination to determine the initial structure of the soil, see equation (3.25).

$$x_0 = \frac{r_{si} - r_{s\,min}}{r_{s\,min}} \tag{3.25}$$

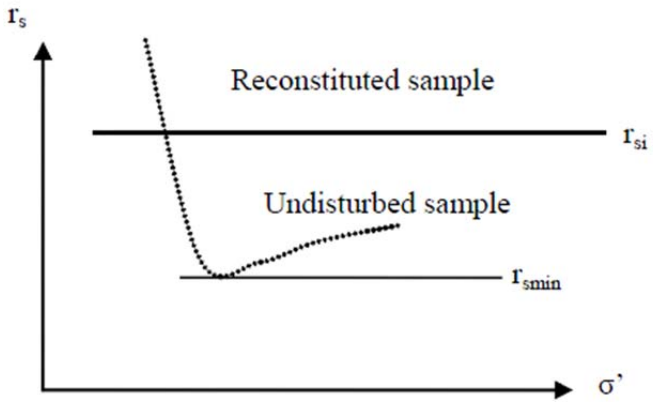

Figure 3.8. Concept of destructuration contra effect on time resistance number (Grimstad & Degago, 2010).

- Two stiffness parameters, E_{oed}^{ref} and E_{ref}, are needed to define the hardening parameter ζ_i via equation (3.26).

$$\zeta_i = p_{ref}\left(\frac{1}{\{E_{oed}^{ref}\}_i} - \frac{3(1-2\nu)}{E_{ref}}\right) = \lambda_i^* - \kappa^* \qquad (3.26)$$

where p_{ref} is the reference pressure commonly set to 100 kPa, and the λ^*_i which is the slope of normal compression line for a reconstituted soil sample, see Figure 3.9.

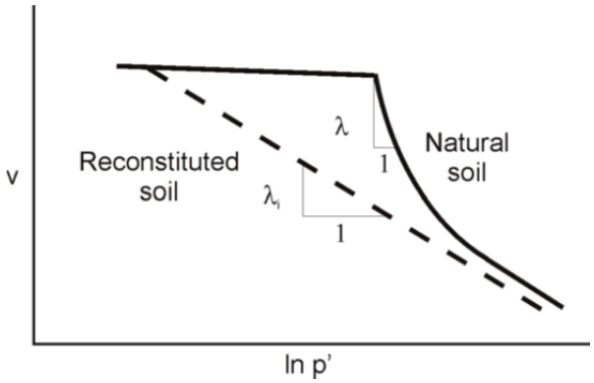

Figure 3.9. Definition of the soil parameter λ_i (Wheeler et al., 2003a).

4 Laboratory tests and soil parameter evaluations

When carrying out the simulations of real soil response under engineering constructions by models, it is of critical meaning to obtain representative soil parameters which can reflect the soil strength and stiffness correctly. In this chapter, the most commonly applied soil tests in laboratory are firstly described, including the different instruments and their testing methods. Then the evaluation of the important soil parameters required by models is discussed.

4.1 Description of laboratory tests

In this section, the oedometer test, which includes the incremental loading test and the continuously loading test, and the triaxial test will be described.

4.1.1 Oedometer test

When attempting to investigate the compressibility of soils, the oedometer test is the most common choice. The tests can be performed as either incrementally loaded tests or as continuously loaded tests (Larsson, 1986). In an oedometer test the sample is enclosed by a ring that is connected to a bottom plate. In order to reduce the friction inside the ring, it is applied with a silicon paste or the ring itself could be made of Teflon. The standard inner diameter and the height of the sample are 50 mm and 20 mm respectively (Hansbo, 1975).

There are porous filter stones located both on the top and bottom, which allow the sample to be two sided drained. The top one is connected to a stamp where the load is added vertically, see Figure 4.1. It is also possible to prevent drainage from the bottom filter stone which results in a one sided-drainage test (Sällfors, 2001). The excess pore water pressure can then be monitored by implementing a pressure transducer at the bottom. In practice, 2/3 of the bottom measured pore pressures are taken as the average pore pressure to calculate the effective stress for the sample (assuming that the water pressure has a parabolic distribution).

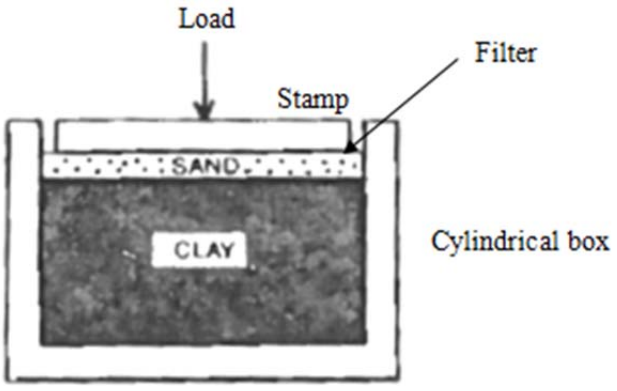

Figure 4.1. Oedometer constructed by the Geotechnical Commission of Swedish National Traffic Administration (Sällfors, 1975).

The two kinds of oedometer test (the incremental loading test and the constant rate of strain test) with different features are described below.

4.1.1.1 Incremental Loading (IL) test

The incremental loading oedometer test is used worldwide to determine the compression index, especially the creep properties. A standard IL test procedure is consisted of several incremental loading steps, for instance, 10, 20, 40, 80, 160, 320, 640 kPa. Each increment is equivalent to the previous consolidation load (i.e. a load increment ratio LIR = 1). Each step is allowed to sustain for 24 hours until the next load is applied (Sällfors, 1975). Figure 4.2 illustrates the incremental loading oedometer apparatus used at Chalmers.

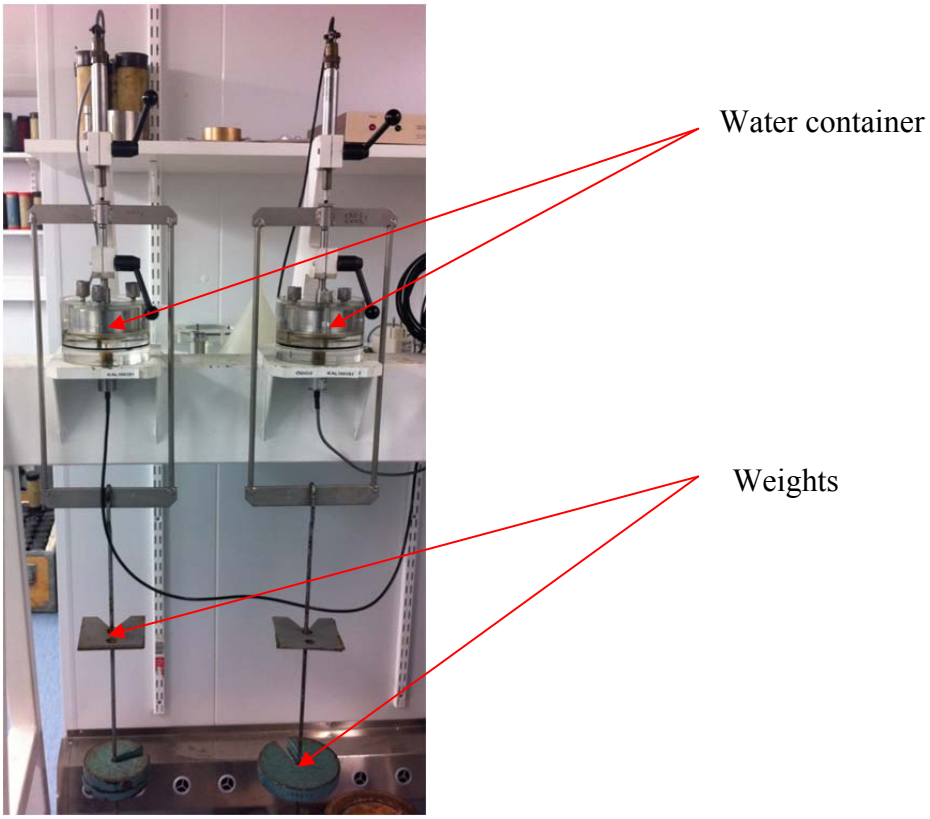

Figure 4.2. IL oedometer test apparatus used at Chalmers. The test sample is located in the water container. The load is applied with the help of weights. The figure illustrates two separate apparatus (Photo: Pär Gustafsson, 2011).

The main results from an IL test are given by the compression within each single step which is plotted against the measurable intervals (defined by users) shown in Figure 4.3. The compression that is received after 24 hours is plotted as a function of the logarithm for an applied effective vertical stress which is shown in Figure 4.4.

With the help of the stress-strain curve, the compression modulus and preconsolidation pressure can be evaluated (Sällfors, 2001). Also, it is able to determine the secondary compression index parameter from the compression curve in each step.

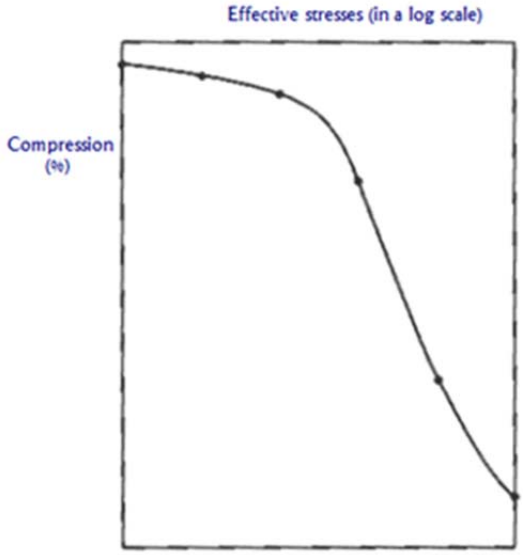

Figure 4.3. Results from a standard IL test illustrated as a stress-strain curve (Sällfors, 1975).

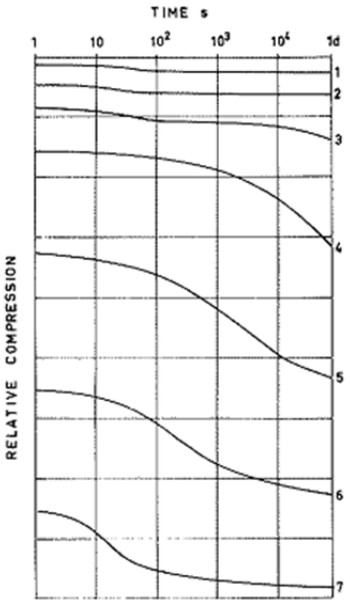

Figure 4.4. Results from a standard IL test illustrated as a time-compression curve for each step (Larsson, 1986).

A main disadvantage with the IL test is that the stress-strain curve obtained is discontinuous, with only a few points obtained and defined on the curve. The accuracy of the results very much depends on the skill of the drawer of the curve. This results in variation of the preconsolidation pressure. Moreover, the 24-hour compression line is discussed as an overestimation of the creep parameters.

To avoid these deficiencies, a reduced load increment ratio (LIR) can be applied to obtain more points in the curve (however, the continuous loading CRS test discussed

later in this chapter is a better choice in this way). And, to evaluate the creep properties appropriately, a longer duration in each step is required to reach the realistic linear relationship between the time and strains.

4.1.1.2 Constant Rate of Strain test (CRS)

For the last thirty years in Sweden, the CRS test is conducted extensively to determine the preconsolidation pressure, compression modulus as well as the coefficient of permeability. In CRS test, the sample is deformed with a constant speed (the standard test speed in Sweden is 0.0024 mm/min, i.e. 0.72%/h). The applied load, deformation and the pore water pressure are continuously measured during the test. The test instrument is shown in Figure 4.5.

Figure 4.5. CRS test apparatus used at Chalmers. The test sample is located in the water container. The load is applied by pushing the canister up. The test sample is then exposed to load from the rod (Photo: Pär Gustafsson, 2011).

Typically, the results from CRS-tests are plotted as several curves; the stress-strain curve, Figure 4.6a, the stress-modulus curve, Figure 4.6b, and the permeability-strain curve, Figure 4.6c (Larsson, 1981).

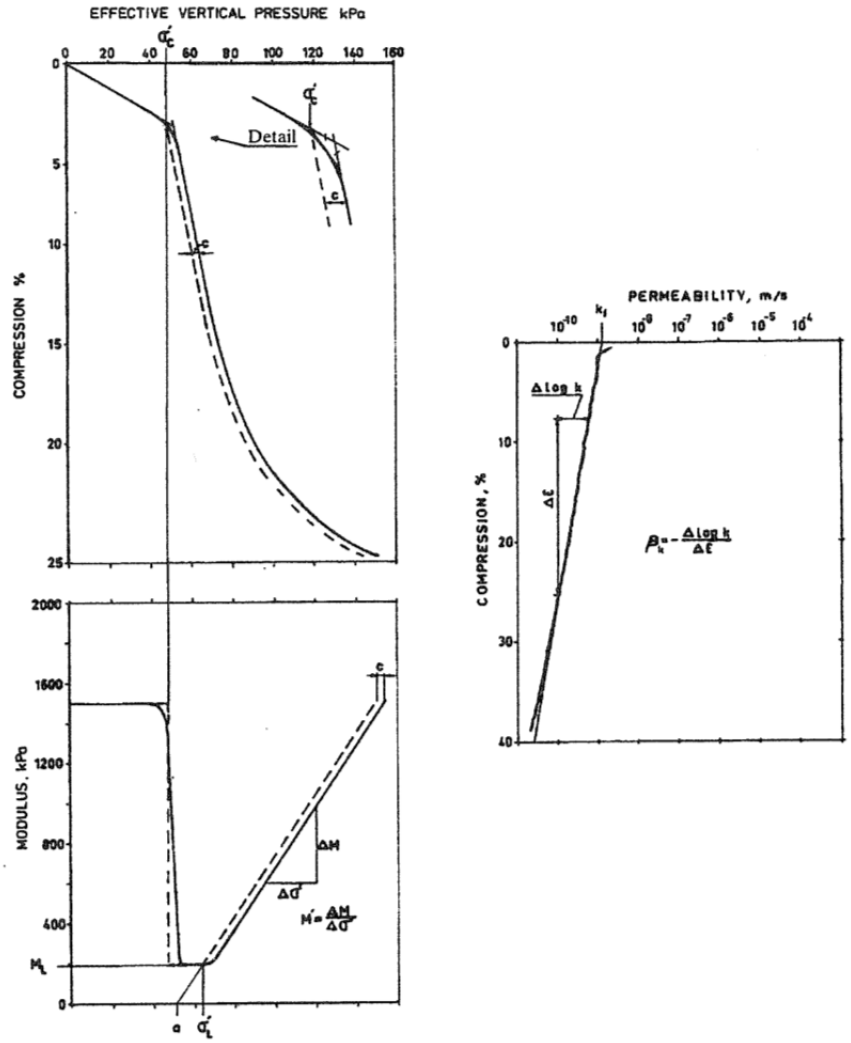

Figure 4.6. Results from CRS test and evaluated compression parameters (Larsson 1986).

a) *Plotted vertical effective stresses with compression both in linear scale.*

b) *Plotted variations of compression modulus against the effective stress.*

c) *Plotted variations of permeability against the strains.*

Considering the strain-rate effect, the preconsolidation pressure is evaluated according to Sällfors's method to be able to represent the realistic soil behaviour at full-scale loading in the field. The evaluation method and the reason behind it are described in the next soil parameter evaluation part, see Chapter 4.2.

To compensate the shortage of information about soft soil creep behaviour in the CRS test, tests with different strain rates can also be performed. In Figure 4.7, a stress-strain curve obtained from CRS test with changing strain rate conducted by Claesson (2003), it is shown that the stress-strain curve exhibits distinct alteration when the strain rate was altered. Moreover, it can also be detected that the plotted curves consistently follow a certain pattern for the respective strain rates. The reason behind this is explored in the process of parameter evaluations later, see Chapter 4.2.

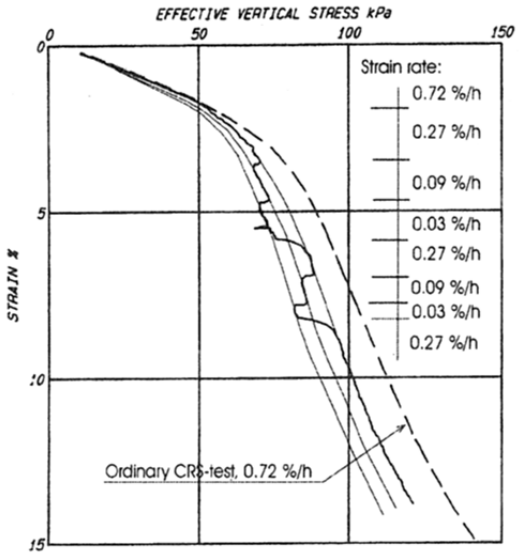

Figure 4.7. Stress-strain curve from CRS test with different strain rates (Claesson, 2003).

4.1.2 Triaxial test

A reliable soil testing always starts with the soil sample being in a condition approximating as closely as possible to its in-situ condition in the ground. Therefore, the triaxial testing apparatus that allows performing some lateral stresses on the sample gain more advantages compared with the confined oedometer test, see Figure 4.8 and Figure 4.9.

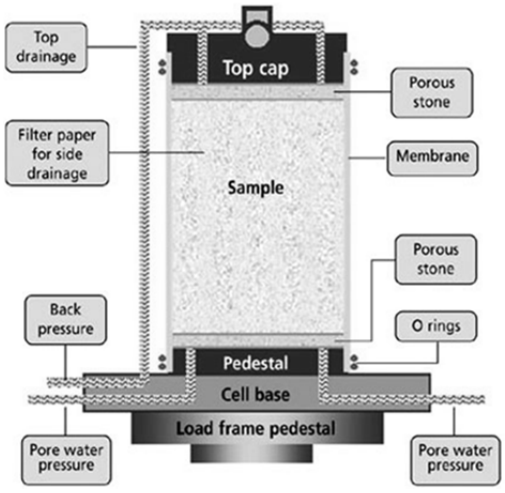

Figure 4.8. A sketched triaxial apparatus (Controls, 2011).

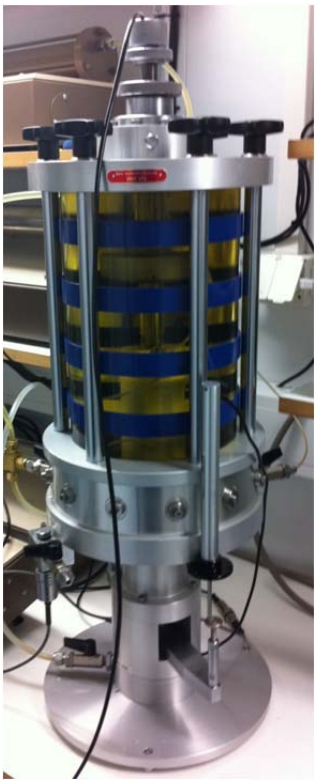

Figure 4.9. Triaxial test apparatus used at Chalmers. The soil sample is enclosed by a membrane and surrounded by paraffin oil (the yellow liquid). Load is applied from the top by a rod (Photo: Pär Gustafsson, 2011).

In the testing cell, a cylindrical soil sample with the dimension of 50 mm diameter and 100 mm height is first enclosed in a thin rubber membrane which isolates the sample from the surrounding cell fluid, i.e. typically water or paraffin oil. The filling cell fluid would then be pressurized, usually to a constant cell pressure. The sample sits in the cell between a rigid base and a rigid top cap which can be loaded by means of a ram passing out of the cell. Commonly, the rod would be pushed down at a constant rate (triaxial compression test). In the drained tests, part or all of the rigid base and/or the top cap is porous to allow the drainage of pore water. Alternatively, if undrained condition is required, the excess pore pressure is measured. Usually, the tests are carried out in two stages; an isotropic cell pressure around the sample is performed firstly to compress the soil sample, and in the second stage a vertical force by the ram is added to shear the sample until failure being observed.

Another type of triaxial test is the conventional triaxial extension test. If the steel rod at the top is pulled upward, then it is possible that the vertical force and the deviator stresses become negative, while the cell pressure keeps constant.

In general, triaxial test measurements are including:

- The cell pressure σ_r, which provides an all-round pressure on the sample;
- The vertical force F loading by the ram;
- The change in length of the sample, δl, which corresponds to the axial strain;
- For drained cases, the change in volume, δv, measured as the amount of pore

water flowing in or out of the sample;
- For undrained tests, the excess pore water pressure u.

These measurements are helpful to deduce the shear strength parameters, including the friction angle, cohesion, dilatancy angle and other parameters. The stress path in p'-q plane and the stress-strain curve can also be plotted.

4.2 Evaluation of soil parameters for the models

This section will describe the evaluation of different soil parameters required by different material models.

4.2.1 Preconsolidation pressure

A correct determination of the preconsolidation pressure is of great importance for soft clay when settlement analysis is interested. How to evaluate the p_c-value properly from the stress-strain curve obtained from oedometer test becomes of focus therefore.

Based on the standard IL test developed by Terzaghi in 1925 (with a load increment ratio equals to 1 and a time duration of each load for 24 hours), several evaluation procedures for preconsolidation pressure was developed, in which the Casagrande construction is the most widely used approach, see Figure 4.10.

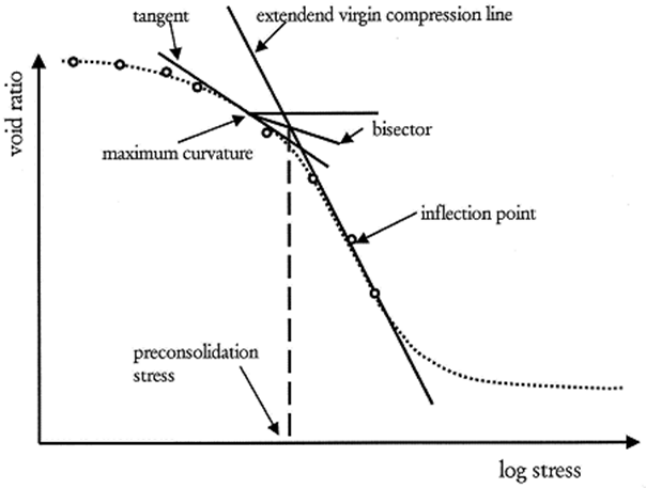

Figure 4.10. Illustration of the Casagrande method for determination of the preconsolidation pressure (Casagrande, 1936).

However, such kind of method does not take the time-dependency into account. Observations show that when the duration of each load is longer, more compression of the soil sample is reached and a lowered stress-strain curve is plotted. Thus a decreased p_c-value is estimated by the standard procedures. Varied load increments are also observed influencing the evaluation of p_c. Bjerrum (1973) described a modified IL test procedure in which the sample is compressed up to the in-situ effective stress in three steps (the increment being $\sigma_0'/3$) and followed by three steps

up to the standard evaluated preconsolidation pressure (the increment being $((\sigma_c'^{est} - \sigma_0')/3)$, the duration of those steps are controlled by the end of pore pressure dissipation. After $\sigma_c'^{est}$ has been exceeded, the loading is adapted to the standard IL test procedure. This modified procedure is to obtain a well-defined compression curve, while a high value of the preconsolidation pressure is assessed since this test occurs rapidly. Hence, it is clear that the evaluation way of the p_c-value is sensitive. One should be always bear in mind that the preconsolidation pressure from IL test is related to the specific test procedure.

By comparison, in a CRS test, the evaluation of the p_c-value is highly strain-rate dependent. In order to modify a standard strain rate (0.0024 mm/min) performed in the laboratory tests compared with the relatively low strain rate in the field for natural clay (the different strain rates, see Figure 4.11a), Sällfors (1975) proposed the following method to obtain a representative in-situ preconsolidation pressure, see Figure 4.11b.

- The pressure-compression curve is firstly plotted on arithmetic scales; normally the two axes are fixed in a ratio of 10 kPa pressure/1% compression;
- The two linear parts are extended to intersect each other at B;
- An isosceles triangle is inscribed.

In the end, the point B' is determined as the preconsolidation value p_c.

This method is proved to be reliable for good agreements with the preconsolidation pressure measured in field tests and has been widely applied in engineering practice.

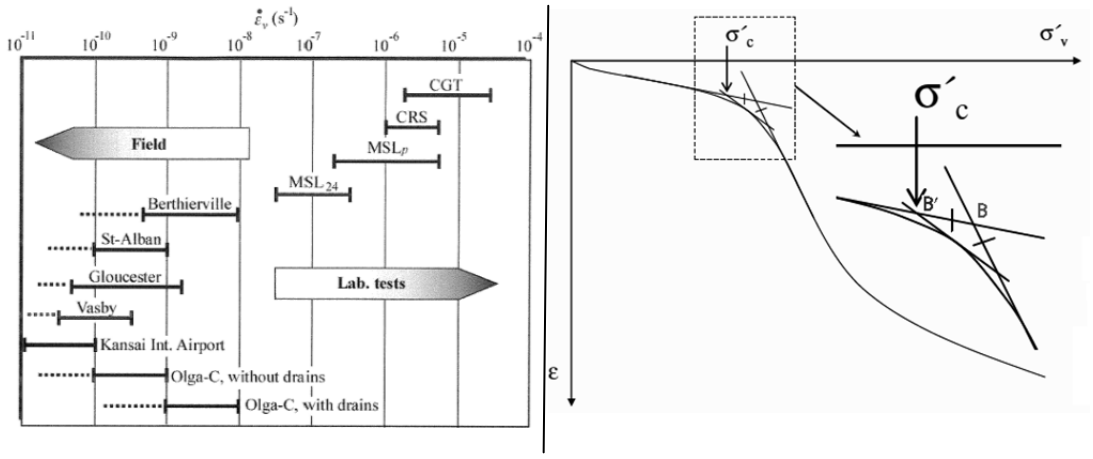

Figure 4.11. a) Ranges of strain rates in lab tests and in-situ conditions (Leroueil, 2006). b) Method for evaluation of the preconsolidation pressure (Sällfors, 1975).

As mentioned in Chapter 2, it is observed that there is a linear relationship between the preconsolidation pressure and the strain rate when both are plotted in logarithmic scales. This means that each strain rate is corresponding to a unique preconsolidation pressure, thus a specific compression curve. When the strain rate is being changed, the soil would adapt to the respective compression curve promptly. Particularly, the soil

sample can have a preconsolidation pressure smaller than its in-situ effective stresses when the test is performed with extremely slow strain rate. As a result, the preconsolidation pressure itself is never a static value but a result of time effect. Any estimation of it should be related to a specific time period.

When applying advanced numerical models incorporating the creep effects already, the advantage is that there is no need to adjust the preconsolidation pressure manually as suggested by Sällfors. The input parameter of p_c, thus the *OCR*-value becomes a reference value corresponding to a certain loading period experienced by the soil. Meanwhile the laboratory tests under specific testing condition turns out to be a useful tool to verify the correction of input parameters and the model performance.

4.2.2 Soil stiffness parameters

In a settlement analysis, the distinct soil stiffness parameters for elastic and plastic deformations have to be known. They are usually derived from the normally consolidated line and an unloading-reloading line from an oedometer test. There are different names and definitions for those parameters, but in general they are all attempting to describe the same soil behaviour.

A pair of parameters commonly used worldwide for the description of the consolidation of soft clay, are the compression index, C_c, and the swelling index, C_s, for effective stress smaller and greater the preconsolidation pressure condition respectively. Their definitions are, according to equations (4.1) and (4.2):

$$C_s = \frac{\Delta e}{\Delta \log \sigma'} \text{ for } \sigma' < p_c \tag{4.1}$$

$$C_c = \frac{\Delta e}{\Delta \log \sigma'} \text{ for } \sigma' > p_c \tag{4.2}$$

where e = void ratio

In Sweden, however, the compression modulus concept $M = \frac{d\sigma'_v}{d\varepsilon}$, is more common practice to use. There are two constant compression modulus, M_0 and $M_{L;}$ one for the over consolidation stress range and one for the normal consolidation stress range. If the effective stress is greater than a certain stress, the modulus is defined to increase linearly with the effective stress, see Figure 4.12.

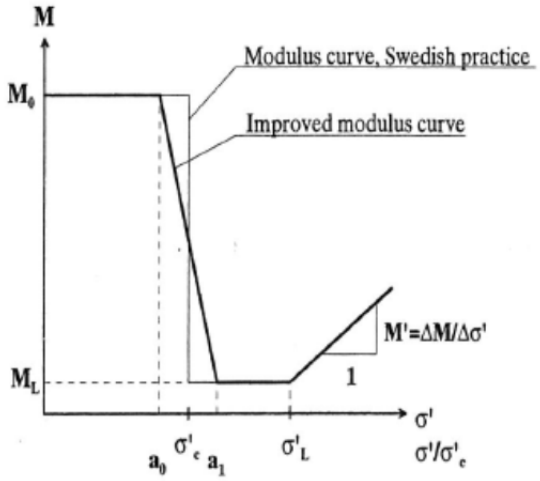

Figure 4.12. An illustration of variation in the compression modulus in Sweden (Claesson, 2003).

For the Modified Cam Clay model, the modified compression index, λ^*, and modified swelling index, κ^*, are used which are defined by the mean effective stress and the volumetric strain as in equations (4.3) and (4.4).

$$\kappa^* = \frac{\Delta \ln p'}{\Delta \varepsilon_v} \text{ for } p' < p'_{pc} \tag{4.3}$$

$$\lambda^* = \frac{\Delta \ln p'}{\Delta \varepsilon_v} \text{ for } p' > p'_{pc} \tag{4.4}$$

In general, the calculations from one parameter to another parameter that are both describing the same soil behaviour are quite straightforward, if with clear understanding of the parameter definition, see illustrations in Figure 4.13.

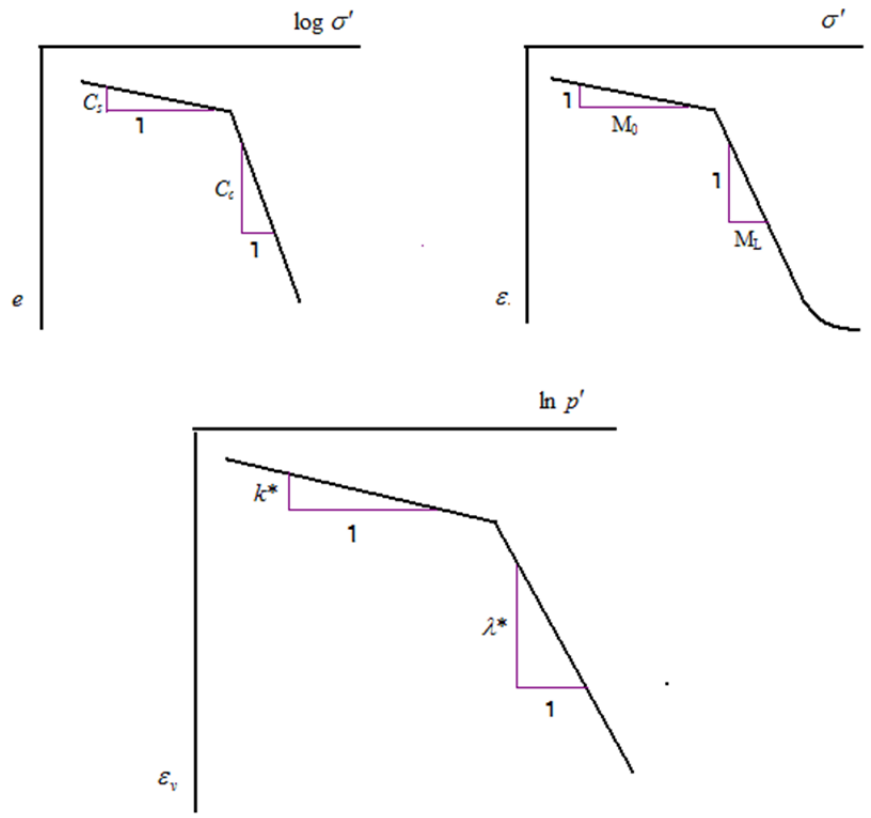

Figure 4.13. Diagram illustrating the definitions of the various stiffness parameters, where σ' is the vertical effective stress, and p' the mean effective stress.

However, a special case is that according to the Modified Cam Clay model. The determination of λ^* and κ^* is made from isotropic consolidation curves. This results in a need to appropriately transfer the compression index from a one-dimensionally loaded oedometer test to these three-dimensional parameters. With the help of K_0-values, it is possible to have the relationship between the mean effective stress and the vertical effective stress, see equations (4.5) and (4.6).

$$p' = \frac{(1+2K_0)\sigma'}{3} \tag{4.5}$$

$$p'_0 = \frac{(1+2K_0)\sigma'_0}{3} \tag{4.6}$$

This results in an equality of:

$$\frac{\Delta \ln p'}{\Delta \varepsilon_v} = \frac{\Delta \ln \sigma'_v}{\Delta \varepsilon_v} \tag{4.7}$$

when $K_0 = K_0^{NC} = constant$ in the normal consolidated range. However, for the over consolidation range, K_0 is not a constant but dependent on the degree of over

consolidation and the direct relation cannot be valid. For such situation, it has an expression as equation (4.8).

$$\frac{\dot{p}'}{p'} = \frac{1+\nu_{ur}}{1-\nu_{ur}} \frac{1}{1+2K_0} \frac{\dot{\sigma}'}{\sigma'} \tag{4.8}$$

Consequently, based on empirical assumptions of the values of K_0 and ν_{ur} (Poisson's ratio for unloading-reloading), it can be deduced out that (equation (4.9)):

$$\Delta \ln p' = \frac{1}{2} \Delta \ln \sigma_v' \tag{4.9}$$

An illustration for determination of λ^* and κ^* in a one-dimensional oedometer curve is illustrated in Figure 4.14.

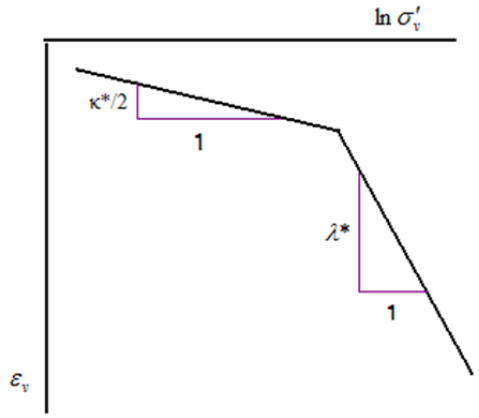

Figure 4.14. Adjustment of the three-dimensional parameters in an oedometer test curve.

Additionally, attention has to be taken when the reloading-unloading line is not performed in the oedometer test. This is because after sampling, the soil swells to some extent and negative pore pressure can be built up, which makes the sample easier compressed in the beginning, and therefore an under estimation of the soil stiffness from the initial loading curve. In fact, the real M_0-value in Sweden is empirically obtained by multiplying a factor of 3-5 on the original M_0-value evaluated from an initial compression curve.

4.2.3 Creep parameters

The secondary compression index, C_α, is the most commonly applied parameter to describe the creep behaviour in soft soil. It is defined by Taylor (1942) as (equation (4.10)):

$$C_\alpha = \frac{\Delta e}{\Delta \log t} \tag{4.10}$$

Alternatively, in Sweden there is a similar parameter, the coefficient of secondary compression, α_s, which is defined as equation (4.11).

$$\alpha_s = \frac{\Delta \varepsilon_{cr}}{\Delta \log t} \tag{4.11}$$

where ε_{creep} = creep strains

The time resistance number, r_s, becomes the third choice to exhibit the creep property according to Janbu's time-resistance concept, equation (4.12).

$$r_s = \frac{\partial \ln t}{\partial \varepsilon_{cr}} \tag{4.12}$$

Moreover, required by the Modified Cam Clay model, a new creep parameter μ^* also deserves to be mentioned, see equation (4.13).

$$\mu^* = \frac{\Delta \varepsilon_{cr}}{\Delta \ln t} \tag{4.13}$$

In general, those parameters can be usually evaluated from an IL oedometer test and also easily be calculated from one to another. Figure 4.15 illustrates, for instance, the evaluation of α_s, from a standard IL compression curve.

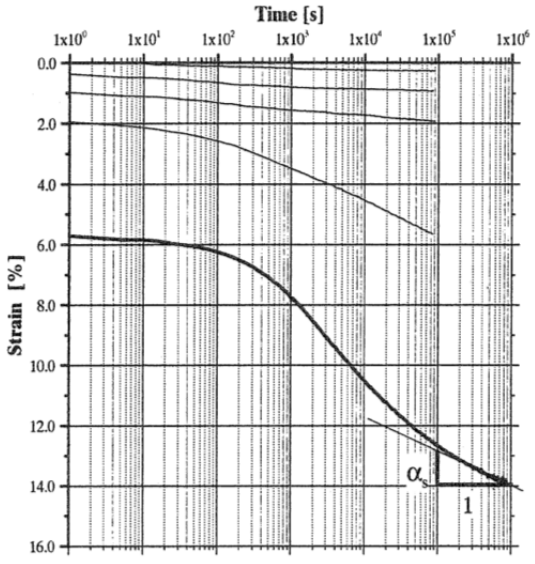

Figure 4.15. Evaluation of α_s from an IL test (Claesson, 2003).

As it can be seen in Figure 4.15 for small load steps, the compression curves are flat and show little creep strain. This indicates that the creep parameter α_s, is not a constant value but varied with the stresses. Based on a series of IL tests, it is observed that the value of α_s is strongly dependent on the magnitude of effective stresses (Claesson, 2003). According to Claesson (2003), for a range of effective stresses smaller than the preconsolidation pressure (below approximately $0.7p_c$), there is very low values of α_s being obtained, while when the effective stresses approach to the preconsolidation pressure, the value of α_s increases significantly and reaches to a maximum at stresses slightly greater than the preconsolidation pressure (about $1.2p_c$). After that it remains at the high value or decreased a little even when the effective stresses keep increasing, see Figure 4.16.

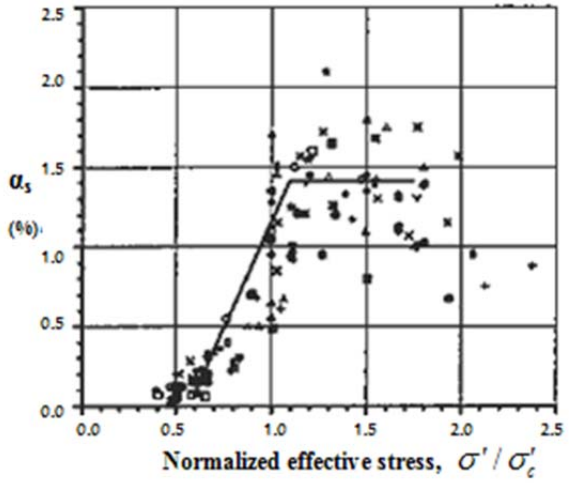

Figure 4.16. Variation of αs with effective stresses interpreted by Claesson for Änggården clay (2003).

Another way to describe the variation of α_s is as a function of the accumulated strains. There is a general model used in Sweden to present the variation of α_s with strains shown in Figure 4.17.

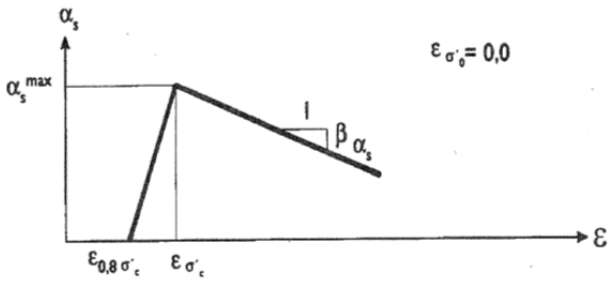

Figure 4.17. Variation of α_s with strains according to Swedish practice (Bengtsson & Larsson, 1994).

It is also possible to evaluate the creep parameters from CRS tests according to Kim & Leroueil (2001). By performing CRS tests with different strain rates, if plotting the evaluated preconsolidation pressure and the respective strain rate both in logarithmic scale, it gives rise to a so-called preconsolidation index, C_p, from their linear correlation, see Figure 4.18. Equation (4.14) describes how to calculate the preconsolidation index.

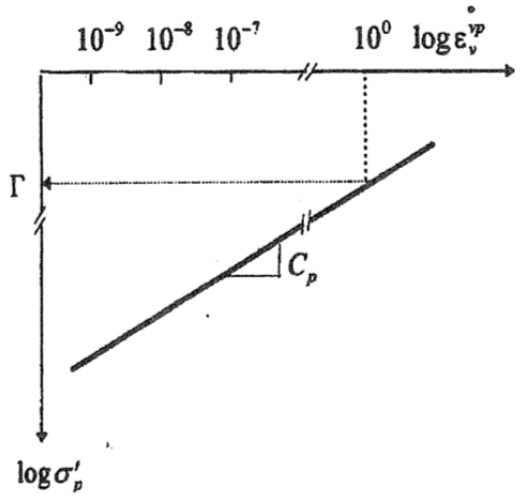

Figure 4.18. Definition of the parameter C_p (Kim & Leroueil, 2001).

$$C_p = \left(\frac{\partial \log \sigma'_p}{\partial \dot{\varepsilon}_v^{vp}}\right) \tag{4.14}$$

The preconsolidation index, C_p, turns out to be equal to the ratio of C_α / C_c, which is usually in a range of 0.04 ± 0.01. In this way the creep parameter C_α can then be well defined.

Moreover, the following empirical expression relationship between natural water content and the minimum time resistance number also provides a possibility to determine the creep parameter when oedometer test data is not available. Equation (4.15) describes this relationship.

$$r_1 = \left(\frac{75}{w_n^{1.5}}\right) \tag{4.15}$$

In general, despite of the variations within the creep parameters, the SSC and ACM models are only requiring a single value as the input. Usually the maximum creep index around the preconsolidation pressure is chosen as the representative value. This leads to an unrealistic large creep strain when the effective stresses are small during a short time period after the undrained loading. Therefore, adjustment of the value of creep parameter is necessary during the construction phase and the further consolidation.

5 Modelling of laboratory test data

When attempting to investigate the performance of advanced computer models for the modelling of soft soil behaviour, simulations of small-scale laboratory tests turns out to be the quickest approach, if considering the convenience of data collection. By modelling lab tests it is then helpful to achieve:

- A familiarity of soil parameter evaluations from the laboratory test curve;
- An adjusting of the evaluation methods by comparing the model prediction and laboratory measurement data;
- A validation whether the models perform as anticipated with the input parameters;
- An investigation of the sensitivity of related soil parameters.

5.1 Background of the data

The laboratory test data in this chapter originates from the reconstruction of highway E45 between the cities of Trollhättan and Gothenburg, see Figure 5.1. The project is called "BanaVäg i Väst" and is managed by the Swedish Traffic Administration (Trafikverket, 2011).

Figure 5.1. Graphic figure of the stretch Gothenburg – Trollhättan. Yellow line is road and red line is railway (Trafikverket, 2011).

The E45 is an important piece of the infrastructure on the Swedish west coast, both regarding personnel traffic and goods traffic. The old E45 was constructed during the 1960's and the increasing traffic of both motor vehicles and trains has proven the road and railroad to be inadequate regarding capacity and safety. A new double railway

with a capacity of 120 trains per day and a 4-lane road for motor vehicles will solve this problem. Geotechnical problems have arisen during the project since the area consists of deep layers of clay, in some places as deep as 100 m. This leads to the need of extensive reinforcements of the ground, e.g. in the form of lime cement columns. The project is to be completed in 2012 (Trafikverket, 2011).

The data has been supplied by the supervisors in the form of Excel- and PDF-files and contains CRS and triaxial test data from bore hole FB2203 at the depths 12, 18, 24 and 30 m respectively.

5.2 Modelling of CRS test

Since the CRS test is the most commonly applied soil test pattern in Sweden for obtaining the compressibility property of soil, it is therefore chosen to be simulated to check the performance of the models.

An axis-symmetric geometrical model with 25 mm in x-axis direction and 20 mm in y-axis direction is set to simulate a standard CRS test sample (20 mm in height and 50 mm in diameter). The boundary condition is chosen as the *Standard fixities* in PLAXIS, which represents prevented horizontal displacements at the two sides and a static bottom boundary without movements both horizontally and vertically. The hydraulic condition is set with one-sided drainage at the top and the other three sides sealed boundary condition. The unit soil weight of sample is set as zero to create constant initial stresses. Figure 5.2 illustrates the geometrical model as drawn in PLAXIS.

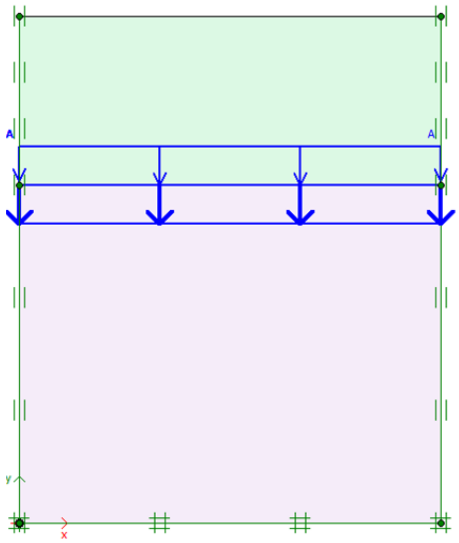

Figure 5.2. A geometric model for the CRS test in PLAXIS.

The following assumptions are then made to start simulating the sample testing:

- Assign a dummy thin soil layer with a calculated soil weight for the *initial K_0 procedure* calculation phase, which is to reproduce the in-situ effective stresses experienced by the sample;
- Inactivate the dummy soil to simulate the unloading of sampling from field to the lab. Add a small amount of load on the sample, which is to simulate the negative pore pressure in the sample due to swelling. This step is performed with *plastic (drained) analysis* in a short time;
- Start the CRS test simulation in the *consolidation analysis* mode by applying a pre-described displacement in a certain time, which corresponds to the strain rate in the lab tests (standard 0.0024 mm/min in this case). The settlements from previous step have been set as zero.

Four CRS tests are simulated with soil materials from different depths using the SSC model. The input parameters are presented in Table 5.1.

Table 5.1. Input parameters of the CRS modelling.

Sample	w_n	e	k	c_k	φ	c	K_0^{NC}	κ^* from stress-strain curve	κ^* (from M_0)	λ^*	μ^*	OCR
12 m	0.75	1.95	5.00E-10	3	30	1	0.5	0.0146	0.021	0.28	0.0087	1.20
18 m	0.70	1.82	5.00E-10	3	30	1	0.5	0.0195	0.025	0.26	0.0078	1.20
24 m	0.63	1.64	5.00E-10	3	30	1	0.5	0.0100	0.017	0.22	0.0067	1.10
30 m	0.59	1.53	5.00E-10	3	30	1	0.5	0.0100	0.017	0.17	0.0060	1.15

Due to that neither IL oedometer test data nor CRS test with different strain rates have been performed to determine the creep index, it is therefore applying the empirical relationship between natural water content and the minimum time resistance number according to Christensen (1995) to get the modified creep index, see equation (5.1).

$$\mu^* = \frac{1}{r_1} = \frac{w_n^{1.5}}{75} \tag{5.1}$$

Two slightly different values of κ^* have been used. One is evaluated directly from the doubling of slope of the over consolidation range in the stress-strain curve as suggested in the previous soil parameter evaluation chapter (Chapter 4.2). Another one is from the relationship between the compression modulus and κ^* mentioned by Olsson (2010) for the over consolidation range, see equation (5.2).

$$M \approx \frac{2\sigma_v'}{\kappa^*} \tag{5.2}$$

where σ_v' denotes the average effective stress in the range of preconsolidation pressure. A simple assumption is taking as the M_0-value (in Swedish practice) corresponds to an average stress as one half of the preconsolidation pressure, see equation (5.3).

$$\kappa^* = \frac{\sigma_c'}{M_0} \tag{5.3}$$

Figure 5.3 to Figure 5.6 illustrates the comparison performed on the SSC simulations of the laboratory data.

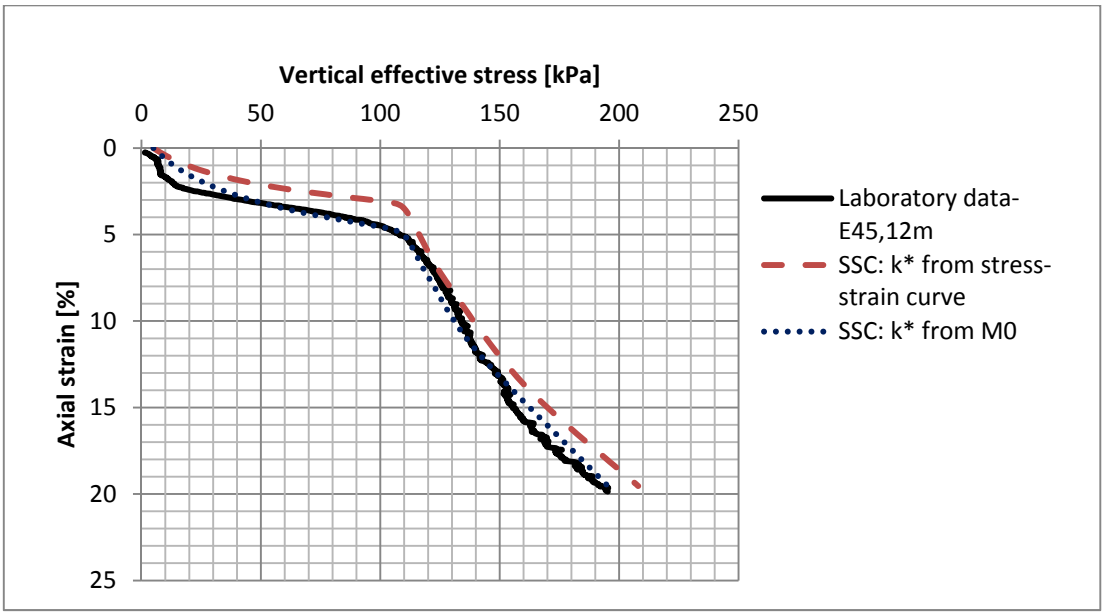

Figure 5.3. Comparisons of SSC simulation with laboratory data for E45-12 m soil samples.

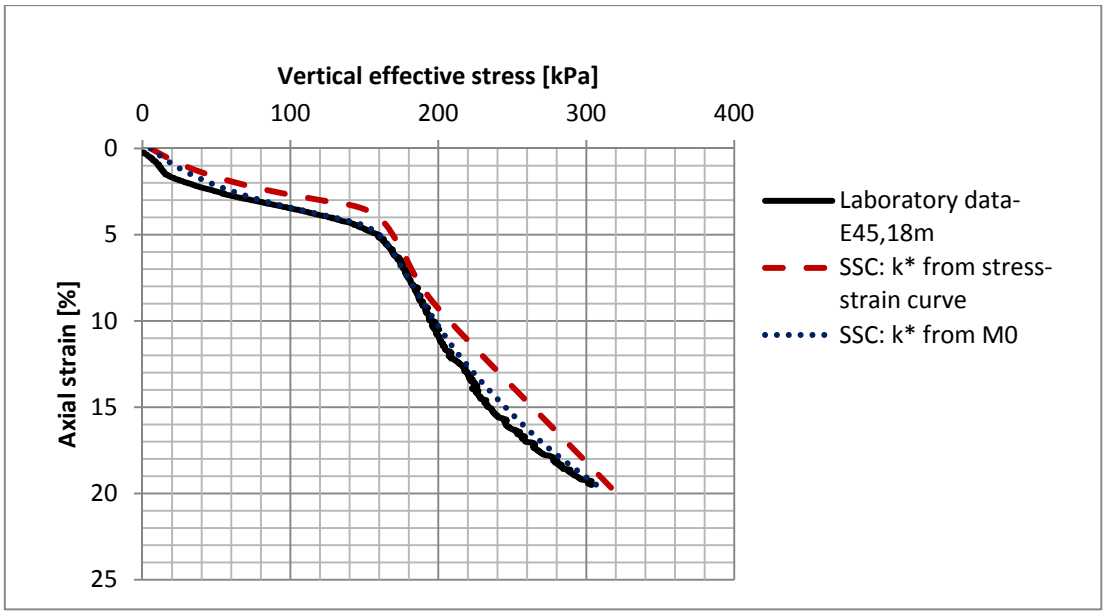

Figure 5.4. Comparisons of SSC simulation with laboratory data for E45-18 m soil samples.

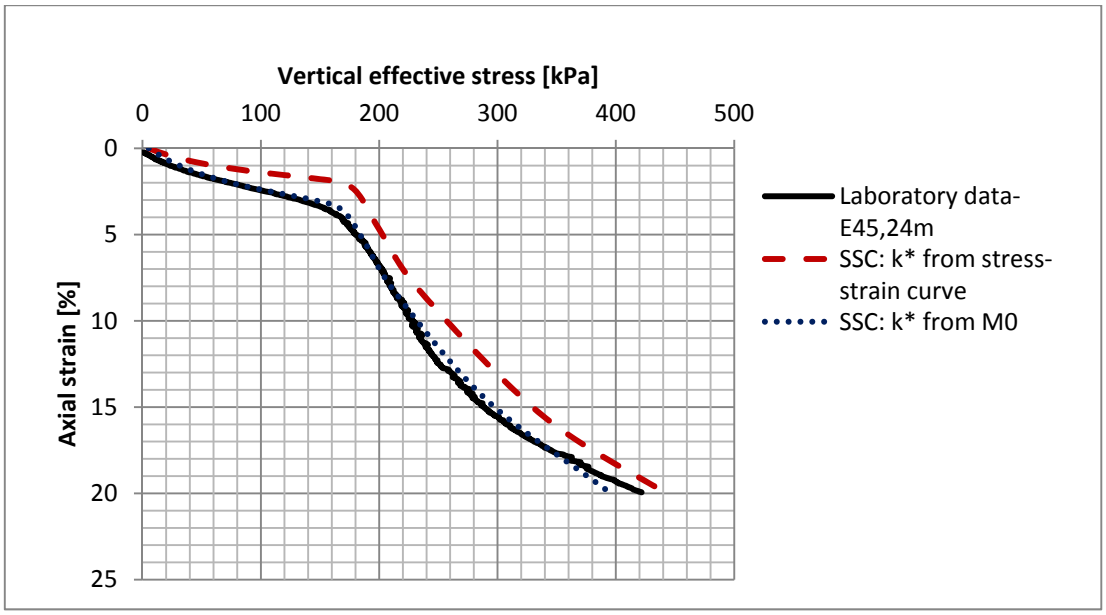

Figure 5.5. Comparisons of SSC simulation with laboratory data for E45-24 m soil samples.

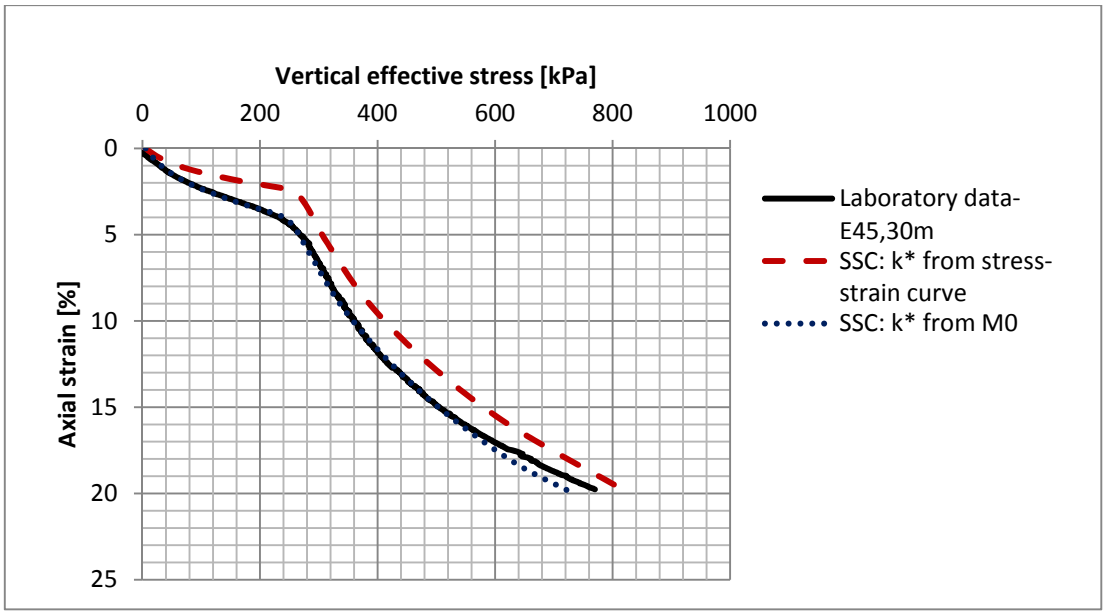

Figure 5.6. Comparisons of SSC simulation with laboratory data for E45-30 m soil samples.

As it can be seen from the results shown in Figure 5.3 to Figure 5.6, the SSC model prediction with κ^*-value derived from stress-strain curve shows some distances to the measurement data, while an increased κ^*-value calculated from the M_0 relation makes the prediction curve more fit to the measured data. A possible explanation can be that the correction of slope of one-dimensional compression curve to that of isotropic compression curve is done by assuming $K_0 = 1$ and $\nu_{ur} = 0.2$. However if ν_{ur} is set as a more general value of 0.15, it would be as equation (5.4) instead:

$$\frac{\dot{p}'}{p'} = \frac{1+\nu_{ur}}{1-\nu_{ur}} \frac{1}{1+2K_0} \frac{\dot{\sigma}'}{\sigma'} \tag{5.4}$$

This equation can be changed into equation (5.5).

$$\Delta \ln p' = \frac{1}{2.22} \Delta \ln \sigma_v' \tag{5.5}$$

which leads to that the κ^*-value is bigger than twice of the slope in the oedometer over consolidation compression curve. Although this slight increase of the κ^*-value could not result in an exactly fit curve to the measured data, it means to some extent that the determination of the isotropic κ^*-value is quite sensitive from the oedometer curve and therefore requires more attention. In comparison, the evaluation of λ^* is more reliable, and for these E45 clay samples, a ratio between the compression index and the swelling index lies in the range of 10-13 which can be suggested by considering the good agreement of the κ^*-value estimated manually from the M_0-value.

Moreover, it has to be noticed that the M_0-value evaluated from lab tests is commonly considered as an underestimation of soil stiffness due to sample disturbance or without the unloading-reloading curve. Therefore when simulating the soil response in the field, the M_0-value has to be modified to be greater value of 3-5 times of the lab-M_0 and therefore the κ^*-value has to be decreased accordingly.

Since there is no IL oedometer test data available for those samples, it is difficult to investigate the correction of empirical determination of creep index. Only the model performance itself can be studied by assuming a simple virtual IL test to check whether the creep parameter works properly. This has been done by doing the following steps:

- Start after the first unloading step in the CRS test simulation, add the first load of 10 kPa instantaneously and then apply a consolidation phase of 1 day;
- Then increase to instant 20 kPa loads and another 1 day consolidation;
- Do the same way to 40 kPa, 80 kPa, 160 kPa and 320 kPa;
- For the last step of 640 kPa, choose 100 days of consolidation instead of 1 day.

The results for the E45-18 m soil sample are shown in Figure 5.7. From the last part of the curve it is possible to back-calculate the modified creep index according to equation (5.6) below.

$$\mu^* = \frac{\Delta\varepsilon_1}{\ln\left(\frac{\Delta t}{t_0}\right)} \approx 0.0078 \qquad (5.6)$$

where $t_0 = 1$ day, which agrees the input parameter well.

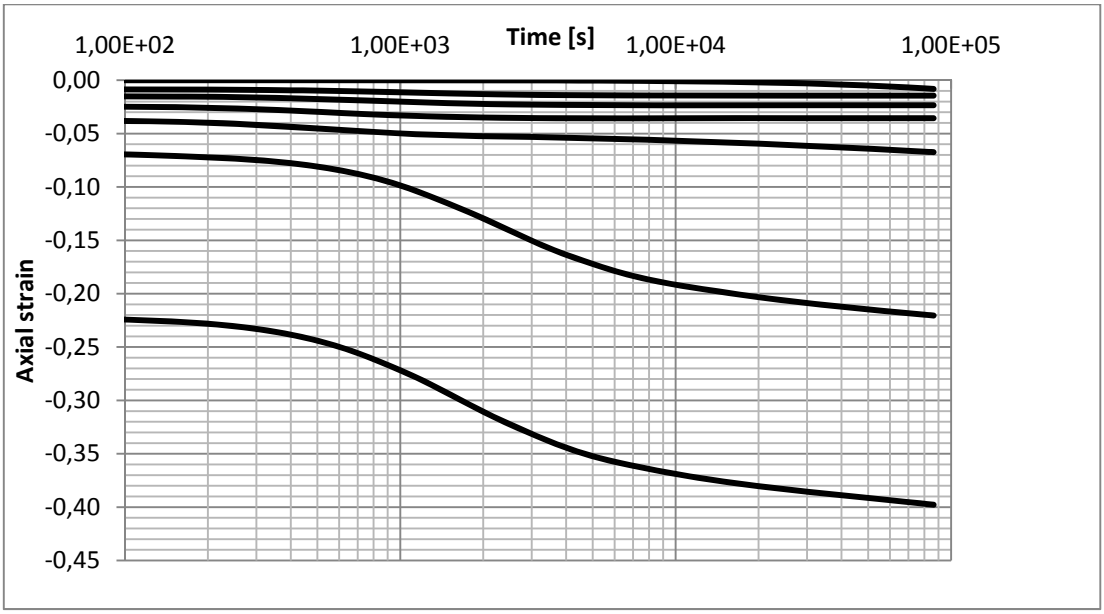

Figure 5.7. A diagram presenting the strain-time curve from the IL test simulation.

Since the stiffness parameters are the same for the ACM as the SSC model, no back-calculation of these parameters needs to be done again.

The CRS test modelling has also been conducted for the n-SAC model, in which several different parameters are required and their determinations are not at all as straightforward as the other models studied in this thesis and hence deserves more investigation.

Due to lack of data for remoulded samples, there are a couple of input parameters left undefined:

- The time resistance number, r_{si}, for remoulded soil;
- The slope of intrinsic compression line, λ_i*, which is much lower than the value of natural clay.

Alternatively, the latter parameter can be determined by linking it to the compression modulus number m' for natural clay when observing the inclination of the compression curve. After the less stiff response when crossing the preconsolidation pressure, soil shows hardening with the accumulated strain. The compression modulus number can be calculated with equation (5.7) which follows.

$$m' = \frac{dM}{d\sigma'} = \frac{d\left(\frac{\partial\sigma'}{\partial\varepsilon}\right)}{d\sigma'} = \frac{d\ln\sigma'}{d\varepsilon} = \frac{1}{\lambda^*} \tag{5.7}$$

Moreover, since the combination of r_{si} and $r_{si,min}$ provides information of the initial amount of structure x_0 that natural soil has, it is a possible way to first find the x_0 which is related to the value of sensitivity of a natural soil by the expression $sensititvty \approx 1 + x_0$ (Wheeler et al., 2003a) and then obtain the estimation of r_{si}. However, there is no data recorded with the soil sensitivity for the E45 soil samples which means that assumption has to be made. Soil with a sensitivity value from 4 to 10 would be considered as high sensitive soil (Jin, Liu & Shao, 2001). Therefore, the r_{si}-value is chosen initially with the assumption of x_0 in a range of 3-9 and adjusted further if big difference found between the predictions with the measurement.

The so-called deviatoric destructuration parameter, ω, which according to Grimstad and Degago (2010) is determined by an undrained triaxial compression test at an OCR in the interval of $1 \sim OCR_{max}$ has not been obtained. The details about how to evaluate this parameter is not provided by the developers, which makes it quite difficult to determine a proper value. A possible value applied by Grimstad and Degago (2010) for the n-SAC model testing would therefore be adopted here, and further analysis of the influence of this parameter on the results is conducted.

All the initial input parameters for the n-SAC model to simulate the CRS test are presented in Table 5.2 below, in which the E_{ref} and $r_{si,min}$ are directly calculated from the κ* and μ* in SSC.

Table 5.2. Input parameters for n-SAC model.

Sample	p_{ref} [kPa]	E_{ref} [kPa]	E_{oed}^{ref}	$r_{s,min}$	$r_{s,i}$	ω	φ_p [°]	φ_{cs} [°]	τ [days]	OCR_τ
18 m	100	8400	1300	128	1280	0.3	25	33	1	1.2

As it can be seen from the results shown in Figure 5.8, the simulated results is far different from the measurements. Firstly, the stiffness for the effective stresses in the over consolidated range is too high in the model simulation. Also, when after crossing the preconsolidation pressure, the soil becomes hardened too fast to approach the intrinsic compression line with larger strains.

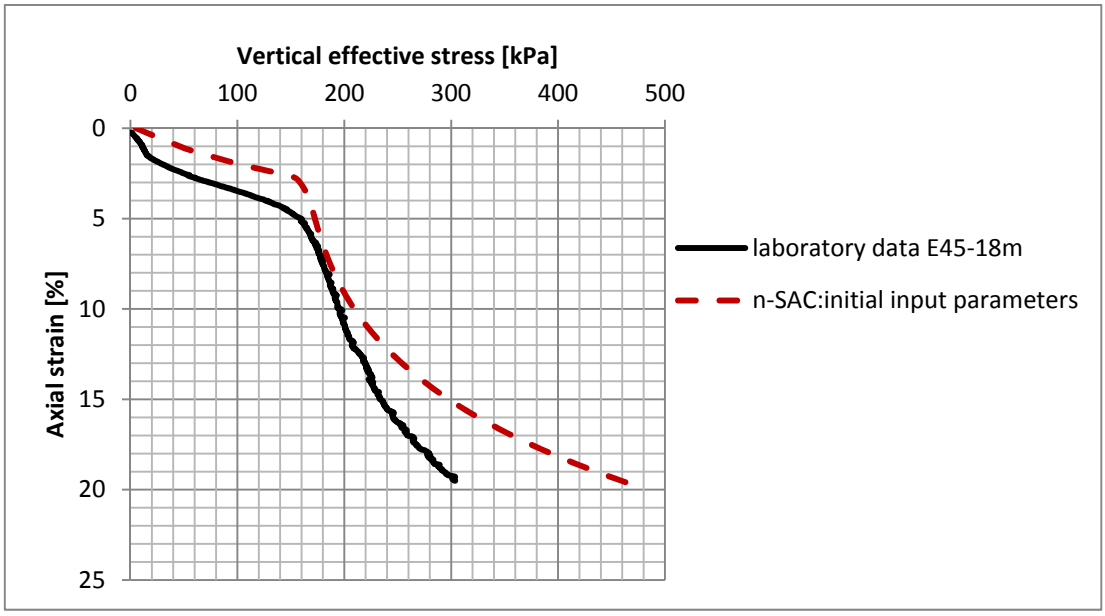

Figure 5.8. Comparison between measurement data from E45 project and n-SAC simulation with initial parameters.

To adjust the model simulations so as to obtain better fit with measurement data, it is of necessity to carry out sensitivity analysis of those important input soil parameters such as E_{ref} and E_{ref}^{oed}. Three different E_{ref} are therefore applied to investigate how it would affect the results with all the other parameters being the same. Similarly, three different E_{ref}^{oed} are also used to check its influence on the model simulation. The results are illustrated in Figure 5.9 and Figure 5.13 respectively.

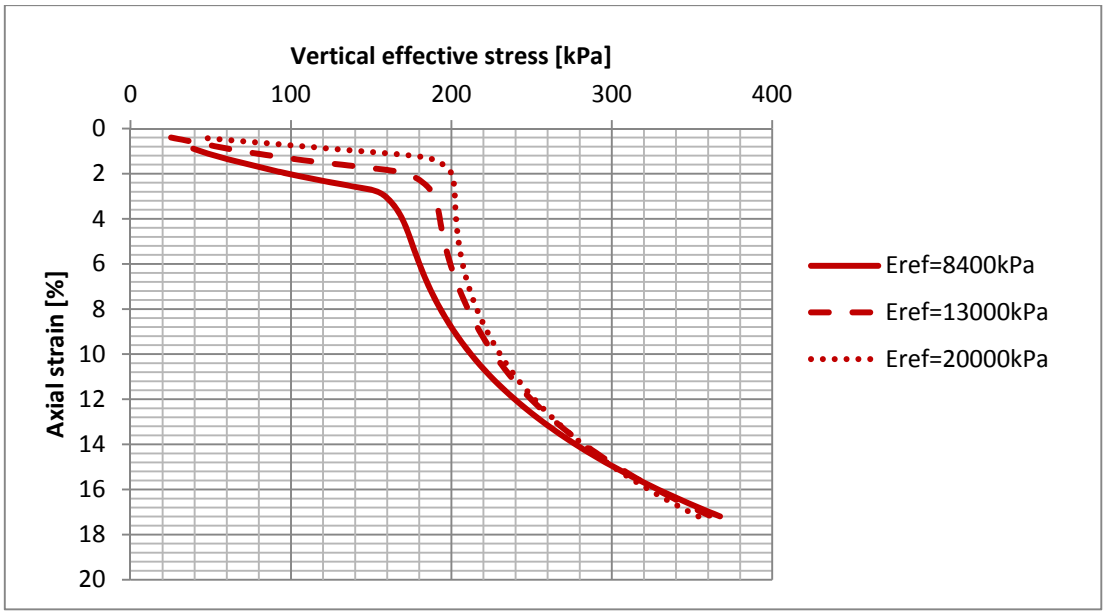

Figure 5.9. Simulation results with three different E_{ref}-values using the n-SAC model.

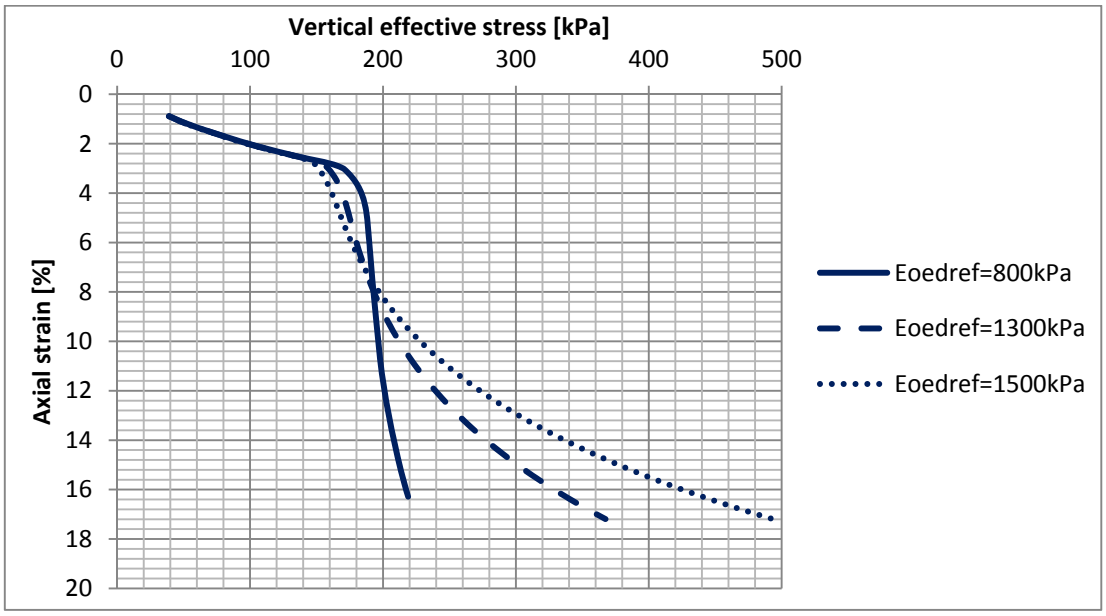

Figure 5.10. Simulation results with three different E_{ref}^{oed}-values using the n-SAC model.

It can be found that the E_{ref}-value is not only influencing the soil stiffness in the over consolidation range but also changing the apparent preconsolidation pressure significantly and controlling how fast soil being destroyed. Similarly, the E_{ref}^{oed}-value is affecting the soil stiffness for large strains as well as the destructuration process. The complexity of the parameters' sensitivity in the n-SAC model can be well explained by its feature of considering the soil structures. There is a hardening parameter ζ_i controlling the destructuration rate significantly, see equation (5.8), which is determined via the difference between the λ_i* and κ*. For example, a decrease of E_{ref}-value results in a smaller value of ζ_i , which then leads to a higher

destructuration rate; the high rate of losing the extra soil structure results in a lower effective stress for a certain strain. While, a decrease of E_{ref}^{oed} gives the opposite result of lower destructuration rate and higher apparent preconsolidation pressure. Therefore, a reasonable combination of E_{ref} and E_{ref}^{oed} is critical for the n-SAC model predictions.

$$\frac{dx}{d\lambda} = \frac{x}{\zeta_i}\frac{3}{3+2\omega}\left(\left|\frac{\partial Q}{\partial p'}\right| + \omega\sqrt{\frac{2}{3}\left\{\frac{\partial Q}{\partial \sigma_d}\right\}^T \frac{\partial Q}{\partial \sigma_d}}\right) \tag{5.8}$$

where $\zeta_i = p_{ref}\left(\frac{1}{\left\{E_{oed}^{ref}\right\}_i} - \frac{3(1-2\nu)}{E_{ref}}\right) = \lambda_i^* - \kappa^*$ (5.9)

Moreover, it is also very important to back-calculate the clay age determined by the combination of E_{ref}, E_{oed}^{ref} , r_{si} and the *OCR*-value, see equation (5.10), to check whether an appropriate creep rate is applied in the model simulation. Clay in Gothenburg area is expected to be about 2000~5000 years old.

$$t_{max} = \tau \cdot (OCR_{max})^{r_{si}\cdot\zeta_i} \tag{5.10}$$

Also, it is commonly recognized that the laboratory CRS test gives unfavourable soil response for the small stress range due to sample disturbance and contact problems etc. Therefore, instead of applying an unreasonable low E_{ref}-value, it could be more realistic to correct the lab test curve by taking away some part of small strains manually to eliminate the problems. In Figure 5.11, the comparison between corrected lab curve and the n-SAC model simulation with initial input parameters is shown. It is very clear that after removing the uncertainty in the lab curve for small stress range, the n-SAC model simulation gives more similar result as lab measurements. However, still there are some differences in the large strain part since the n-SAC model shows higher stiffness in the normal consolidated stress range. Based on the sensitivity analysis, decreasing the Erefoe-valued can be an effective approach to modify the simulation. Meanwhile, to achieve appropriate prediction of the clay age, the r_{si}-value has also to be adjusted. New combination of soil input parameters for the n-SAC model are therefore listed in Table 5.3. The calculated clay age results in about 2300 years, which turns to be reasonable for Gothenburg clay. Good agreement between corrected lab curve and the final adjusted simulation are depicted in Figure 5.12.

Table 5.3. Adjusted input parameters for the n-SAC model.

Sample	p_{ref} [kPa]	E_{ref} [kPa]	E_{oed}^{ref}	$r_{s,min}$	$r_{s,i}$	ω	φ_p [°]	φ_{cs} [°]	τ [days]	OCR_τ
18 m	100	8400	1000	128	1000	0.3	25	33	1	1.2

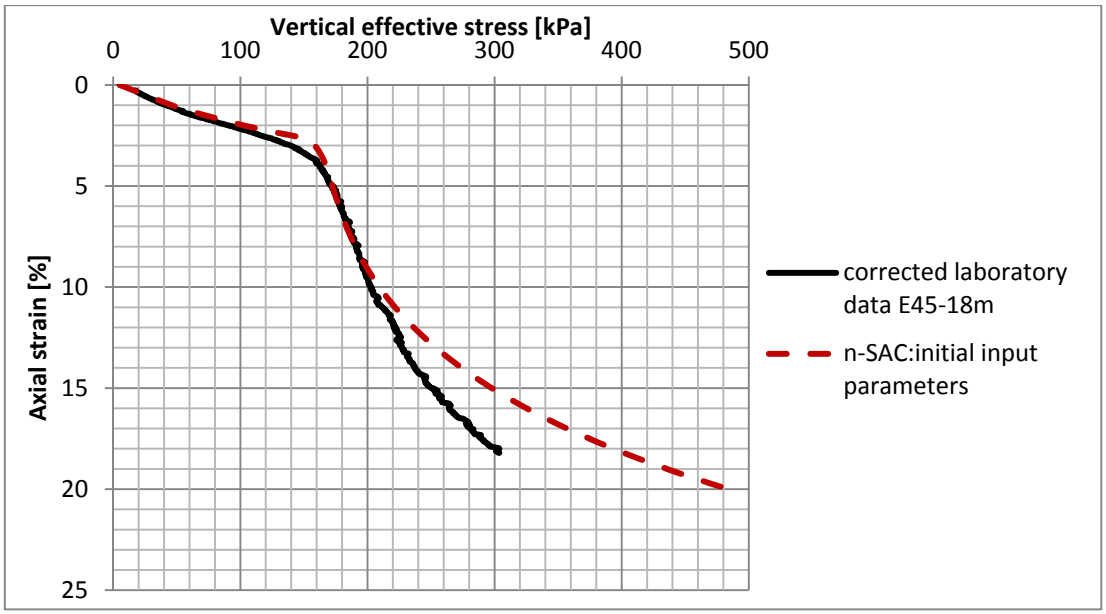

Figure 5.11. Comparison between corrected laboratory measurement data from E45 and n-SAC simulation with initial input parameters.

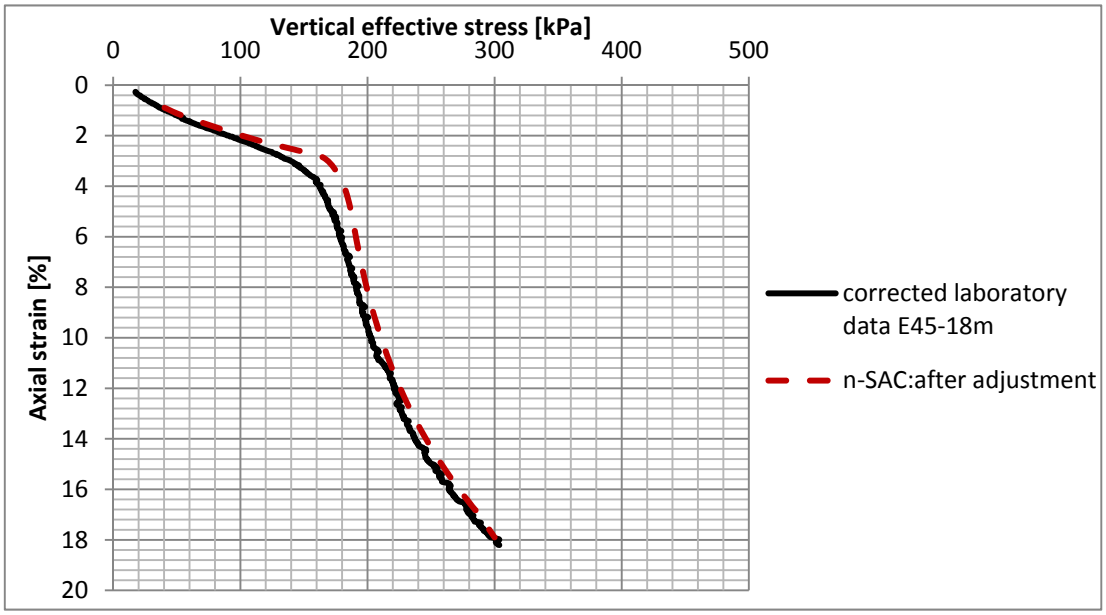

Figure 5.12. A diagram illustrating the adjusted n-SAC simulation and the corrected lab data from the E45 project.

Moreover, in order to investigate the effect of the deviatoric destructuration parameter ω, various ω-values are applied to compare the difference. As it can be seen in Figure 5.13, it is showing that the higher value of ω, the lower value of the preconsolidation pressure. This is considered as reasonable results since high destructuration rate makes the soil being destroyed earlier and thus the portion of preconsolidation pressures gained from extra structures is lost.

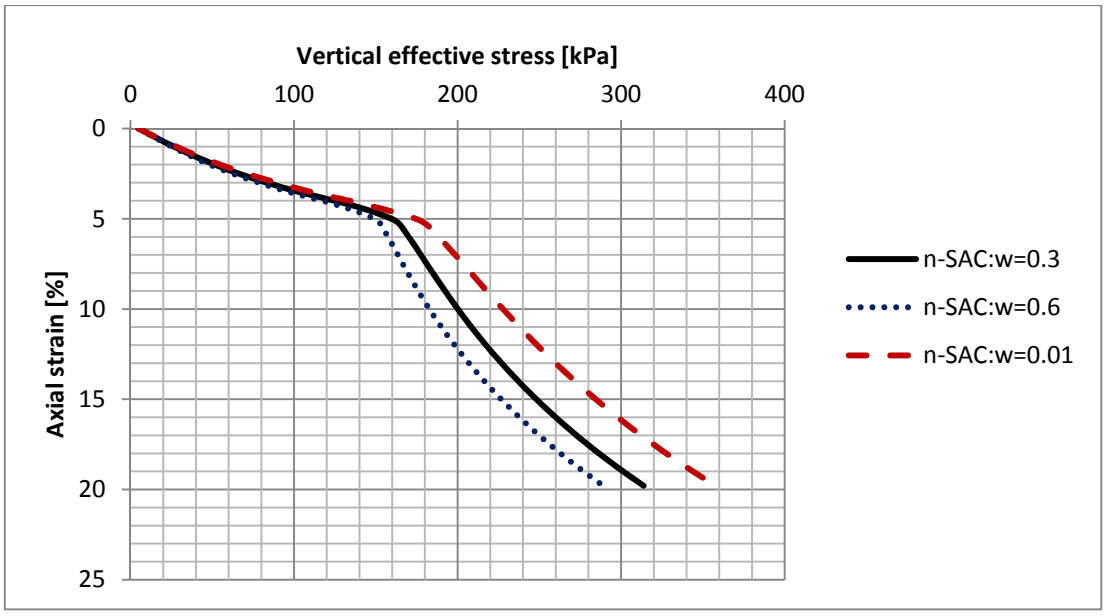

Figure 5.13. Comparison of simulation results with different ω-values.

In general, as it has been explored, the laboratory soil sample shows indistinct structures, soil tests on remoulded material is absent and the deviatoric destructuration rate parameter is poor-defined. It is therefore difficult to determine all the input parameters for the n-SAC model properly and the simulation results turn out to be less reliable. The modelling process thus was aimed to study the effects of various parameters, which then could found a base for the further field test modelling.

5.3 Modelling of undrained triaxial test

To investigate the response of soft clay under relatively rapid constructions, the undrained triaxial test is the most applied soil test to obtain the undrained shear strength as well as to study the stress path during loading. Reliable soil tests are those which are performing tests on soil samples along the stress path in the field (Wood, 1984). Hence, in this part, simulation of undrained triaxial test is carried out to verify whether the models are capable to follow those stress paths and therefore be reliable to predict the soft soil behaviour.

Initially, a general description of the stress path in triaxial tests is provided so as to give fundamental ideas of the further stress path analysis.

5.3.1 General description of stress path in triaxial tests

In a conventional triaxial compression test, an equation can be written as equation (5.11).

$$p = \frac{\sigma_a + 2\sigma_r}{3} = \frac{\sigma_r + q + 2\sigma_r}{3} = \sigma_r + \frac{q}{3} \qquad (5.11)$$

where σ_a = the axial stress

σ_r = the radial stress

The cell pressure is commonly defined as constant, which gives according to equation (5.12):

$$\delta\sigma_r = 0 \tag{5.12}$$

which follows that (equation (5.13)):

$$\delta p = \frac{\delta q}{3} \tag{5.13}$$

These equations describes that the total stress path (TSP) in a conventional triaxial compression test would follow a gradient of 3 from an initial stress state. Alternatively, in a conventional triaxial extension test, this relationship still holds with the deviator stress q as negative. It is often assumed that in drained triaxial test, the effective stress path would coincide with the TSP since the pore water is free drained. The illustrations of the stress path in drained triaxial tests are present in Figure 5.14a.

By comparison, in undrained condition, the effective stress path (ESP) would have a curvature from the TSP. The distance between TSP and ESP is representing for the excess pore water pressure, see Figure 5.14b.

Especially, for a slightly over consolidated soil sample (common in nature) in an undrained triaxial test, the effective stress path would initially go up vertically and then turn left after soil yielding. This is explained by that soil deforms elastically inside the yield surface firstly and no plastic volumetric strain occurs. Consequently there has to be no elastic volumetric strain neither since the total volumetric strain is zero under undrained condition. The mean effective stress therefore remains constant before the preconsolidation pressure.

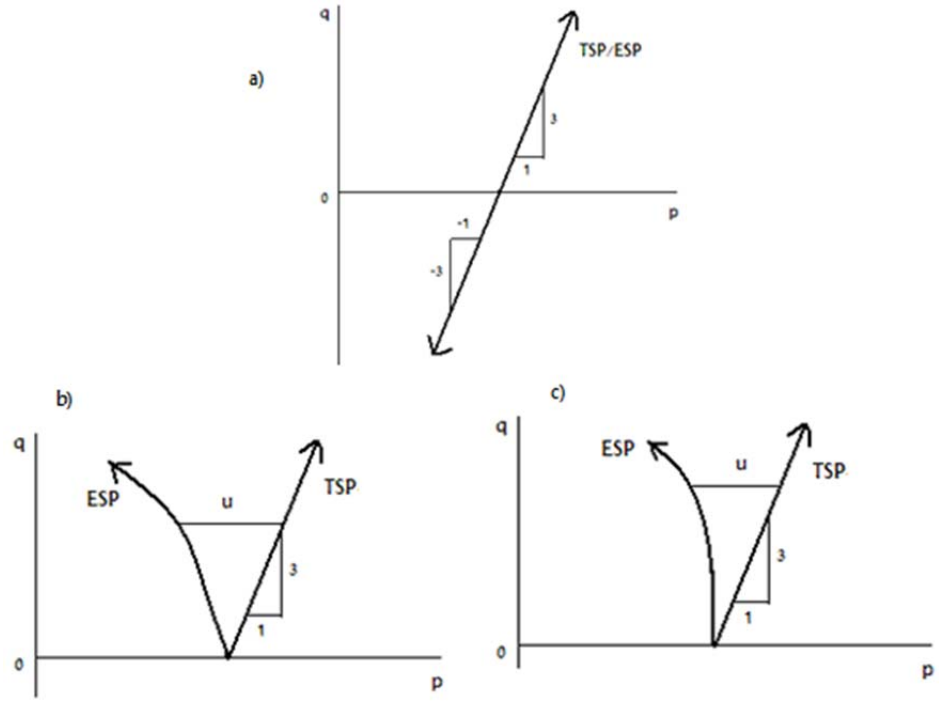

Figure 5.14. Diagram illustrating stress paths in triaxial test (modified after Wood, 1990).

a) *Total stress path and effective stress path in drained triaxial test.*

b) *Total and effective stress path in undrained triaxial test for normal consolidated soil.*

c) *Total and effective stress path in undrained triaxial test for slightly over consolidated soil.*

5.3.2 Model simulations

An axis-symmetric geometry model with 25 mm in x-axis direction and 100 mm in y-axis direction is first built to simulate a standard triaxial sample (100 mm in height and 50 mm in diameter) in PLAXIS. The boundary conditions are set as the right side can move free both vertically and horizontally. The left side can only move vertically due to symmetry and the bottom side can only move horizontally, see Figure 5.15 below. In the consolidation phase, the sample is three-sided drained with only sealed bottom in the lab test while in the models, it is two-sided drainage since left side is also sealed due to symmetry. The soil weight is set as zero to create constant initial stresses.

The simulations of the calculation phase are then described as follows:

- K_0-consolidate the sample to $0.8\sigma'_c$ by adding a certain amount of vertical load and horizontal load (for the E45 samples, K_0 is set as 0.6), the time period is set about approximately six hours to obtain a steady pore pressure;
- Slightly unload the sample to its corresponding in-situ effective stress state;

- Keep the horizontal load and start the undrained shearing by applying a prescribed displacement either downwards or upwards depending on the triaxial compression or extension test in a certain time, the constant strain rate has to be equal to the laboratory stain rate (0.6%/hr in this case).

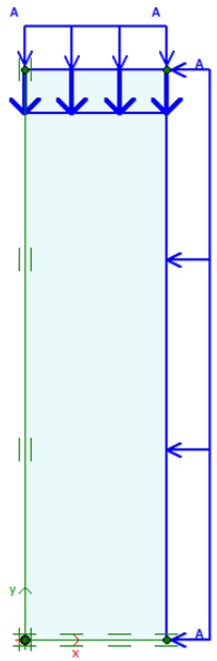

Figure 5.15. Geometry model for triaxial tests simulation in PLAXIS.

The SSC model simulation results of the triaxial compression test for E45-18 m sample are presented in Figure 5.16 as the p'-q stress path and in Figure 5.17 as the deviatoric stress-axial strain curve. Good agreement between the SSC predictions and the measurement is observed which proves the capability of SSC model to capture the undrained shear strength of soft soil.

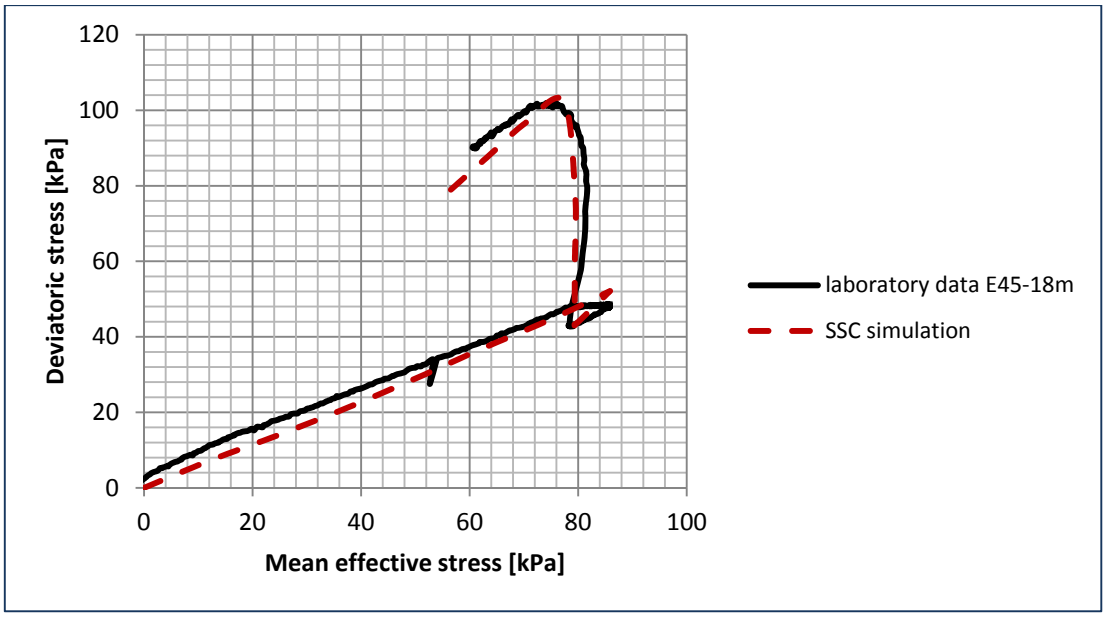

Figure 5.16. Comparisons of the SSC model simulations and measurement in triaxial compression test, here presented as the p'-q stress path.

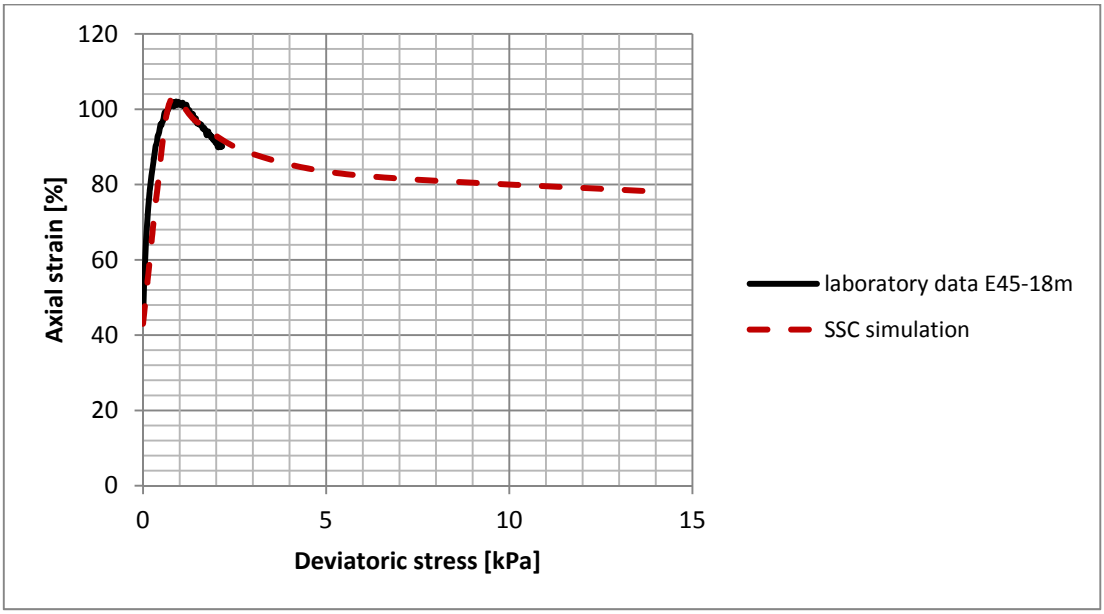

Figure 5.17. Comparisons of the SSC model simulations and measurement in triaxial compression test, here presented as the deviatoric stress-axial strain curve.

Particularly, to investigate whether the SSC model is able to distinguish the creep effect on the undrained shear strength of soft soil, two other strain rates (0.06%/hr and 6%/hr respectively) are used alternatively in the last shearing step. The results of the triaxial test simulations under three different shearing rates are shown in Figure 5.18 and Figure 5.19, which clearly demonstrate that the higher the strain rate the higher the undrained shear strength would be.

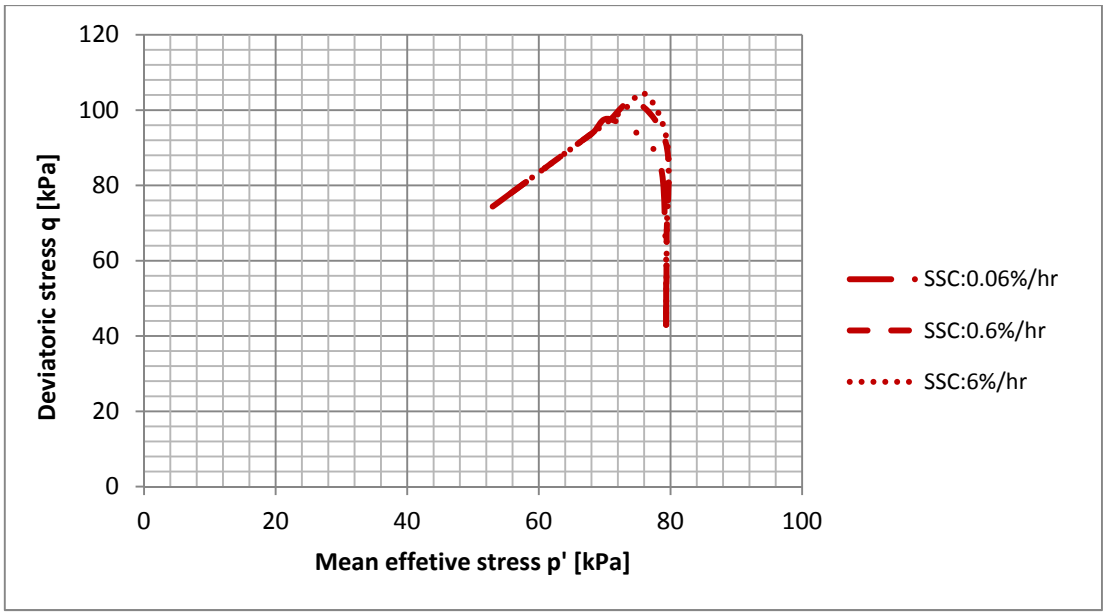

Figure 5.18. Triaxial compression test simulations with different strain rates, here presented as the p'-q stress path.

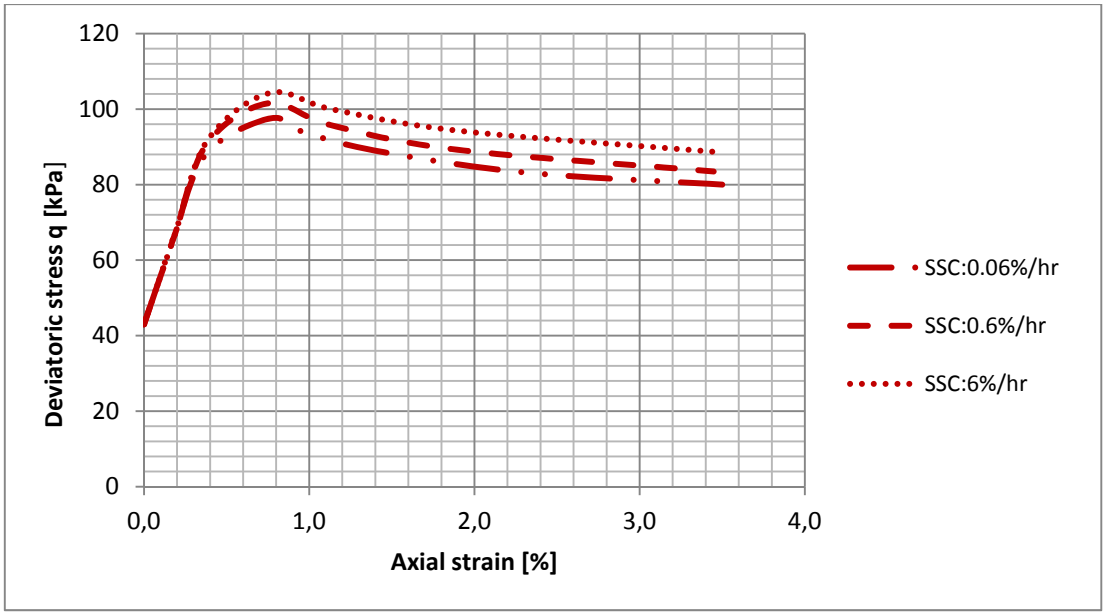

Figure 5.19. Triaxial compression test simulations with different strain rates, here presented as the deviatoric stress-axial strain curve.

Moreover, it is well known that the ACM model, which incorporates the soil anisotropy, would gain more advantages in capturing the different undrained shear strength horizontally and vertically. Therefore, a simulation of triaxial extension test is of necessity to verify this idea.

The input parameters for the ACM model in the triaxial test are listed in Table 5.4 below.

Table 5.4. Input parameters for the ACM model.

Sample	κ^*	λ^*	μ^*	M_e	M_c	α_0	ω_d	ω
18 m	0.0250	0.26	0.0078	0.90	1.29	0.49	0.85	11

In Figure 5.20 and Figure 5.21, the predicted results of both triaxial compression and extension tests by the SSC, n-SAC and ACM models are presented.

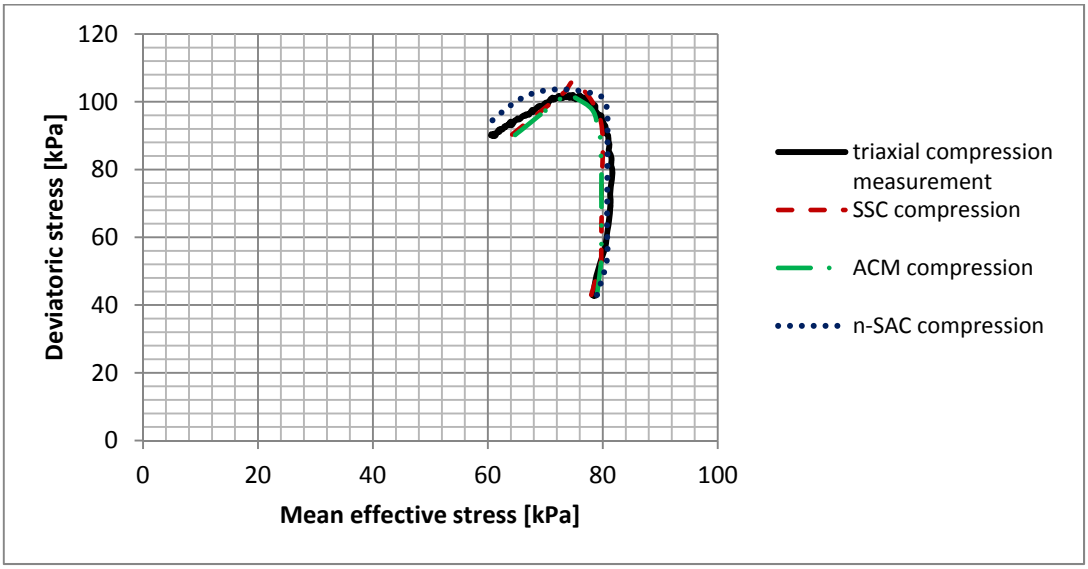

Figure 5.20. Comparison of different stress paths in triaxial compression tests using all the three studied models.

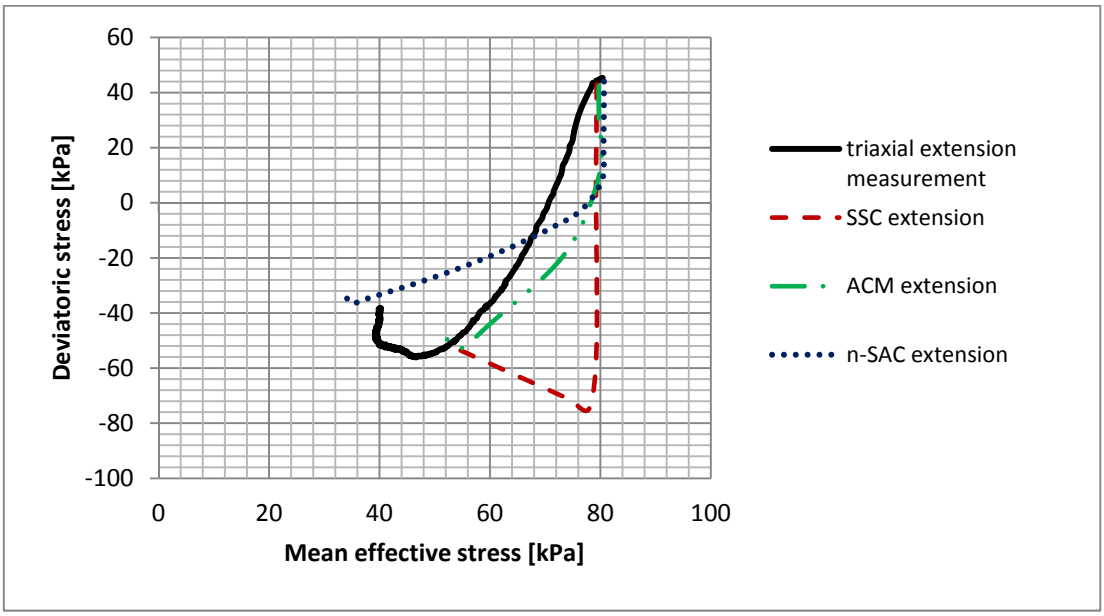

Figure 5.21. Comparison of different stress paths in triaxial extension tests, using all the three studied models.

Overall, in triaxial compression tests, all the three models captured the undrained shear strength (the stress path) well.

In contrast, regarding to the undrained extension test, the three models exhibit big differences in prediction. The SSC model shows the largest deficiency to predict the peak shear strength. The stress path in the SSC simulation stays as a straight line in shearing, which illustrates that the soil is deformed elastically mainly before failure and therefore the yield surface for extension is incorrect if compared with a bending stress path of the laboratory measurement. In the end, the over-predicted peak shear strength in the SSC is too far to be accepted. The n-SAC model also shows inadequacy to capture the measured stress path. Lower peak shear strength has been predicted by n-SAC, which might be due to more significant destructuration occurred in extension tests and more investigations are necessary. By comparison, the ACM model, which has an application of rotated yield surface and the elastic region for the extension side being adjusted by the inclination parameter $\alpha_{0,}$ simulates a gradually bending path and the reasonable peak shear strength.

6 Modelling of real case test data

It is considered that an ultimate goal of the development of any soil model is to give reliable predictions regarding the respective soil behaviour in engineering practice, e.g. settlements, soil strength etc. In this thesis, the three models; the SSC, the ACM and the n-SAC models, are mainly aimed to predict the soft soil deformations incorporating creep, therefore the performance of these models in a real case scenario needs to be evaluated. Test sites with long term measurement data provide the opportunity to achieve this goal. Consequently, the Lilla Mellösa test fill is selected as the real case scenario for model evaluation.

6.1 Site investigation

Lilla Mellösa is located near Upplands Väsby north of Stockholm, Sweden, see Figure 6.1. The test fills was constructed by the Swedish Geotechnical Institute (SGI) in 1945 and the purpose of the construction was to search for an appropriate site for a new airfield, which was to be located outside the Swedish capital of Stockholm. Lilla Mellösa was later decided not suitable for an airport and was instead built at Halmsjön and is today known as Stockholm-Arlanda Airport (Larsson, 1986).

Instead, a new test fill was constructed in order to continue and extend the field tests. The unsuitable conditions for an airport turned out to be highly suitable for a geotechnical test site due to the subsoil conditions with 10 to 15 m of highly compressible soils. The site today functions as a full-scale loading test site with deposits of soft clay. The clay has consolidated under the load of the fill over a long period of time. The data acquired from the test field is unique in terms of long term monitoring and data gathering, stretching back to the mid 1940's (Larsson, 1986).

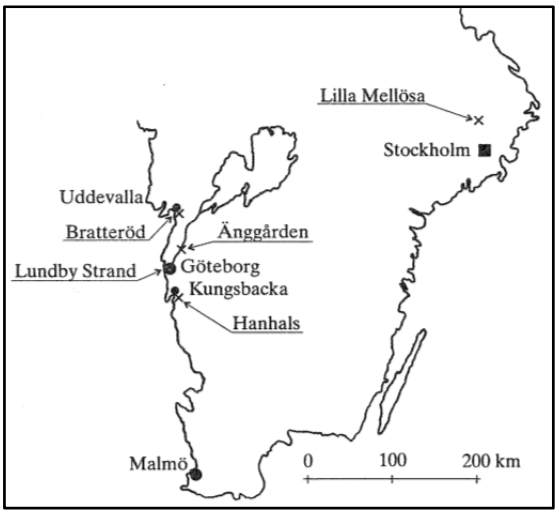

Figure 6.1. The location of Lilla Mellösa (Claesson, 2003).

6.1.1 Soil conditions

Based on comprehensive site investigations by e.g. Chang (1969) and Larsson (1986), the soil profile at Lilla Mellösa is elaborately constructed as shown in Figure 6.2.

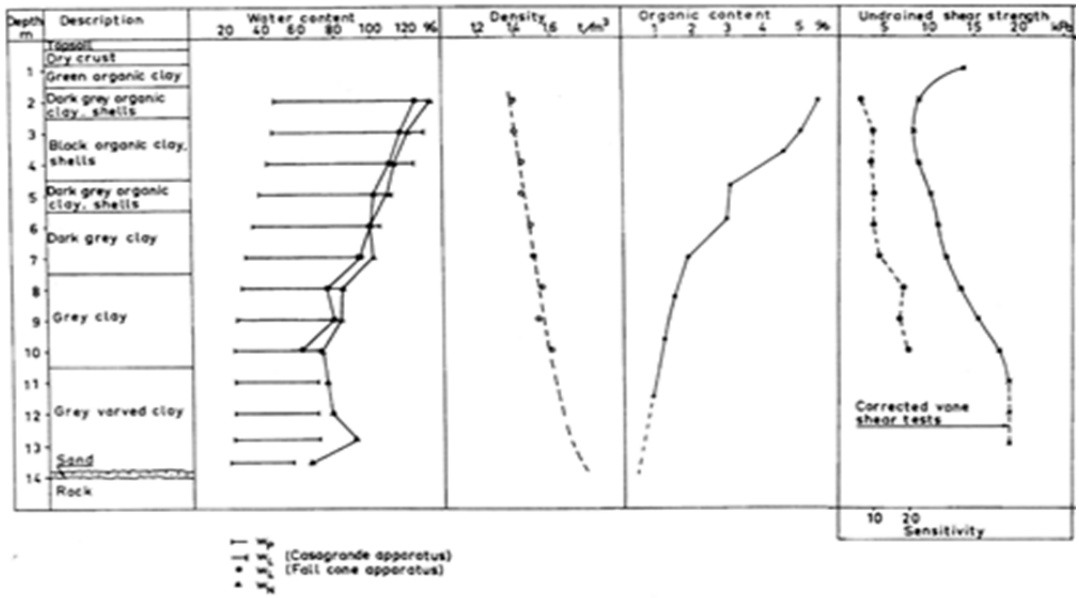

Figure 6.2. Soil profile of the test field at Lilla Mellösa, Sweden (Larsson, 1986).

The top layer consists of a 0.3 m thick layer of organic topsoil. This layer was scraped off before the fill was constructed (Larsson, 1986). The dry crust is 0.5 m thick and consists of organic soil. The soft clay layers of interest is underlying the dry crust down to 14 m with varied organic content along the depth (starting at ca. 5% below the crust and decreasing to less than 2% from 6-7 m depth and below). A thin sand layer is below the soft clay and on top of the bedrock with less importance.

The colour of the clay varies from green to black but becomes grey with the depth. The reason for the black colour is the presence of sulphides in the clay (Larsson, 1986). The clay layer is also characterized with high water content, from a maximum of about 130% in the upper part to a gradually decreased value of 70% in the bottom. The bulk density of clay increases from ca. 1.3 t/m^3 to ca. 1.8 t/m^3 along the depth. The undrained shear strength determined by vane shear tests has a minimum value of 8 kPa at 3 m depth and is then with an increase of 1.3 kPa/m. The clay becomes varved after 10 m depth. They are at first diffuse however the characteristics become more clear with depth (Larsson, 1986).

In Figure 6.3, the evaluated preconsolidation pressure profile from both CRS tests and incremental tests demonstrates that the upper 0.8-2 m of clay is highly over consolidated with an OCR in a range of 2-4 (mainly due to the dry crust effect). In contrast, the downward 2-6 m layer of clay is almost normally consolidated, with only a small amount of pre-overburden pressure (2-4 kPa). In the lower clay part, the over consolidation effect increases again to about 12 kPa, corresponding to an OCR of about 1.2.

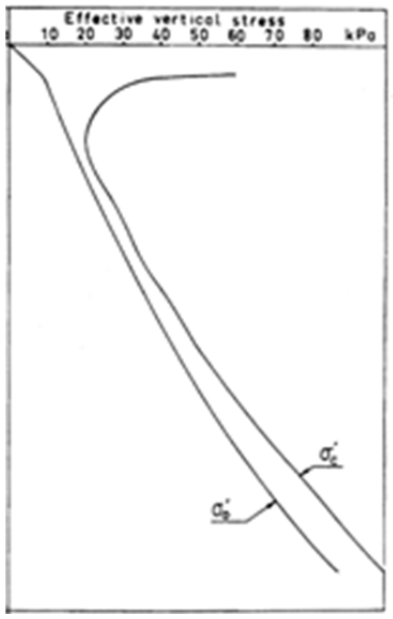

Figure 6.3. Evaluated preconsolidation pressure and the initial effective stress (Larsson, 1986).

The soil parameters used for model simulations are those evaluated by Larsson (1986), shown in Figure 6.4.

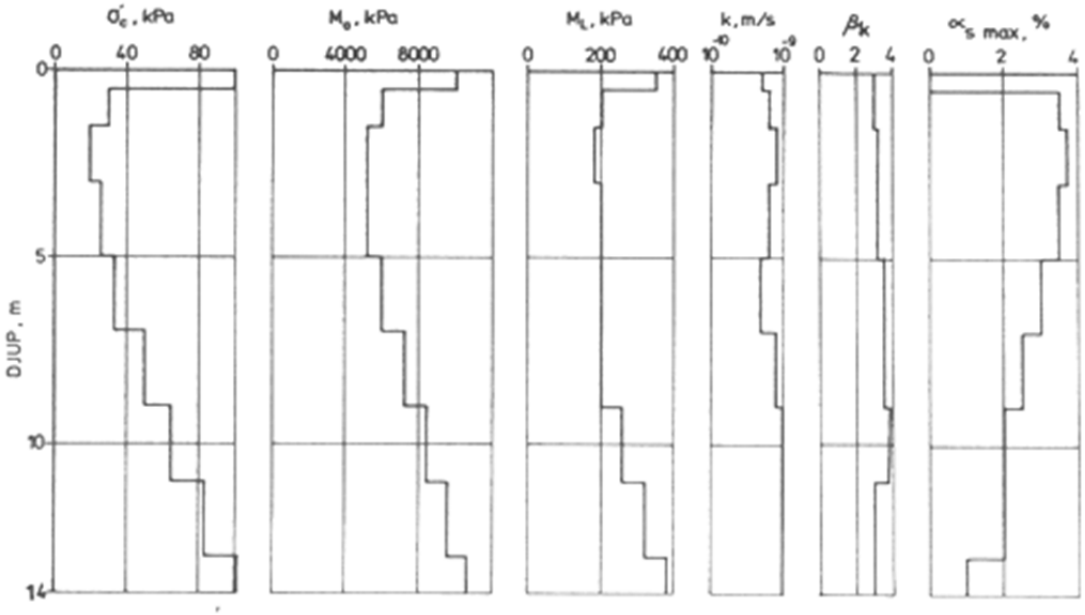

Figure 6.4. Evaluated compression modulus, permeability, coefficient of secondary compression (Larsson, 1986).

The over consolidation compression modulus, M_0, for the clay layer shows a minimum value of about 5 MPa in the upper 5 m and is increased to about 10 MPa in the bottom. The normal consolidation compression modulus, M_L, is about 200 kPa at a depth of 9 m and then starts to increase to about 380 kPa at 14 m depth. The

coefficient of secondary compression presents high values in the upper 7 m and decreases gradually to 0.01 in the bottom. In general, the small compression modulus M_L and the high coefficient of secondary compression are interpreting the high compressibility of this soft clay deposit.

The ground water level is about 0.8 m below the ground surface and the pore water pressure distribution is observed as hydrostatic. The hydraulic conductivity of the clay layer varies from $7 \cdot 10^{-10}$ to $10 \cdot 10^{-10}$ m/s along the depth.

6.1.2 The undrained test fill

The test fill was constructed in October-November 1947. As mentioned above, the topsoil (0.3 m) was scraped off before the construction. The construction consists of 2.5 m high fill of gravel with a density of 1.7 t/m^3. The bottom dimension of the fill is 30 x 30 meters^2 with a slope of 1:1.5. The construction took 25 days to complete and the load has not been changed since then, other than natural variations. The net load increase on the fill was calculated to 40.6 kPa. After some 20 years, the fill settled beneath the ground water table which created a hydraulic up-lift and thereby decreasing the overburden load to about 27 kPa, i.e. a load reduction of 32.5% (Chang, 1981).

6.1.3 Measured settlements and pore pressures

The field measurements of settlements and pore pressures in Lilla Mellösa have been recorded for a period of 57 years from 1945 to 2002, which gives valuable data for creep studies.

Several piezometers and settlement markers were installed in the ground at various depths before constructing the test fill. They had however ceased to function and new ones have been installed, but many of them were out of action with time as well (Larsson, 1986). In order to be able to evaluate the settlement distribution, it is therefore primarily performed by measuring the change in water content in the different layers of the profile (Chang, 1981). The prerequisite of this is however that the lateral deformations may be assumed to be small compared to the amount of consolidation settlements (Larsson, 1986).

The initial settlement during the short construction period was measured to 0.065 m. After 21 years of consolidation, the surface settlements reached to 1.40 m and the excess pore pressure was still in the order of 30 kPa at that time, which states that there were some parts of clay layer with almost no increase of the effective stresses. In 1979, the measured total settlements increased to 1.65 m and the remaining pore pressure was still greater than 20 kPa. The latest measurement data available originates from 2002 and is published by Claesson (2003), which indicates a total settlement of 2 m and excess pore pressure in the order of 10 kPa.

In general, the total settlements within a period of 57 years are shown by Figure 6.5. The distribution of settlements along the depth has been recorded two times in 1967 and 1979 presented in Figure 6.6. The measurements of excess pore pressure distribution in 1967, 1979, and 2002 are plotted in Figure 6.7. While, it is found that there might be some errors regarding to the excess pore pressure data, since after 20 years the fill had settled down to the depth of 1.4 m, at least there would not be any excess pore pressure above the 1.4 m due to the high permeability of the gravel-fill.

Similarly, in 1979 the fill had continued to settle to 1.65 m which indicates no excess pore pressure in this range of depth.

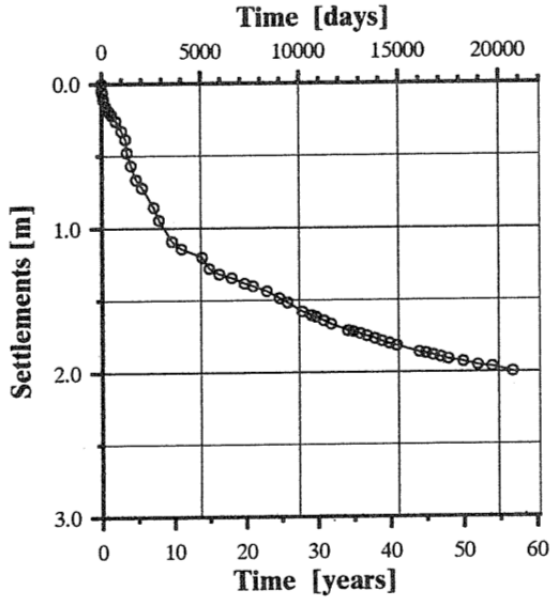

Figure 6.5. The measured total settlements versus time (Claesson, 2003).

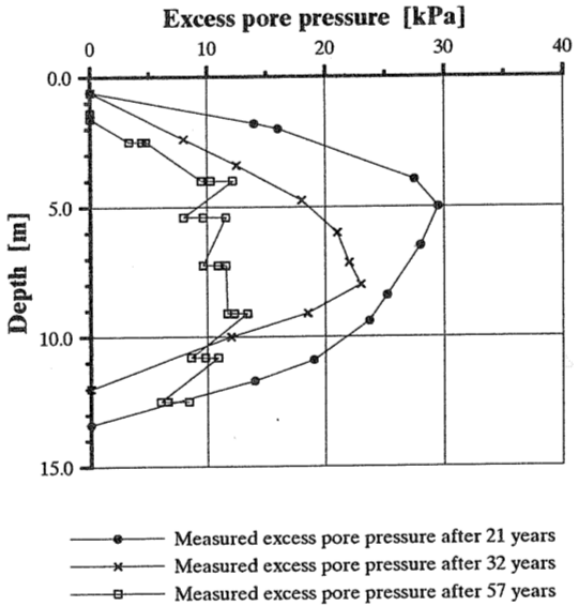

Figure 6.6. Excess pore water pressure distribution along the depth (Claesson, 2003).

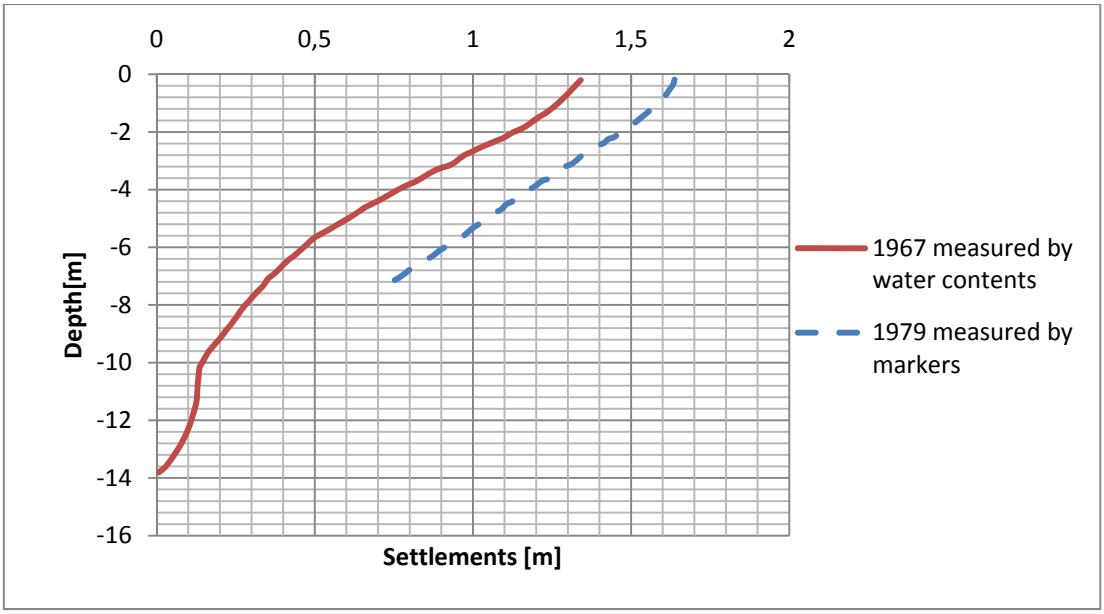

Figure 6.7. Measured settlements distribution (after Larsson, 1986).

6.2 Simulations and comparisons

After general studies of the Lilla Mellösa site, simulations in PLAXIS are then carried out.

6.2.1 Finite element model

An axis-symmetric geometrical model for Lilla Mellösa test fill is built in PLAXIS. It is considered to simulate a horizontal distance of 50 m far from the fill toe and set the initial ground surface height as zero.

In order to capture more details of the variation of soil parameters along the depth, the soft clay is divided into eight sub-layers as shown in Figure 6.8. The boundary condition is set as the *Standard fixity* in PLAXIS, i.e. prevented horizontal displacement at the two sides and a fixed bottom. The mesh generation is set as *fine* of the global coarseness, and with *refined line* for the fill bottom and *refined cluster* in the areas near the fill.

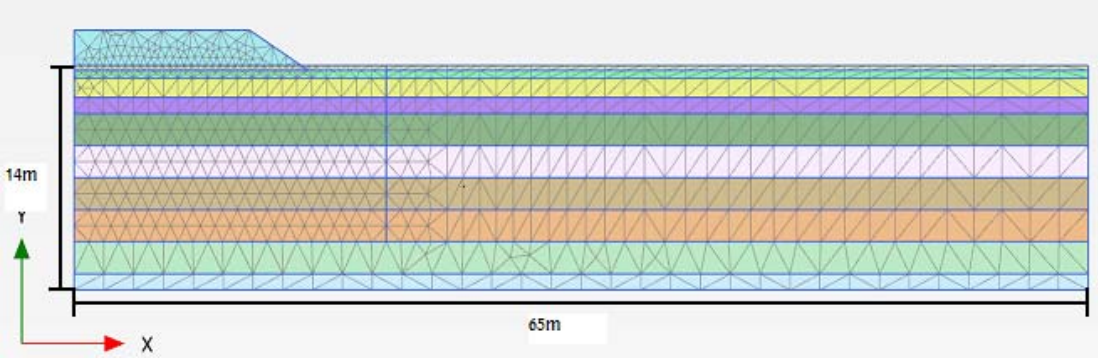

Figure 6.8. An overview of the Lilla Mellösa model drawn in PLAXIS.

6.2.2 Input parameters

The input parameters for models are mainly calculated based upon the evaluated compression modulus and the coefficient of secondary consolidation presented in Table 6.1.

For the n-SAC model, the modulus number *m'* is required to estimate the λ_i-value. However, due to that no record data for this parameter exist, an empirical relationship between the modulus number with natural water content proposed by Larsson (1981) is used, as in equation (6.1).

$$m' = 4.5 + \frac{6}{w_n} \tag{6.1}$$

Table 6.1. Evaluated fundamental soil parameters for Lilla Mellösa.

Layer	γ [kN/m^3]	w_n [%]	e_{init} [-]	M_0 [kPa]	M_L [kPa]	m' [-]	σ'_c [kPa]	α_s [-]	k [m/s]	c_k [-]
0.8-2 m	14	125	3.25	6000	200	9	20-30	0.035	7.00E-10	3
2-3 m	14	125	3.25	5000	190	9	20-22	0.038	7.00E-10	3
3-5 m	14	110	2.86	5000	200	10	22-32	0.035	7.00E-10	3
5-7 m	15	100	2.60	6000	200	10	32-40	0.030	7.00E-10	3
7-9 m	15	85	2.21	7000	200	12	40-58	0.025	7.00E-10	3
9-11 m	16	75	1.95	8400	260	12	58-72	0.020	1.00E-09	3
11-13 m	17	80	2.08	9500	320	12	72-90	0.020	1.00E-09	3
13-14 m	18	70	1.82	10800	380	13	90-100	0.010	1.00E-09	3

Additionally, the CRS tests conducted on the sample from the depth of 5 m and 9 m, which could be representative for the normal consolidated clay layer and slightly over consolidated clay layer respectively, are simulated so as to validate the suitability of the input parameters and obtain possible corrections, see Figure 6.9 and Figure 6.10.

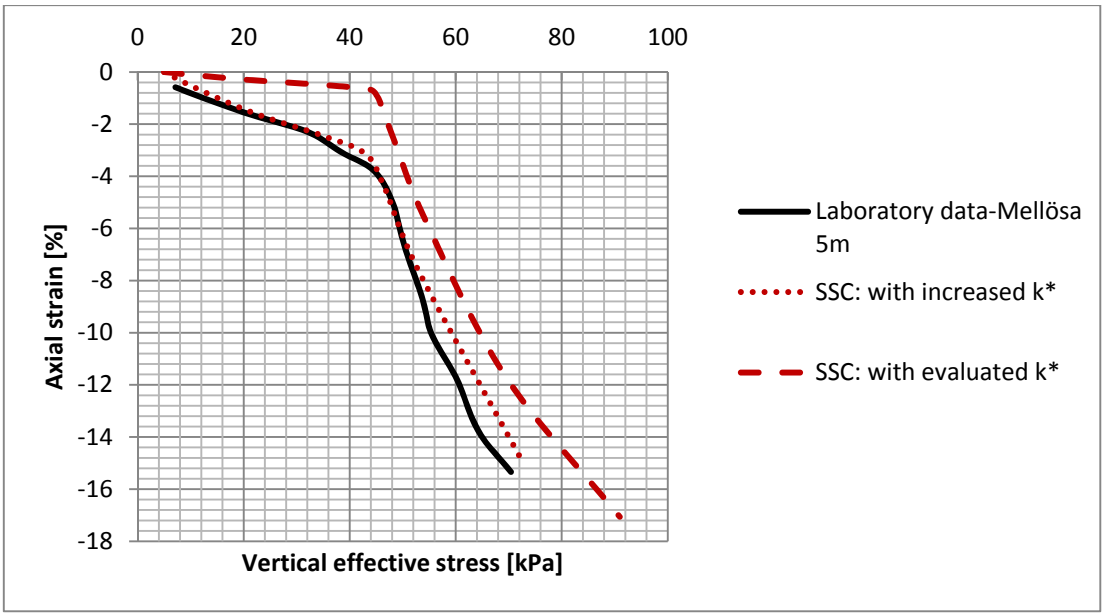

Figure 6.9. Comparison of SSC simulation with measurement in CRS tests for the 5 m sample from Lilla Mellösa.

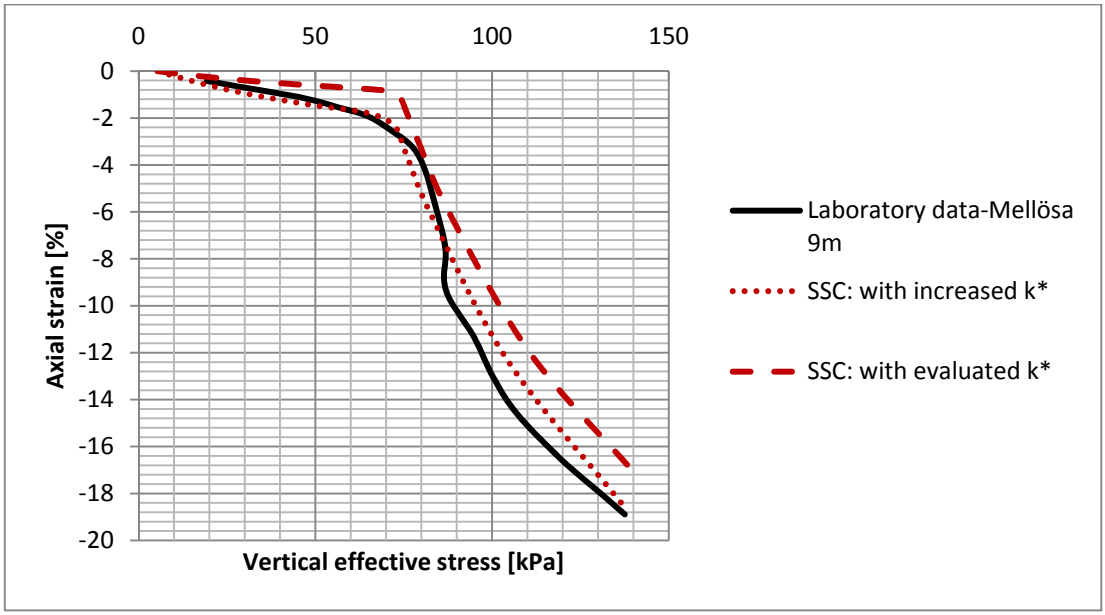

Figure 6.10. Comparison of SSC simulation with measurement in CRS test for the 9 m sample from Lilla Mellösa.

As it can be seen from the results shown in Figure 6.9 and Figure 6.10 above, the SSC simulation with evaluated k^*-value for both the 5 m and 9 m samples shows higher stiffness during the over consolidated stress range compared with the measurements. An increased k^*-value would fit the laboratory curve better, see Figure 6.11a and Figure 6.11b.

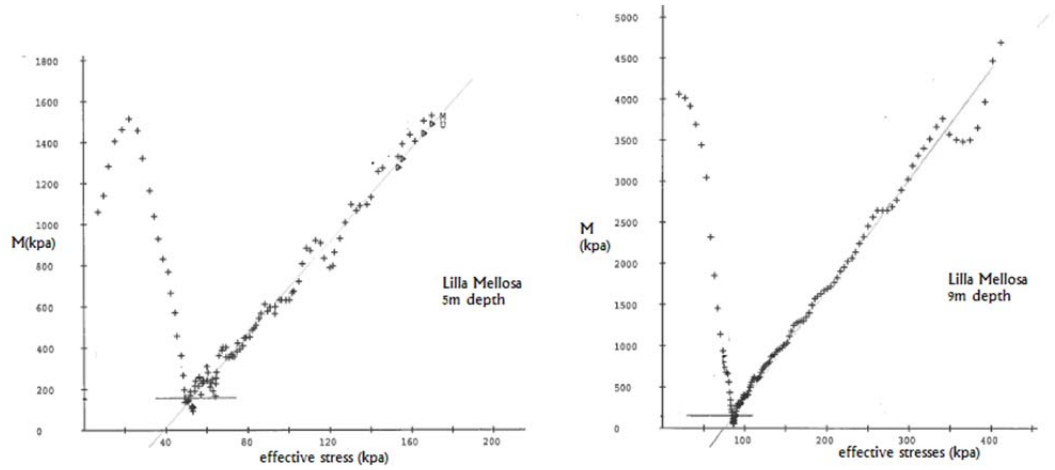

Figure 6.11. Variations of compression modulus with effective stresses from CRS tests on the samples of 5 m (a) and 9 m (b) samples in Lilla Mellösa.

This is quite reasonable if looking at the compression modulus directly from the CRS tests shown in Figure 6.11, in which the compression modulus in the over consolidated range, is much smaller than the evaluated M_0-value by Larsson (1986). Hence, it is concluded that Larsson has already multiplied a factor of 3~5 on the CRS-modulus data to modify the sample disturbance and inaccuracy without unloading-reloading curve thus to obtain a more suitable M_0-value for the field condition. Therefore it is decided to use the originally evaluated k^*-value here for the SSC and the ACM simulations.

For the CRS test simulations using the n-SAC model, similarly with SSC model, the evaluated E_{ref} predicts higher stiffness than the measurement, and a decreased E_{ref} (corresponding to the lower M_0 in CRS tests) gives more agreement with the laboratory curve, see Figure 6.13 and Figure 6.13). In addition, as discussed before, the E_{ref}-value also influences on the increase of stiffness after yielding (hardening). The decreased E_{ref}-value results in smaller hardening parameter, ζ_i, which in turn simulates rapid hardening in the large strain range.

Moreover, the r_{si}-value has been adjusted several times assuming a structure parameter, x_0, in the range of 4~10 to get a reasonable compression curve for the normal consolidated range. It is finally found that a $r_{si} = 10r_{si,min}$gives good prediction, which then is used for the fill simulation in n-SAC.

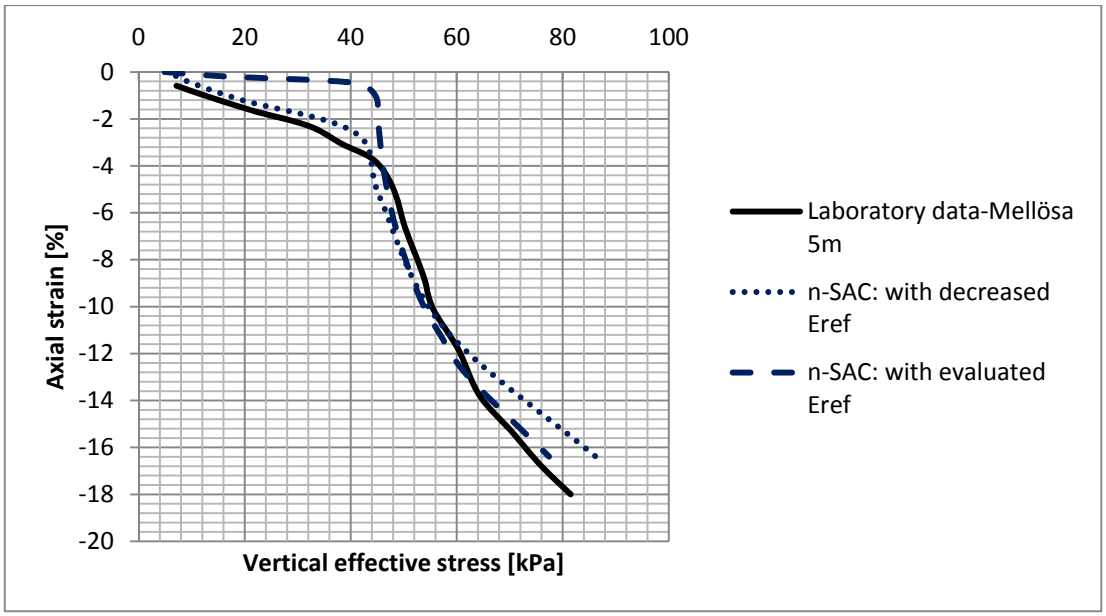

Figure 6.12. Comparison of n-SAC simulation with measurements in CRS tests for the 5 m sample from Lilla Mellösa.

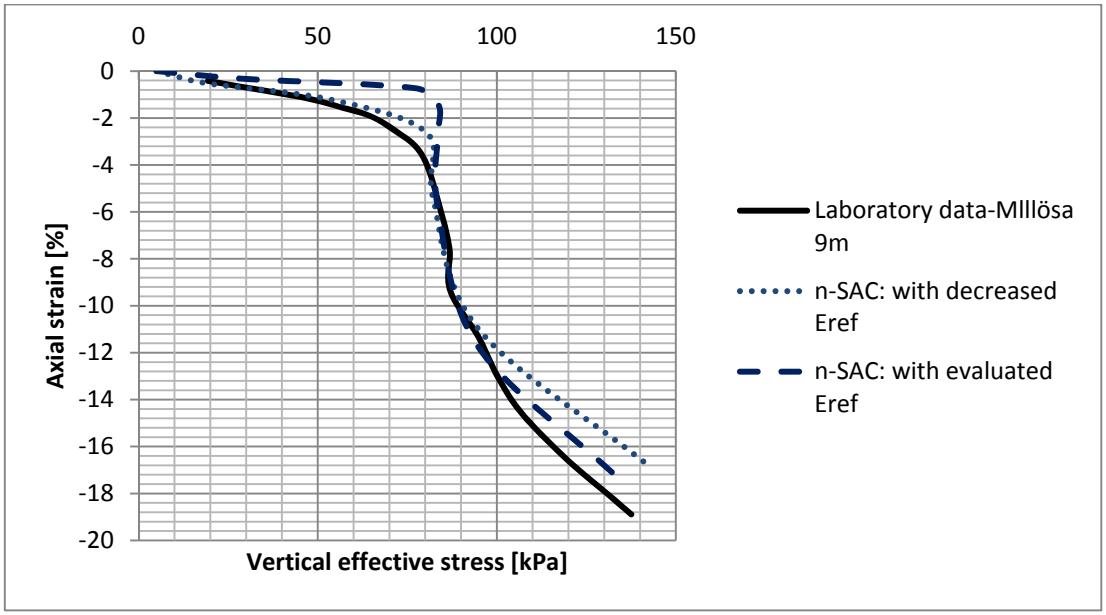

Figure 6.13. Comparison of n-SAC simulation with measurements in CRS tests for the 9 m samples from Lilla Mellösa.

In the end, all the input parameters for the simulations of Lilla Mellösa are presented as follows in Table 6.2, Table 6.3 and Table 6.4.

Table 6.2. Input parameters for the SSC model.

Layer	κ^* [-]	λ^* [-]	μ^* [-]	φ' [°]	c' [kPa]	K_0^{NC} [kPa]	OCR [-]	POP [kPa]	ν_{ur} [-]
0.8-2 m	0.0050	0.18	0.0152	30	1	0.5	/	16	0.15
2-3 m	0.0050	0.23	0.0165	30	1	0.5	/	2	0.15
3-5 m	0.0064	0.25	0.0152	30	1	0.5	/	3	0.15
5-7 m	0.0067	0.25	0.0130	30	1	0.5	/	4	0.15
7-9 m	0.0083	0.27	0.0109	30	1	0.5	1.2	/	0.15
9-11 m	0.0086	0.27	0.0087	30	1	0.5	1.2	/	0.15
11- 13 m	0.0095	0.29	0.0087	30	1	0.5	1.2	/	0.15
13-14 m	0.0093	0.29	0.0043	30	1	0.5	1.2	/	0.15

Table 6.3. Input parameters for the ACM model.

Layer	κ^* [-]	λ^* [-]	μ^* [-]	φ' [°]	c' [kPa]	M []	ν_{ur} [-]	ω []	ω_d []
0.8-2 m	0.0050	0.18	0.0152	30	1	1.2	0.15	0.76	16
2-3 m	0.0050	0.23	0.0165	30	1	1.2	0.15	0.76	13
3-5 m	0.0064	0.25	0.0152	30	1	1.2	0.15	0.76	12
5-7 m	0.0067	0.25	0.0130	30	1	1.2	0.15	0.76	12
7-9 m	0.0083	0.27	0.0109	30	1	1.2	0.15	0.76	12
9-11 m	0.0086	0.27	0.0087	30	1	1.2	0.15	0.76	11
11- 13 m	0.0095	0.29	0.0087	30	1	1.2	0.15	0.76	10
13-14 m	0.0093	0.29	0.0043	30	1	1.2	0.15	0.76	10

Table 6.4. Input parameters for the n-SAC model.

Layer	p_{ref} [kPa]	E_{ref} [kPa]	ν [-]	E_{oed}^{ref} [kPa]	$r_{s,min}$ []	r_{si} []	ω []	t_{max} []	τ [day]	OCR_τ [-]
0.8-2 m	100	42000	0.15	930	66	660	0.3	365yr	1	3
2-3 m	100	42000	0.15	930	61	610	0.3	365yr	1	1
3-5 m	100	33000	0.15	1000	66	660	0.3	365yr	1	1
5-7 m	100	31500	0.15	1050	77	770	0.3	365yr	1	1
7-9 m	100	25000	0.15	1100	92	920	0.3	365yr	1	1.2
9-11 m	100	24500	0.15	1250	115	1150	0.3	365yr	1	1.2
11- 13 m	100	22000	0.15	1200	115	1150	0.3	365yr	1	1.2
13-14 m	100	22000	0.15	1300	230	2300	0.3	365yr	1	1.2

The fill itself is simulated by the Mohr-Coulomb model, with a Young's Modulus of 40 MPa, friction angle of 37° and non-cohesion as well as a soil weight of 17 kN/m^3. The topsoil and dry crust layers are modelled simply by linear elastic model, both with E = 11 MPa and unit weight of 20 kN/m^3.

6.2.3 Calculations and comparison

In this section, calculation steps and the results are described in details at the first. The discussions with the different predictions are then presented.

6.2.3.1 Calculations

The calculation phase in PLAXIS is built by stages as:

- An *initial K_0-procedure* to create the in-situ stress state, with a hydrostatic pore pressure generated from a groundwater table level at the top of clay layer (0.8m below the ground);
- A 25-days construction phase;
- Several consolidation phases to 1967, 1979 and 2002 for measurement comparisons. The hydraulic boundary condition is set closed in both sides and open at the top and bottom. The calculation mode is *consolidation analysis (EPP)* with *updated mesh* to simulate the hydraulic lift due to settlements of fill.

6.2.3.2 Results

For the result analysis, it is determined to focus on the comparison of the time-settlement curve and the generated excess pore pressure. The settlement distributions

that had been measured along the depth at specific years are also of interest so as to investigate the different compressibility of different layers. Although there is no field measurement data about horizontal displacement, it is of necessity to compare the differences in terms of horizontal displacements prediction among soil models.

The ACM model has only succeeded to complete the calculation in the construction phase and failed for long-time calculation due to numerical difficulties within the model itself. As a consequence, comparisons of long-term settlements have been done between the SSC and the n-SAC models only.

After the completion of the fill construction, the predicted settlement is 0.0568 m, 0.0670 m and 0.1100 m by the SSC, the n-SAC and the ACM models respectively. The field measurement of immediate settlement was about 0.06 m after construction. The ACM model turns out to predict larger short-term settlements than the SSC model, which is in agreement with previous researches due to the incorporation of soil fabric anisotropy (Berengo, Leoni & Simonini, 2008; Leoni & Vermeer, 2009).

In Figure 6.14, results are illustrated as the vertical settlements versus time under the centre of the fill. The total predicted period is 57 years. Both of the models show good capability to capture the long-term settlements in terms of 21 years calculations (resulted in 1.4 m settlements). As the increase of consolidation time, the SSC model predicted a total settlement of 1.9 m after 57 years while the n-SAC model calculated a slightly small amount of settlements about 1.74 m.

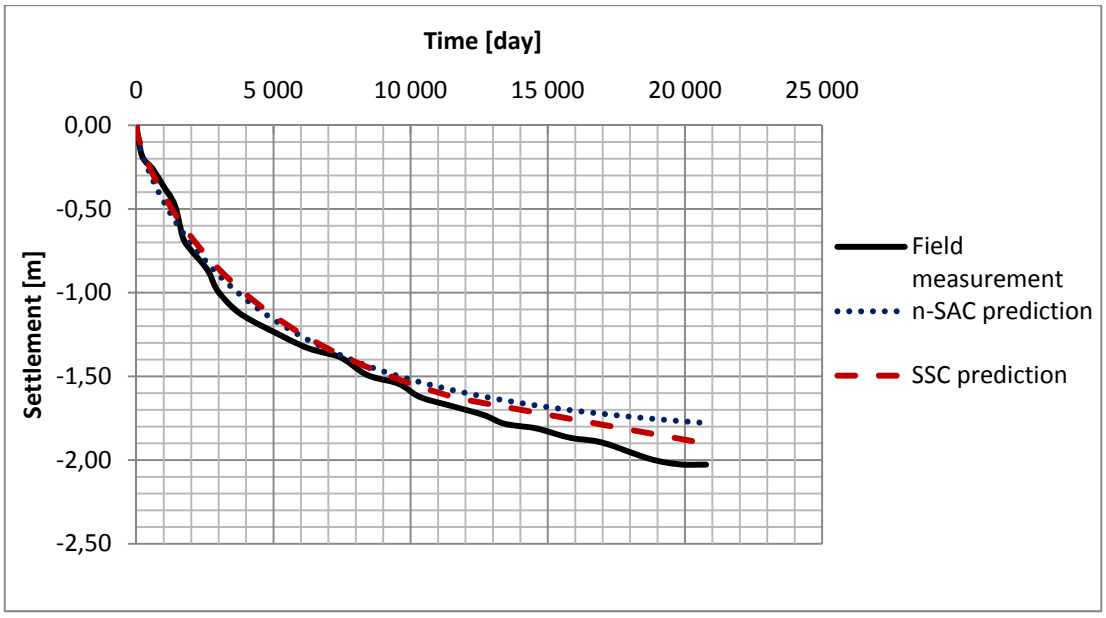

Figure 6.14. Time-settlement curves for measured and calculated data.

In Figure 6.15, Figure 6.16 and Figure 6.17, the measured and predicted distributions of excess pore pressure after 21 years, 32 years, and 57 years of consolidation are presented. Since it has been described above, there might be some error within the field measurement of excess pore pressure. It is therefore difficult to evaluate whether the models exactly give good or bad predictions in terms of the generated excess pore pressure. In general, the two models captured the shape of excess pore pressure distribution with the highest generated pore pressure in the middle layers. Moreover, a

general tendency of the SSC model to predict more excess pore pressure than the n-SAC model can be found. But this difference is less significant when compared to the field measurement.

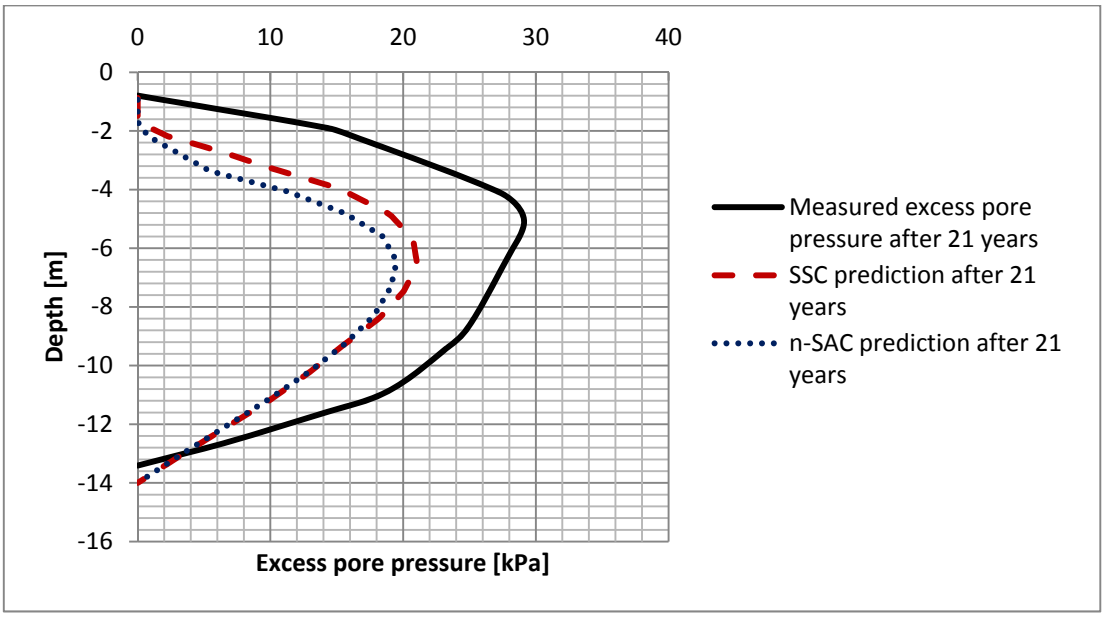

Figure 6.15. Excess pore pressure after 21 years of consolidation.

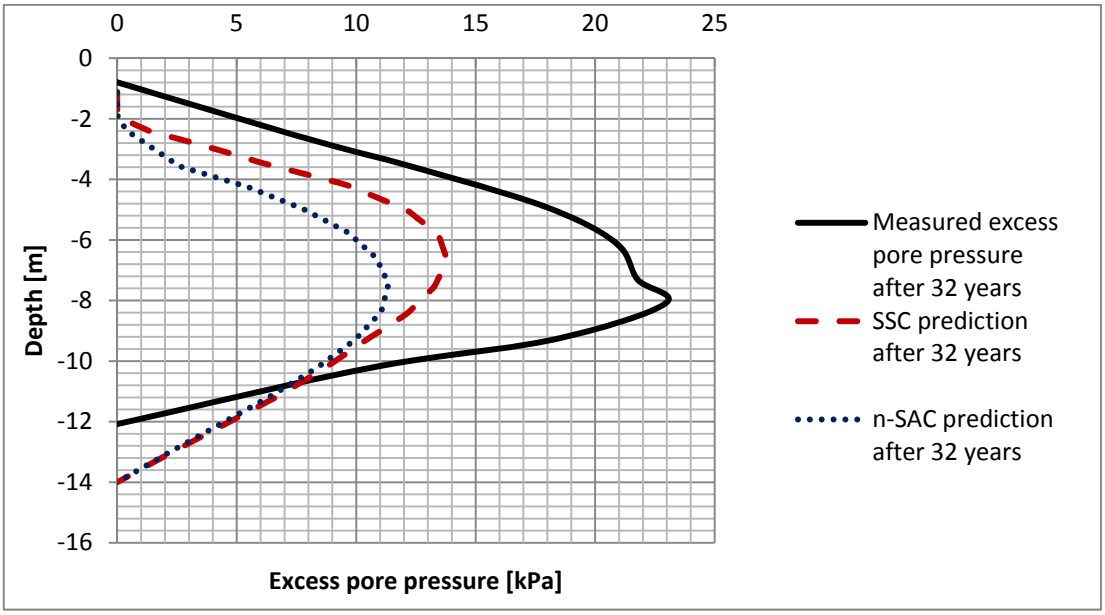

Figure 6.16. Excess pore pressure after 32 years of consolidation.

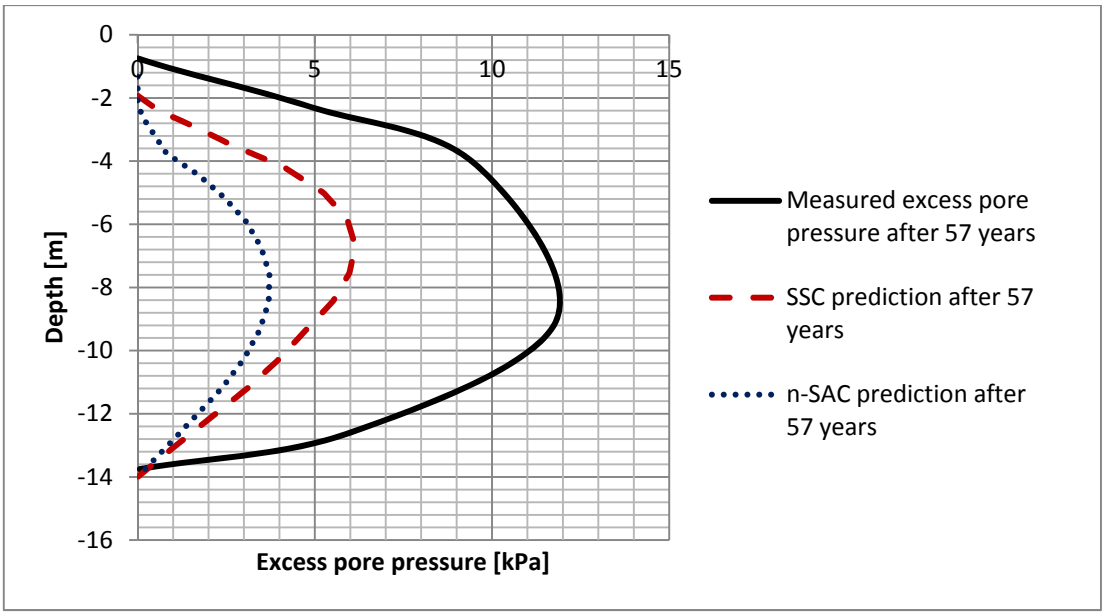

Figure 6.17. Excess pore pressure after 57 years of consolidation.

Figure 6.18 describes the comparisons among the model simulations and field measurements in terms of settlement distribution after 21 years. There are two in-situ measured values, in which one is from installed markers and the other one is from water content changes. Both of the models are capable to predict the overall distributions of the settlements in different layers. While, the biggest difference lies in the prediction of settlements for the upper 2 to 3 m of soils.

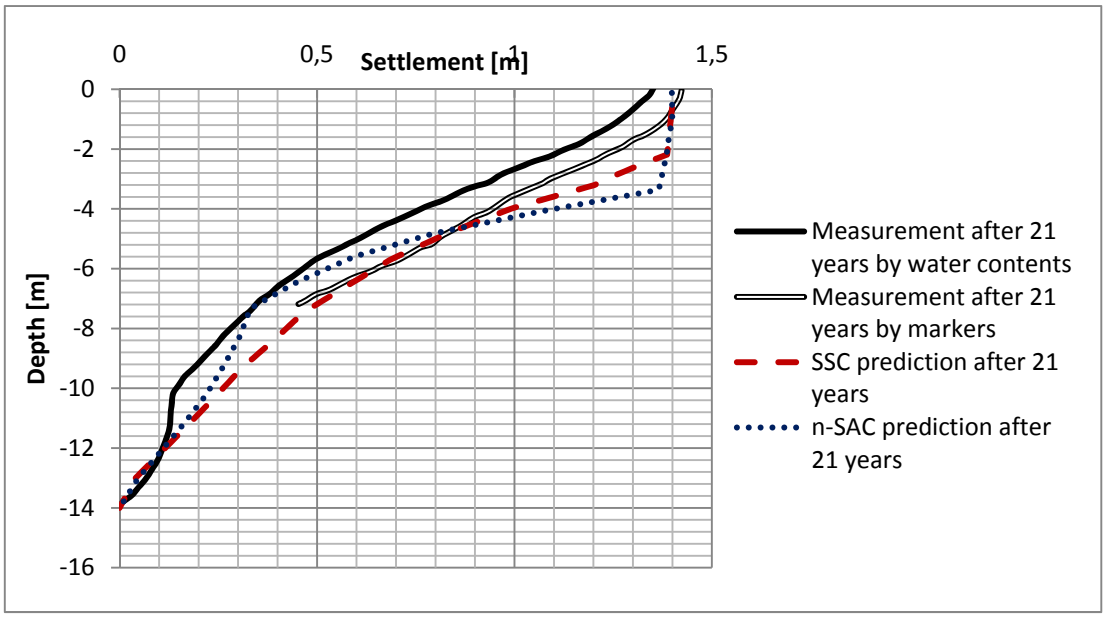

Figure 6.18. Settlement distribution after 21 years.

Moreover, it is also possible to compare the differences of horizontal displacements calculation for both the short-term period and in the long run shown in Figure 6.19

and Figure 6.20 in different models. Figure 6.19 shows the horizontal displacements under the fill toe at the end of construction, in which both the ACM model and n-SAC model predict larger horizontal displacements than the SSC model. In Figure 6.20 and Figure 6.21 the simulated long-term horizontal distributions are compared between the SSC and the n-SAC models. Overall, both of the models predict the largest horizontal displacement in the normally consolidated layer of 2~6 m.

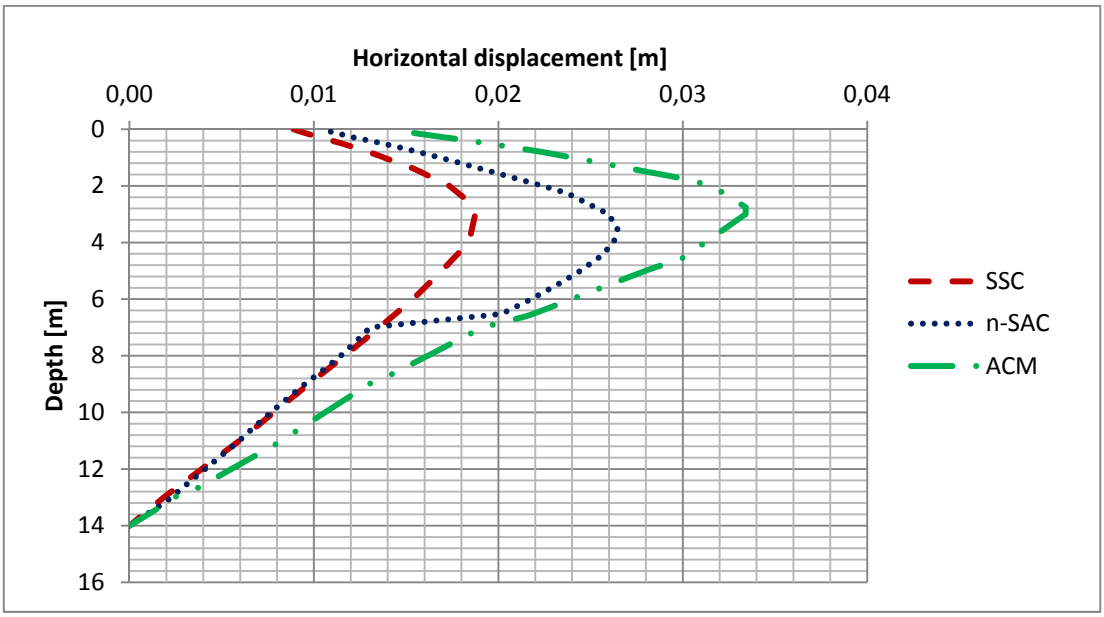

Figure 6.19. Horizontal displacement distributions at the end of construction.

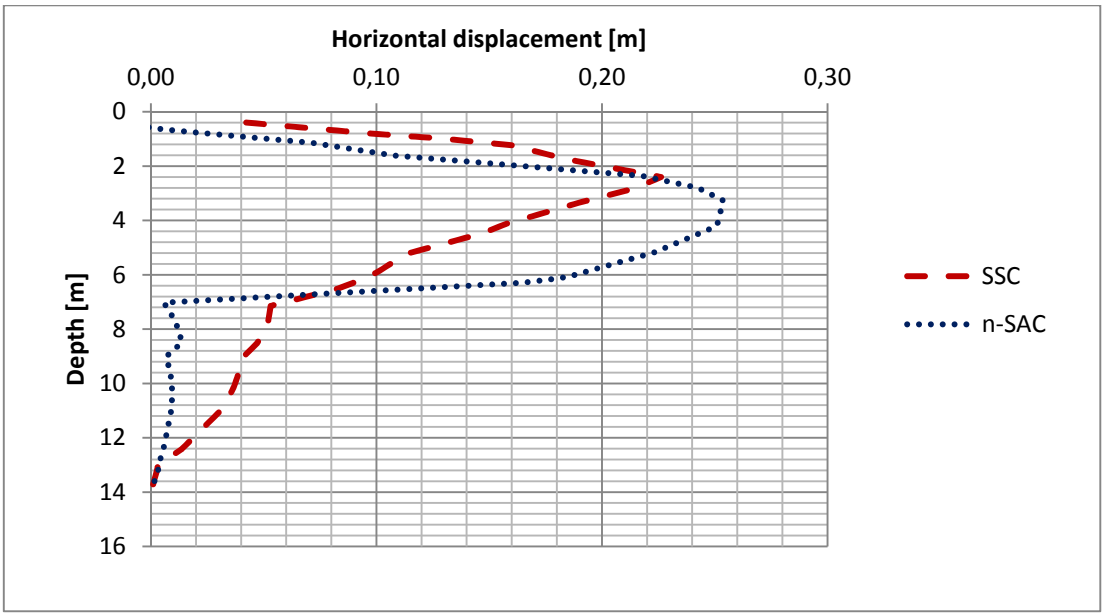

Figure 6.20. Horizontal displacement distributions after 21 years of consolidation.

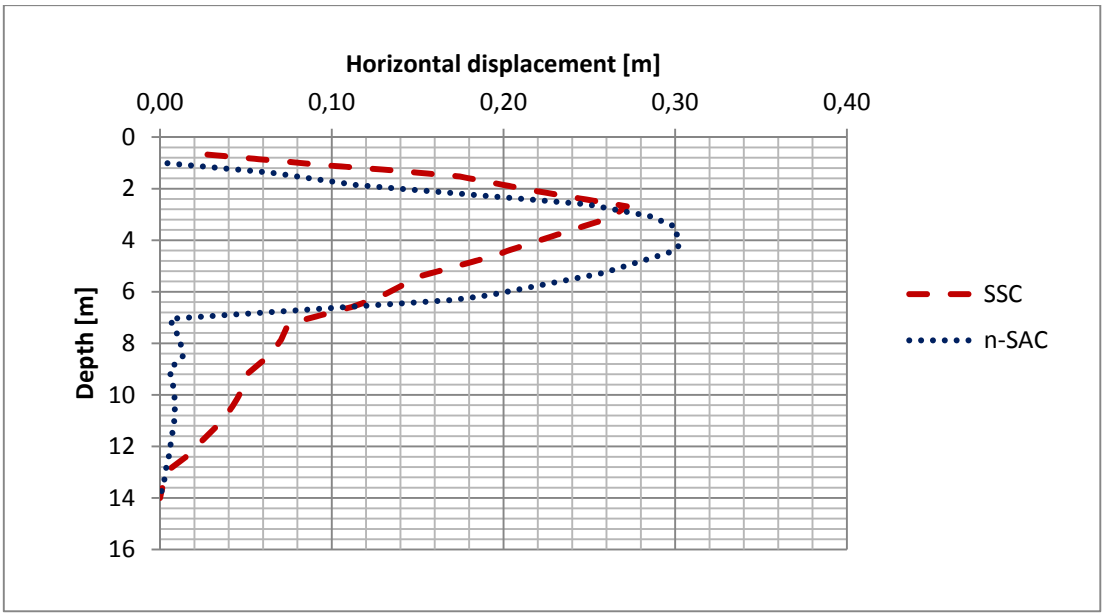

Figure 6.21. Horizontal displacement distributions after 57 years of consolidation.

It is expected that the ACM model would also predict more horizontal deformations in the long run since more plastic zones are developed with consolidation time, and therefore the more significance of the plastic anisotropy.

6.2.3.3 Discussion

Both the SSC and the n-SAC models show overall adequate capabilities to capture the long-term settlement of the fill, even though there are still some differences between the final measured settlements and predictions after 57 years and in both models, the decrease in settling rate with time is more significant compared with the measurements.

As mentioned before, the stiffness parameter for the over consolidated stress range has been empirically adjusted to match the real field condition. And therefore lower κ^*- and higher E_{ref}-values are applied in the model simulations. However, this might result in a risk of overestimating the soil stiffness and also influences on the change of creep rate in predictions, since the combined parameters of $(\lambda^*-\kappa^*)/\mu^*$ in the SSC model and $r_{si}\cdot\zeta$ in the n-SAC model are controlling the creep rate variations in time respectively. Hence, lower κ^*- and higher E_{ref}-values give fast change of creep rate in modelling.

The determination of the creep index also requires more attention. It has been commonly discussed that the 24 hour duration of each load in the standard incremental loading oedometer test would likely give rise to an overestimation of the creep parameter as the consolidation has not been completed yet or the creep just starts in a fast rate after one day. Moreover, Šuklje (1957) accounted for the fact of that the thickness and drainage condition of the soil sample are also influencing the creep behaviour, which means that the thin laboratory sample with restricted drainage condition during tests give more discrepancy in the determination of creep index. Specifically, the higher the ratio between the initial thickness of soil layer and the sample, the more creep would occur during the tests.

One has to bear in mind that these input soil parameters are determined by limited amount of laboratory tests, usually of one-dimensional loading on samples, and there are some sample disturbances and also influences by the testing environment. It is hard to get perfect representative parameters from the soil sample to describe the realistic behaviour of the whole soil layer, which therefore could explain the discrepancy between the model simulations and the in-situ measurements well.

Moreover, given that natural clays are fabric anisotropic, inter-particle bonded and viscous materials, any predictions disregarding these characteristics are likely to be unconservative in terms of settlement prediction. This is to say that the creep effect, anisotropy and the destructuration would all contribute to a larger amount of total settlements in soil layers. However, it seems that the n-SAC model calculated smaller settlement than the SSC model in the long run. The reason behind this is due to the inherent difference in the constitutive creep law of these two models. The n-SAC model attempts to describe the creep strain rate on the influence of soil destructurations and a varied creep number is applied, see Figure 6.22. However, the SSC model used the constant modified creep index μ^*. Consequently, it is difficult to say that the two models have consistent input soil parameters and thus the destructuration would result in more settlements. Instead, the value of $r_{si,max}$ in the n-SAC model is corresponding to the μ^*-value in the SSC model, which means that the SSC model calculation is with a higher creep rate. Similarly, the SSC model calculated higher excess pore pressure during the consolidation compared with the n-SAC model. Additionally, there are large uncertainties within the determination of destructuration parameter ω and the intrinsic creep number r_{si}, which means that more studies should be focused on the understanding of destructuration parameters thus they can be easily evaluated from standard laboratory tests.

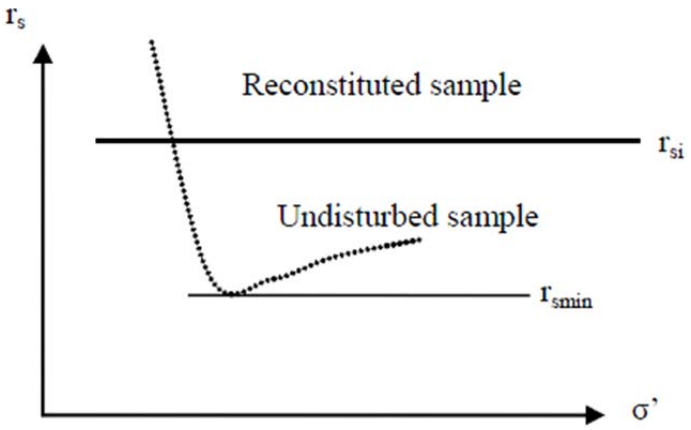

Figure 6.22. Variations of creep number in the n-SAC model (Grimstad & Degago, 2010).

It is also worth to discuss that there is a difference within the slope of the critical state line (i.e. the *M*-value) in models, which in turn influences the soil plasticity. The SSC model adopts an increased value of *M* according to the Modified Cam Clay theory so as to capture realistic K_0^{NC}-consolidated soil behaviour. However, the ACM and the n-SAC models apply a real value of *M* being consistent with Jaky's formula and a rotated yield surface which achieve the prediction of soil response in K_0^{NC}-consolidation also. This difference in results is a discrepancy in the ratio of horizontal

displacements and vertical settlements. Since the higher the slope of the critical state line, the steeper the yield surface would be, and therefore the lower ratio of horizontal displacements and vertical settlements based on the definition of plastic potential. In Figure 6.19, both the n-SAC and ACM models predicted larger short-term horizontal displacements under the fill toe than the SSC model, and the n-SAC model estimated larger horizontal displacements in long run as well. The evaluation of model predictions can be further performed when field measurements are available.

In general, it is never an easy task to predict the behaviour of soft soil when creep is considered and this task becomes even tougher when soil anisotropy and bonding effects are also incorporated. The more parameters are needed to describe the different features of soil, the more complexity of the numerical predictions it would be. What is more, the complexity that lies in those soil models is also that there is no single parameter that only affects one specific aspect of the soil behaviour, but instead each parameter is linked with others and then influences the over-all soil deformations in a combined way.

For future researches, since the anisotropy and destructuration of soft clay are not limited to the problems of long-term settlements, it is also of great importance to evaluate the ACM model and the n-SAC model for other types of geotechnical problems such as a deep excavation and a tunnel.

7 Conclusions

In this thesis, three advanced soil models, the Soft Soil Creep model (SSC), the Anisotropic Creep Model (ACM) and the non-associated creep model for Structured Anisotropic Clay (n-SAC), have been tested and evaluated by simulating several laboratory tests, including the CRS test and undrained triaxial test, and a field test located at Lilla Mellösa, Sweden. Even though the ACM model failed to predict the long term settlements for the field test, the overall performance of the ACM model can still be described and discussed together with the other two models. In the following, the advantages and drawbacks of the three models are concluded briefly and their further applications in engineering practice are also mentioned.

All three models are advantageous when the creep is of interest by incorporating the creep parameter (μ^* or r). Compared with conventional elastic-plastic models, the viscosity of soft soil is well described in these models. However, the evaluations of creep parameters are of challenge due to the need of incremental loading tests with longer loading duration or several CRS tests with different strain rates when incremental loading tests are missing and also correctly evaluated approaches. In general, the creep parameter is observed as stress-dependent or in another way strain-dependent, which means that the determination of a representative value of creep index for the models has large sensitivity. Therefore, in future studies, the incremental oedometer tests are suggested to be simulated so as to evaluate the performance of the creep index.

From a theoretical point of view, it would seem that the n-SAC model which incorporates all the three features of soft clay, i.e. the time-dependency, anisotropy and the structures, turns out to be the best choice in terms of soft soil behaviour prediction. However, the n-SAC model requires several parameters which are difficult to be defined from standard laboratory test practices, such as the destruction parameter. Based on the experiences of simulating both the lab tests and field case, it is found that the complexity in determining the soil parameters is counteracting the advantages of the n-SAC model. Therefore, more investigations regarding to the input parameters for the n-SAC model are of most importance.

The ACM model shows good capability in predicting the undrained shear strength in extension tests compared with the other two models, which demonstrates that the ACM model would be quite suitable for applications in deep excavation practice. Moreover, in the field test simulation, though it is only found that the ACM model predicts larger short-term horizontal displacements than the SSC model, it is reasonable to expect larger horizontal displacements in long term also when referring to previous studies (Berengo, Leoni & Simonini, 2008, Leoni & Vermeer, 2009). Therefore, the ACM model is valuable to be applied in cases of which the horizontal displacement is of big interest. Also, compared with the n-SAC model that requires the destructuration parameters and extra soil test on the reconstituted sample, the ACM model is without any difficulties in the determination of soil parameters since all the parameters are calculated from basic soil relations.

Overall, in terms of numerical simulation, the SSC model is very stable and performs its calculations fast compared with the other two models. The reason behind this might be due to the fact that the ACM and the n-SAC models are still just implemented as user-defined models into PLAXIS and more testing needs to be carried out. To conclude, at present the SSC model is an attractive choice when dealing with soft soil predictions in real cases. Further works regarding to the

implementations of the ACM and the n-SAC models have to be carried out so that they can also have wide applications in the industry.

8 References

Adachi, T. & Oka, F. (1982): Constitutive equation for normally consolidated clays based on elasto-viscoplasticity. *Soils and Foundations*, Vol. 22, pp. 57-70.

Anandarajah, A., Kuganenthira, N. & Zhao, D. (1996): Variation of fabric anisotropy of kaolinite in triaxial loading. *Journal of the Geotechnical Engineering Division, American Society of Civil Engineers,* Vol. 122, No. 8, pp. 633-640.

Bengtsson, P.E. & Larsson, R. (1994): *Användarhandbok Program Embankco, version 1.02*. (User Manual Program Embankco, version 1.02. In Swedish). Swedish Geotechnical Institute and National Road Administration, Linköping, Sweden.

Berengo, V., Leoni, M. & Simonini, P. (2008): Numerical modelling of the time-dependent behaviour of Venice Lagoon silts. *The 12th International Conference of International Association for Computer Methods and Advances in Geomechanics,* Goa, India, pp. 929-934.

Bjerrum, L. (1967): Engineering geology of Norwegian normally-consolidated marine clays as related to settlements of buildings. *Géotechnique*, Vol. 17, No. 2, pp. 81-118.

Bjerrum, L. (1973): Problems of soil mechanics and construction on soft clays and structurally unstable soils (collapsible, expansive and others). *State of the Art Report to Session IV, 8th International Conference on Soil Mechanics and Foundation Engineering,* Moscow, Union of Soviet Socialist Republics.

Brinkgreve, R.B. J., Broere, W. & Waterman, D. (2006): *PLAXIS Manual 2D - Version 8,* Netherlands.

Buisman, K. (1936): Results of long duration settlement tests. *Proceedings 1st International Conference on Soil Mechanics and Foundation Engineering*, Cambridge, Massachusetts, USA, Vol. 1, pp. 103-107.

Burland, J.B. (1990): On the compressibility and shear strength of natural clays. *Géotechnique*, Vol. 40, No. 3, pp. 329-378.

Casagrande, A. (1936): The determination of the preconsolidation load and its practical significance. *Proceedings of the 1st International Conference of Soil Mechanics and Foundation Engineering*, Cambridge, Massachusetts, USA, Vol. 3, p. 60.

Chang, Y.C.E. (1969): *Long term consolidation beneath the test fills at Väsby, Sweden*. Diss. University of Illinois, Urbana, Illinois, USA.

Chang, Y.C.E. (1981): *Long term consolidation beneath the test fills at Väsby, Sweden*. Swedish Geotechnical Institute Report 13, Linköping, Sweden.

Christensen, S. (1995): *Long-term processes in geomaterials. Creep parameters from oedometer tests on Illitic clays*. SINTEF Geotechnical Engineering, Trondheim, Norway.

Claesson, P. (2003): *Long term settlements in soft clays*. Ph.D. thesis, Department of Geotechnical Engineering, Chalmers University of Technology, Gothenburg, Sweden.

Controls (2011): Triaxial Cell Accessories. [Online]
Available:
http://www.controls.it/products.php?code=260&page=Triaxial_Cells&product=603&product_name=Heavy_Duty_Banded_Triaxial_Cells&language=1
[2011-05-25]

Garlanger, J.E. (1972): The consolidation of soils exhibiting creep under constant effective stress. *Géotechnique,* Vol. 22, pp. 71-78.

Grimstad, G., Degago, S.A., Nordal, S. & Karstunen, M. (2008): *Modelling creep and rate effects using the time resistance concept in a model for anisotropy and destructuration*. Nordic Geotechnical Meeting, Sandefjord, Norway, pp. 195-202.

Grimstad, G. & Degago, S.A. (2010): A non-associated creep model for structured anisotropic clay (n-SAC). *Proceedings of the 7th European Conference on Numerical Methods in Geotechnical Engineering*, Trondheim, Norway, pp. 3-8.

Hansbo, S. (1975): *Jordmateriallära* (Soil material science. In Swedish). AWE/GEBERS, Stockholm, Sweden.

Havel, F. (2004): *Creep in soft soils*. Ph.D. thesis, Geotechnical Division, Department of Civil and Transport Engineering, Norwegian University of Science and Technology, Trondheim, Norway.

Hinchberger, S.D., Qu, G. & Lo, K.Y. (2010): Constitutive approach for rate-sensitive anisotropic structured clays. *International Journal for Numerical and Analytical Methods in Geomechanics*, Vol. 34, No. 17, pp. 1797-1830.

Janbu, N. (1969): The resistance concept applied to soils. *Proceedings of the 7th International Conference on Soil Mechanics and Foundation Engineering,* Mexico City, Mexico, pp. 191-196.

Janbu, N. (1998): *Slope stability evaluations in engineering practice*. Department of Geotechnical Engineering, Norwegian University of Science and Technology, Trondheim, Norway.

Jin, F., Liu, S. & Shao, G. (2001): The settlement of embankment on soft ground. *Chinese Journal of Geotechnical Engineering*, Vol. 23, No. 6, pp. 659-661.

Kim, Y.T. & Leroueil, S. (2001): Modelling the viscoplastic behaviour of clays during consolidation: application to Berthierville clay in both laboratory and field conditions. *Canadian Geotechnical Journal*, Vol. 38, No. 3, pp. 484-497.

Koskinen, M., Karstunen, M. & Wheeler, S. J. (2002): Modelling destructuration and anisotropy of a soft natural clay. *5th European Conference on Numerical Methods in Geotechnical Engineering,* September 2002, Paris, France, pp. 11-20.

Larsson, R. (1981): Drained behaviour of Swedish clays. Swedish Geotechnical Institute Report 12, Linköping, Sweden.

Larsson, R. (1986): *Consolidation of soft soils*. Swedish Geotechnical Institute Report 29, Linköping, Sweden.

Larsson, R. (2007): *Långtidsobservationer av konsolideringsprocesser - Resultat från mer än 50 års uppföljningar av provbankar på lös lera i Sverige*. (Long-term observations of consolidation processes – results from about fifty years´ monitoring of Swedish test embankments on soft clay. In Swedish). Swedish Geotechnical Institute Report 70, Linköping, Sweden.

Lefebvre, G. (1981): The long-term stability of a cutting slope in an overconsolidated sensitive clay. *Canadian Geotechnical Journal*, Vol. 18, pp. 322-323.

Leoni, M., Karstunen, M. & Vermeer P.A. (2008): Anisotropic creep model for soft soils. *Géotechnique*, Vol. 58, No. 3, pp. 215-226.

Leoni, M. & Vermeer, P.A. (2009): Numerical modelling of creep in soft soils. *17th International Conference on Soil Mechanics and Geotechnical Engineering*, Alexandria, Egypt.

Leroueil, S., Tavenas, F., Brucy, F., La Rochelle, P. & Roy, M. (1979): Behaviour of destructed natural clays. *Journal of the Geotechnical Engineering Division, American Society of Civil Engineers,* Vol. 105, No. 6, pp. 759-778.

Neher, H.P., Wehnert, M. & Bonnier, P.G. (2001): An evaluation of soft soil models based on trial embankments. In Desai et al. (Eds), *Proceedings of the 10th International Conference on Computer Methods and Advances in Geomechanics*, Rotterdam, the Netherlands, pp. 373-378.

Olsson, M. (2010): *Calculating long-term settlement in soft clays – with special focus on the Gothenburg region*. Lic.Eng. thesis, Division of GeoEngineering, Department of Civil and Environmental Engineering, Chalmers University of Technology, Gothenburg, Sweden.

Šuklje, L. (1957): *The* Analysis of the Consolidation Process by the Isotaches Method. *Proceedings of the 4th International Conference on Soil Mechanics and Foundation Engineering*, London, United Kingdom, 1957, pp. 200-206.

Sällfors, G. (1975): *Preconsolidation pressure of soft, high plastic clays*. Ph.D. thesis, Geotechnical Department, Chalmers University of Technology, Gothenburg, Sweden.

Sällfors, G. (2001): *Geoteknik: Jormateriallära, Jordmekanik, 3:e upplagan* (Geotechnics: Soil material science, Soil mechanics, 3rd edition. In Swedish), Chalmers University of Technology, Gothenburg, Sweden.

Tavenas, F. & Leroueil, S. (1977): Effects of stresses and time on yielding of clays. *Proceedings of the 9th International Conference on Soil Mechanics and Foundation Engineering*, Tokyo, Japan, Vol. 1, pp. 319-326.

Taylor, D.W. (1942): *Research on consolidation of clays – Report 82*. Department of Civil Engineering, Massachusetts Institute of Technology, Cambridge, Massachusetts, USA.

Terzaghi, K., (1923): *Die Berechnung der Durchlässigkeitsziffer des Tones aus dem Verlauf der hydrodynamishen Spannungserscheinungen*. Akademie der Wisenschaften in Wien. Mathematisch- Naturwissenschaftliche Klasse. Sitzungsberichte. Abteilung II a., Vol. 132, p. 125-138.

Trafikverket (2011): *Om BanaVäg i Väst* (About BanaVäg i Väst. In Swedish). [Online].
Available: http://www.trafikverket.se/Privat/Projekt/Vastra-Gotaland/BanaVag-i-Vast/Om-BanaVag-i-Vast/ [2011-04-14].

Vermeer, P.A. & Neher, H.P. (1999): A soft soil model that accounts for creep. *Proceedings of the Plaxis Symposium on Beyond 2000 in Computational Geotechnics,* Amsterdam, the Netherlands, pp. 249-262.

Wheeler, S.J., Cudny, M., Neher, H.P. & Wiltafsky, C. (2003a): Some developments in constitutive modelling of soft clays. *International Workshop on Geotechnics of Soft Soils – Theory and Practice,* Noordwijkerhout, the Netherlands, pp. 3-22.

Wheeler, S.J., Näätänen, A., Karstunen, M. & Lojander, M. (2003b): An anisotropic elastoplastic model for soft clays. *Canadian Geotechnical Journal*, Vol. 40, No. 2, pp. 403-418.

Wood, D.M. (1984): Choice of models for geotechnical predictions. *Mechanics of engineering materials*, pp. 633-654.

Wood, D.M. (1990): *Soil behaviour and critical state soil mechanics*. Cambridge University Press, Cambridge, United Kingdom.

Yin, Z-Y., Chang, C.S., Karstunen, M. & Hicher, P-Y. (2010): An anisotropic elastic-viscoplastic model for soft clays. *International Journal of Solids and Structures*, Vol. 47, pp. 665-677.